Mitotic DNA Damage Responses in *Drosophila* Polyploid Rectal Papillar Cells

by

Delisa Ellen Clay

Department of Cell Biology
Duke University

Date:_____

Approved:

_____
Donald Fox, Supervisor

_____
Eda Yildirim

_____
David Kirsch

_____
Jeff Sekelsky

_____
David Sherwood

Dissertation submitted in partial fulfillment of
the requirements for the degree of Doctor
of Philosophy in the Department of
Cell Biology in the Graduate School
of Duke University

2021

ABSTRACT

Mitotic DNA Damage Responses in *Drosophila* Polyploid Rectal Papillar Cells

by

Delisa Ellen Clay

Department of Cell Biology
Duke University

Date:_____
Approved:

_____
Donald Fox

_____
Eda Yildirim

_____
David Kirsch

_____
Jeff Sekelsky

_____
David Sherwood

An abstract of a dissertation submitted in partial
fulfillment of the requirements for the degree
of Doctor of Philosophy in the Department of
Cell Biology in the Graduate School of
Duke University

2021

Abstract

Mitosis involves the faithful segregation of two identical copies of chromosomes into two daughter cells. This process is highly regulated to maintain genome integrity, as mis-segregation of partial or whole chromosomes can lead to genomic instability. Cells are constantly exposed to both endogenous and exogenous forms of DNA damage, which if left unattended to, can contribute to mitotic errors. Cells therefore possess DNA damage responses (DDRs) which involves enacting cell cycle checkpoints, DNA damage repair, and in cases of extreme damage – cell death or senescence.

While several lines of investigation have identified key mechanisms of the DDR during interphase of the cell cycle, there are several key questions that remain with regards to how cells deal with damage that persists into mitosis. Further, there is currently a gap in knowledge on the mechanisms, timing, and conditions in which different aspects of the DDR are active and coordinated. In this dissertation, I will demonstrate how I implemented genetic and imaging tools using our laboratory's previously established model system, *Drosophila* rectal papillar cells [hereafter papillar cells]. Using this model, I studied (1) mechanisms of the DDR during mitosis, (2) mechanisms that act in the absence of key DDR components, and (3) novel regulators and protein-protein interactions of the mitotic DDR. This body of work contributes to the growing knowledge of how cells tolerate DNA damage that persists into mitosis.

Dedication

I dedicate this dissertation to the village that raised me: my loving parents Felicia Brogden and Eddie Clay, who both motivated and encouraged me throughout this process; my dear grandmother Martha Clay, who saved my life; my large and loving family for who I do this for; the community of lovely human beings that I've had the pleasure of knowing throughout my scientific journey including here at Duke. I am truly grateful for the amazing scientists that have fostered my growth during this process. I cannot pay it back but I will try to pay it forward.

Contents

List of Tables

List of Figures

Acknowledgements

I would like to thank my advisor, Dr. Don Fox for his mentorship and support throughout my PhD experience at Duke. Additionally, I would like to thank my mentors outside of the lab, Dr. Devyn Gillette, Dr. Sherilynn Black, Dr. Adrienne Stiff-Roberts, Dr. Paige Cooper, Dean Jacqueline Looney, and Dr. Nina Sherwood. I would also like to acknowledge Dr. Nina Sherwood, Dr. Eric Spana, and Dr. Emily Ozdowski for allowing me to use their lab space for my doctoral work and for providing feedback on my research.

I thank my collaborators who have contributed to my first author manuscript and additional research projects, Dr. Heidi Bretscher, Erin Jezuit, MS, Korie Bush, Dr. Don Fox, and Daniel Buster and Dr. Greg Rogers at the University of Arizona. Thank you to the groups that have provided reagents used in my dissertation: the labs of Dr. Jeff Sekelsky, Dr. Greg Rogers, Dr. Anne Royou, Dr. Jared Nordman, Dr. Paul Fisher, and Dr. James Kadonaga.

I thank Dr. Fu Yang and Dr. Zhao Zhang for comments on my first author manuscript. Thank you for the additional provided reagents used in my first author manuscript: Bloomington Drosophila Stock Center, Developmental Studies Hybridoma Bank, and Vienna Drosophila Resource Center. This project was supported by the NIGMS grant GM118447 to Dr. Don Fox., an NSF GRFP grant to myself., and an NCI

grant F31CA186545 to Dr. Heidi Bretscher. I also thank Dr. Lisa Cameron and Dr. Yasheng Gao at the Duke Light Microscopy Core Facility for assistance.

Lastly thank you to the following lab groups that have provided feedback on my research over the years: The MacAlpine lab, the Goetz lab, the Duronio lab, the Yao Lab, the Zhang lab, the Kirsch lab, the Jinks-Roberston lab, and the Petes lab. Thank you to my dissertation committee members, Dr. Don Fox, Dr. Eda Yildirim, Dr. David Kirsch, Dr. David Sherwood, and Dr. Jeff Sekelsky, for fostering my growth as a scientist over the years. And thank you to the members of the Fox lab for their training, scientific feedback, and support.

1. Introduction

This introduction is a review of the DNA damage response (DDR) with an emphasis on how the specific DDR is influenced by cell cycle stage, ploidy state, and genome instability. I will review the existing literature on DDRs with an emphasis on work in model systems to provide sufficient context for Chapters 2 and 3. These chapters contain published (Chapter 2) and unpublished (Chapter 3) work on DDRs in the *Drosophila* model organism. I will be using human nomenclature to refer to gene and protein names unless otherwise specified.

1.1 The DNA damage response

There are various forms of internal and external sources of DNA damage that pose a threat to genome integrity. Therefore, organisms have evolved a DNA damage response (DDR) to respond to aberrant lesions and ensure faithful segregation of genetic material during cell division [1, 2]. The DDR is a concerted effort involving several factors that sense DNA damage, signal that damage to the cell, and recruit downstream effector proteins that induce transcription, cell cycle arrest, the repair of DNA damage, and in some cases cell death or senescence [3].

1.1.1 Causes of DNA damage and lesion types

The diverse forms of DNA damage will influence which factors are recruited to damaged sites as well as dictate DNA damage pathway choice. Naturally occurring

cellular functions such as metabolic processes, inflammatory responses, or errors in DNA replication and recombination can lead to various forms of DNA damage or aberrations [1, 4]. Common sources of external DNA damage include ultraviolet (UV) radiation from the sun, ionizing radiation (IR), and chemical drugs often used to treat cancer such as cisplatin or mitomycin C (MMC). Several of these agents and processes can result in aberrant DNA structures, single-strand DNA breaks (SSBs), and double-stranded breaks (DSBs)[2].

1.1.2 DNA lesions and SSB pathways

Distinct DNA damage repair processes, each with factors specific to each process, have evolved to respond to erroneous DNA changes. Overall, these responses mainly involve excising the aberrant structure, gap-filling, and ligation. The Base Excision Repair (BER) pathway responds to chemical changes at single base sites and involves various DNA glycosylases [2, 5, 6]. Bulky adducts caused by UV radiation and chemotherapy drugs are removed by the Nucleotide Excision Repair (NER) pathway [1, 2, 5, 6]. Mismatch Repair (MMR) is required for base mismatches that can arise from DNA replication and recombination errors [7]. Interstrand crosslinks (ICL) arise from crosslinking agents such as MMC or nitrogen mustard and depends on the Fanconi Anemia pathway for repair (Covered in more detail in Chapter 3) [2, 6]. Lesions that are not removed from either BER or NER and persist during DNA replication are responded

to through translesion synthesis (TLS), a process that involves switching to specialized DNA polymerases that bypass lesions and synthesize new bases with varying fidelity [8]. Much of what we know about the molecular underpinnings of SSB pathways has emerged from studies performed in human disease models. For example, Fanconi Anemia patient cells and cells from NER-deficient Xeroderma pigmentosum patients have high sensitivity to UV-light [9]. Overall, DNA damage that requires SSB repair pathways are fairly common and pose a smaller threat to genome integrity than DSBs [2].

1.1.3 DSB repair pathways

DSBs, while less common than the aforementioned lesions, are more deleterious in nature as they can lead to loss of large amounts of genetic material during cell divisions if not responded to properly [3, 10]. DSBs can be caused by sources such as IR (X-ray, gamma, etc.), or errors in replication in which stalled forks collapse into DSBs.

Two major repair pathways have been described to respond to DSBs: the Homologous Recombination (HR) pathway and Classical Nonhomologous End-Joining (cNHEJ). Other DSBs repair pathways have also been characterized to a lesser extent, including Alternative End-Joining (alt-EJ, also known as Theta-Mediated End-Joining, TMEJ) and Single-Strand Annealing (SSA) [2, 11]. Several discoveries of conserved DSB

repair pathways have emerged from mutagenesis screens and other DSB repair assays in model organisms such as yeast, *C. elegans*, and *Drosophila* (as reviewed in [12][3-5, 13]).

HR is an error-free mode of repair which involves the processing of DSB ends through short and long-range resection with various endo- and exonucleases. Rad51 is recruited to resected ssDNA and drives the search for a homologous template to allow for accurate repair. cNHEJ is an error-prone form of DSB repair that involves Ku proteins (Ku70/Ku80) binding to either side of the DSB. Enzymes are then recruited to process DNA ends, and the XRCC4-LIG4 complex participates in ligating the processed ends together. Alt-EJ and SSA have similar modes of repair with distinct machinery. During alt-EJ, which primarily depends on DNA polymerase theta (*POLQ*), microhomologies around the site of a break are recognized and annealed together. For SSA to occur, longer regions of homology are required for annealing. Rad52 is thought to be required for this process in yeast(*S. cerevisiae* and *S. pombe*) and humans, though other factors have been hypothesized to be involved such as RECQ5 and SMARCAL1 in *Drosophila* as well [2, 5, 11, 14, 15].

Repair of both SSBs and DSBs is typically coordinated through a signal transduction cascade that mediates cell cycle arrest to allow for DNA repair before continuing the cell cycle. Failure to properly coordinate cell cycle checkpoints with DNA repair can result in persistent DNA damage and may eventually lead to mitotic

catastrophe, which is the activation of cell death pathways during mitosis, or loss of genetic information during cell division [1, 2, 4, 16]. The following section highlights some major players in mediating the signaling that coordinates the DDR to promote the accurate scheduling of repair and return to the cell cycle.

1.1.4 DNA damage response signaling mechanisms

The DDR involves a signal transduction cascade that promotes DNA damage sensing and cellular outputs such as transcription and recruitment of downstream effector proteins. DDR signaling can lead to cell cycle arrest, DNA repair, cell death, or senescence. Similar to repair pathway choice, the type of DNA damage can dictate which signaling factors are recruited early on. A great extent of this signaling is driven by 3 phosphoinositide 3-kinase (PI3K)-related kinases (PIKKs). PIKKs were first identified in *S. cerevisiae* through various genetic screens by independent groups in search of genes involved in both repair and cell cycle progression. The first PIKK, ATM- and Rad3-related (ATR), was found to be important during replication induced DNA damage. The other two PIKKs that were identified were DNA Protein Kinase (DNA-PK) (not found in *S. cerevisiae* or *S. pombe*) and Ataxia telangiectasia mutated (ATM)[13, 17]. While DNA-PK and ATM are often recruited to sites of DSBs, ATR is mainly recruited to ssDNA that arises during errors in replication. In addition to PIKKs,

poly(ADP-ribose) polymerase (PARP) family proteins also mediate the DDRs in the case of both DSBs and SSBs [2].

ATM and ATR amplify signaling cascades through direct and indirect phosphorylation of downstream substrates. Key players in cell cycle control during the DDR, Checkpoint kinase 1 and 2 (Chk1 and Chk2) are phosphorylated directly by ATR and ATM, respectively and then phosphorylate downstream substrates. ATM and Chk2 can both regulate the p53 transcription factor. p53 is a tumor suppressor with several important functions in the DDR, but primarily regulates transcription to induce cell cycle arrest, cell death, or senescence [1, 2, 17]. ATR mediated activation of Chk1 leads to the regulation of CDKs which also leads to cell cycle arrest [17]. DNA-PK, which senses DSBs, primarily activates cNHEJ after recruitment to damaged sites by Ku proteins. All 3 PIKKs can phosphorylate H2Ax (γH2Ax), a histone variant that once activated can recruit downstream factors to repair foci that amplify the DDR signal [2, 17].

Another factor that drives signaling choice during the DDR response involves the stage of the cell cycle. Regulation of DNA damage checkpoints differ during distinct cell cycle phases. For example, p53 suppression is associated with a failed G_1/S phase arrest, but cells may still be capable of arresting in G_2. In contrast, Chk1 is primarily involved in mediating cell cycle arrest during S-phase and at the G_2/M transition [18, 19].

The following section will focus primarily on how cell cycle stage can determine which repair pathway choice is selected to repair DNA lesions.

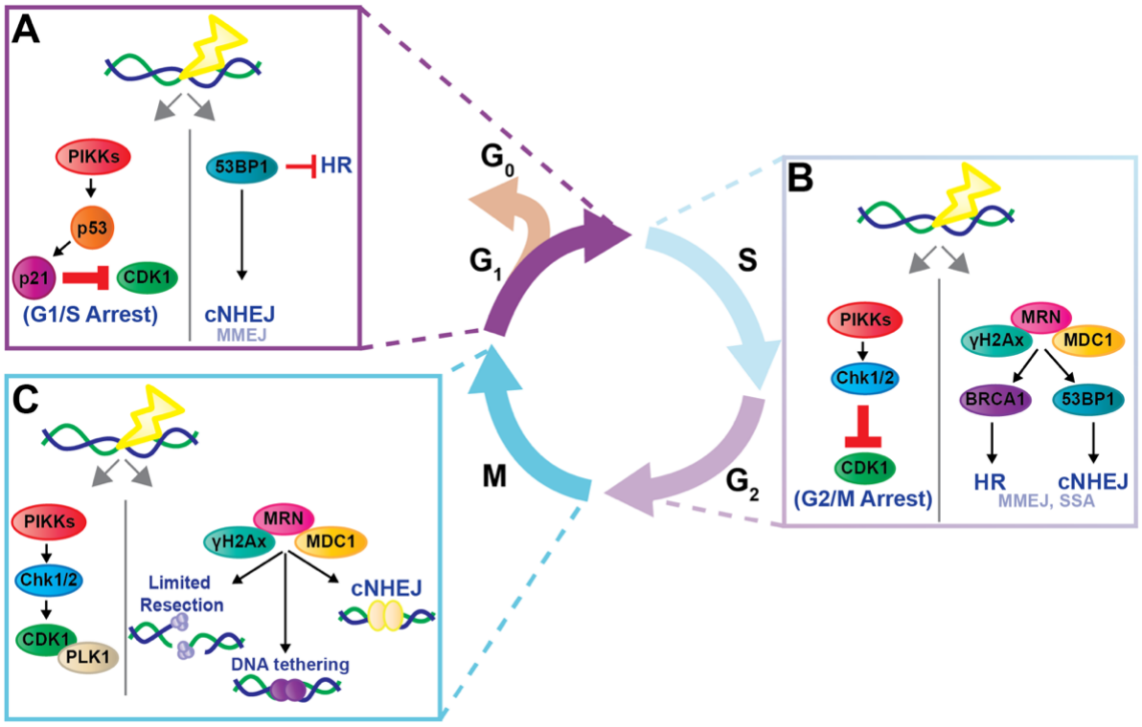

Figure 1: DDRs during the cell cycle.

(A) The DDR during the G_1-phase of the cell cycle. During G_1, cell cycle arrest is predominantly mediated through p53 signaling. cNHEJ is the DSB repair of choice, MMEJ is active in certain contexts and can compensate for cNHEJ loss. HR is activity inhibited. (B) The DDR during S-phase and G_2. Chk1/2 kinases mediate cell cycle arrest. HR is active and there is extensive resection allowing for SSA to also be active. (C) The mitotic DDR. Upstream DDR regulators are recruited after DSBs. Downstream events are less known. Resection is limited, but cNHEJ may occur in some contexts. DSBs can physically tether themselves during mitosis. (See text for details).

1.2 Cell cycle stage and DNA repair pathway choice

The DNA damage response is highly dependent on the cellular context, including the stage of the cell cycle. There are several lines of evidence of how cell cycle stage may dictate repair pathway choice including the availability of a homologous template, chromatin organization, and protein abundance during a particular cell cycle stage [20]. While SSBs constitute the majority of DNA damage and can be repaired throughout the cell cycle, DSB pathway choice is dictated by cell cycle progression [20, 21].

1.2.1 cNHEJ and HR pathway choice during the cell cycle

It had previously been hypothesized that during the G_1-phase of the cell cycle, cNHEJ predominated as the preferred DSB repair pathway. As a sister chromatid is generated during S-phase, it was speculated that HR was the pathway of choice from S-phase to G_2[22, 23]. In 2005, Mao *et. al.*, using the site-specific endonuclease, I-SceI to induce DSBs and fluorescent reporters of HR and cNHEJ repair, reported that in "normal" human cells (non-cancerous, checkpoint-intact), cNHEJ dominates throughout the cell cycle (Fig1A). HR predominates during S-phase and can also occur during G_2 as a sister chromatid is present (Fig1B). It was speculated that in organisms with highly repetitive genomes like humans, erroneous cNHEJ may be preferred [23]. Indeed, mammalian cells are much less sensitive to loss of HR machinery after DSBs compared

to *E.coli* [24, 25]. In other organisms, key machinery involved in major DSB repair pathways appear to be missing or have yet to be identified. This reflects a decrease in efficiency in cNHEJ some organisms, such as in *S. cerevisiae* and *S. pombe*, which lack DNA-PKcs. However, *Drosophila* and other insects also appear to lack DNA-PKcs, but cNHEJ is still efficient in this organism, suggesting evolutionarily divergent mechanisms may drive cNHEJ [5, 26].

Further work in mammalian cells provided evidence for cNHEJ as not only a predominant pathway throughout the cell cycle, but also the first pathway of choice after DSBs induced during G_1 and G_2 as cells defective in HR-components show little radiosensitivity during these stages [25]. Generally, HR plays an important role in repair of DSBs during DNA replication. During mammalian cell S-phase, both damage-inducing agents such as UV radiation and replication fork stalling and collapse can lead to single-ended DSBs. As repair of single-ended DSBs via cNHEJ could lead to deleterious chromosomal rearrangements, HR is the pathway of choice [25, 27]. Aside from single-ended DSBs, HR and cNHEJ can compete for repair of DSBs during S-phase [28]. HR efficiency during cell cycle stages is also regulated by cyclin-dependent kinase (CDK) activity. As CDKs are required for the phosphorylation of key end resection factors, HR is active when CDK activity is higher during S- and G_2-phases (Fig1B). [27, 29]. There is also evidence that within eukaryotes, organisms with larger genomes (and

thus more genome to replicate) such as mammalian cells, are more dependent on HR machinery during S-phase than *S. cerevisiae* or *S. pombe* [26].

1.2.2 Alt-EJ and SSA pathway choice during the cell cycle

While alt-EJ is often described as a "back-up" pathway to cNHEJ, emerging evidence is revealing important roles for this repair pathway in numerous contexts. As the limited end resection that occurs during alt-EJ repair can also serve as a template for cNHEJ, is it plausible that alt-EJ should be active throughout the cell cycle (Fig1A). [28]. In both zebrafish and mouse embryos as well as *C. elegans* germ cells, alt-EJ plays important roles. In zebrafish embryos, the *C. elegans* germline, and mouse zygotes, alt-EJ is the predominant pathway of choice throughout the cell cycle, likely due to decreased availability of key cNHEJ components [30].

As SSA requires extensive long-range resection, this repair pathway potentially occurs as a back-up pathway to HR during S/G_2 (Fig1B). Similar to the dependence on alt-EJ during early development in zebrafish, *C. elegans*, and mice, *Drosophila* germline cells during early development depend on SSA and eventually switch to cNHEJ repair. These findings are similar to what has been observed in yeast (*S. cerevisiae* and *S. pombe)*, *Arabidopsis*, chicken, and mammalian cells in which SSA is prevalent whenever SSA proteins are available and other DSB pathways are not. Taken together these findings support the notion the cell cycle stage, the regulation which can vary depending on

development stage, cell type, and organism type, heavily influence DSB repair pathway choice and competition.

1.2.3 The DDR during mitosis

Much of what is known about the DDR, including DNA repair, is in the context of interphase cells. It was previously believed that during mitosis, the DDR is shut down and DNA repair cannot occur. Recently, however, increasing evidence has shed light on how cells tolerate DNA damage present during mitosis. It is now understood that mitotic cells are capable of activating a rewired DDR [31]. Additionally, both repair protein recruitment and DNA repair synthesis have been observed to occur during mitosis (Fig1C). [32].

It is not surprising that DDR signaling and repair occurs during mitosis. Several factors involved in mediating the DDR are also important for mitotic progression. Increased Cdk1 activity, which is known to promote DNA resection, also promotes mitotic progression and has roles in regulating the spindle assembly checkpoint (SAC) with other mitotic kinases (Aurora-B and PLK1) [33]. Furthermore, Cdk1 and PLK-1 work to rewire the DDR during mitosis, blocking recruitment of downstream repair factors known to participate in HR and cNHEJ [34]. For the most part, upstream DDR signaling during mitosis is similar to what is observed during the G2/M checkpoint. PIKKs phosphorylate H2Ax, and phosphorylated H2Ax (γH2Ax) can then recruit the

DNA damage sensor MDC1. The MRN complex, which functions as a DNA damage sensor and endonuclease, is comprised of the conserved proteins Mre11, Rad50, and Nbs1, and is also recruited to DSBs present during mitosis [31, 34, 35]. However, beyond these upstream events, many further downstream DDR signals are not known to be active in mitosis [33, 34].

DNA damage present during mitosis poses a threat to genome integrity. Mitotic DNA damage can lead to mis-segregation of whole chromosomes or chromosome fragments [36]. This can lead to aneuploidy or micronuclei, a nuclear atypia implicated in cancer initiation and progression. Several groups, including ours, have proposed mechanisms of how cells prevent genome instability when DNA damage is present during mitosis. In human cells, broken chromosome fragments are tethered together through MDC1 binding to TopBP1, and DDR mediator protein [37]. In *Drosophila* neuroblasts, SAC proteins Polo, BubR1, and Bub3, also work to tether broken chromosomes that accumulate either after the G_2/M checkpoint or during mitosis itself [38]. More information on how DSBs are tethered during mitosis in other model organisms are covered in the Introduction section of Chapter 2.

Similar to DNA repair pathway choice during interphase DDRs, the context in which DNA damage arises during mitosis can dictate the DDR as well. Errors in DNA replication can occur at common fragile sites (CFS), which can lead to replication fork

collapse, leading to incomplete replication and repair intermediates during mitosis. DSBs that persist from DNA replication are capable of undergoing mitotic DNA synthesis, or MiDAS, during prophase [31, 32]. A recent study, however, identified that DSBs induced during mitosis were also capable of MiDAS. Contrary to evidence suggesting that downstream repair pathways are not active during mitosis, repair synthesis in this context depends on both NHEJ and HR machinery [39].

In addition to the influence of the cell cycle on differences in DDR signaling pathway, cell cycle arrest, and DNA repair, DNA damage itself can also influence cell cycles [40, 41]. Variations of the mitotic cell cycle are conserved across multiple organisms and can serve as protective mechanisms to DNA damage. The next section will focus on how DNA damage can result in cell cycle rewiring and how cell cycle variations also influence DDRs [42].

1.3 Polyploidy and the DNA damage response

Several forms of DNA damage have been observed to result in polyploidization – whole genome duplications [43-46]. In contrast, induced or naturally forming polyploid cells can also cause DNA damage [47, 48]. In this section I will summarize the literature related to DNA damage induced polyploidy, polyploid DNA damage responses, and how this relates to disease and cancer.

1.3.1 Polyploidy: whole genome duplications

Polyploidy is defined as having more than two copies of chromosomes and occurs commonly in nature. Polyploidy has been observed from single-celled protozoa, widely in plants, and in animals. In humans, polyploid cells are found in nine of eleven organ systems and are most widely studied in the placenta, liver, and heart, and skeletal muscle [49]. Despite the frequency of polyploidy, relatively little is known about polyploid biology compared to its diploid counterpart [48, 50-52]. Polyploidy can arise through various mechanisms as a naturally occurring process during organismal development or during times of stress such as after DNA damage or tissue wounding [48].

Polyploidy can occur via variations in the cell cycle. Endoreplication, the process in which a cell's genomic content is copied more than one time without the cell completely dividing, is a common mechanism of polyploidization. During the mitotic cell cycle, the cell undergoes G_1, S, G_2, and M phases. During endoreplication, cells either undergo cycles of G and S phases (endocycle) or the enter into mitosis without completing cell division (endomitosis). Endoreplication can result in mono- or multi-nucleate polyploid cells depending on whether nuclear division has occurred. Most endocycled cells generate polytene chromosomes, where chromosomes remain closely

associated following repeat S-phases. Cells can also become polyploid through cell-cell fusion, which can give rise to multi-nucleate cells [48, 53, 54].

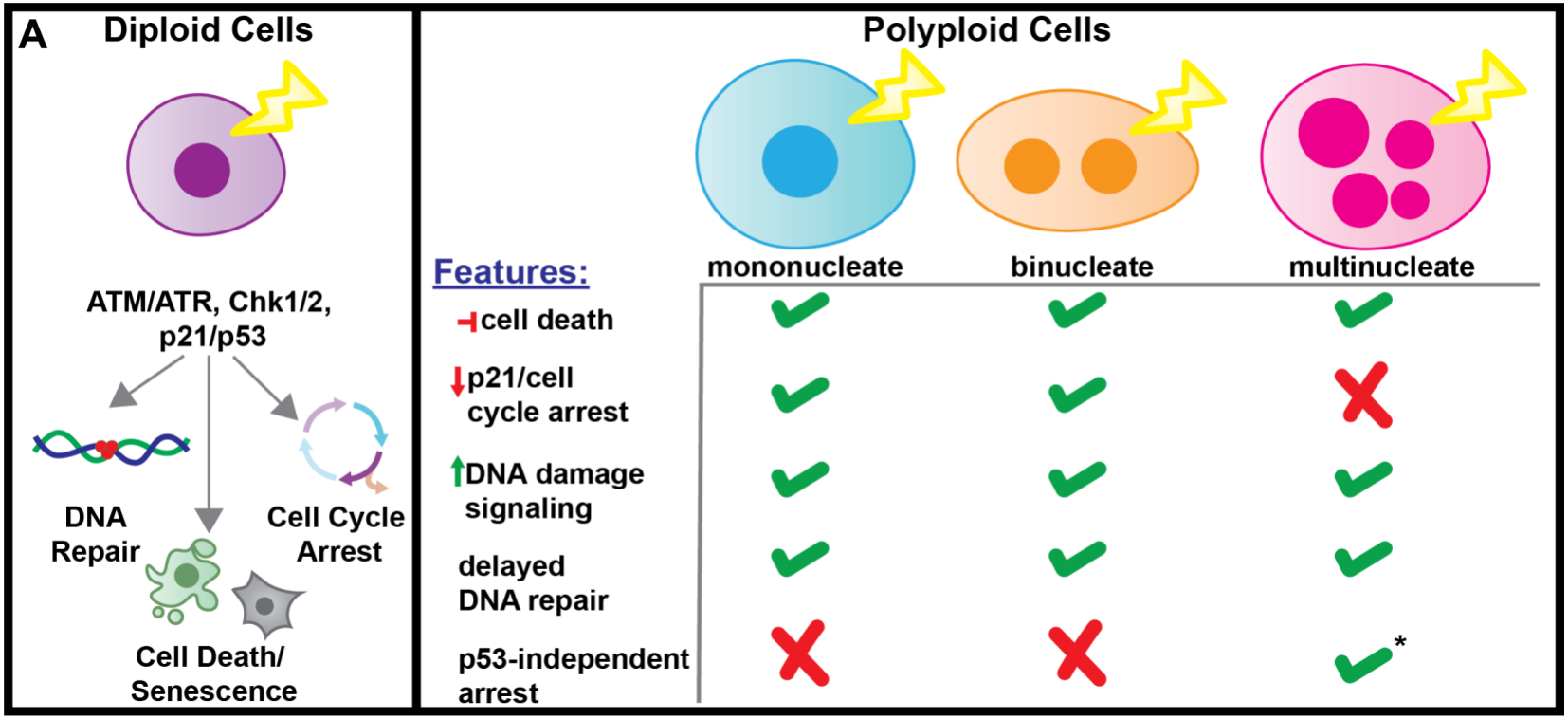

Figure 2: DNA damage responses of diploid versus polyploid cells.

(A) DDRs vary depending on cell ploidy. A majority of DDR mechanisms have primarily focused on diploid cells which use PIKKs to coordinate cell cycle arrest, DNA repair, and cell death or senescence if DNA damage is too severe. In contrast, polyploid cells typically suppress canonical DNA damage checkpoints, cell death and tolerate high levels of DNA damage, and upregulate repair proteins which persist on DNA breaks. *Multinucleate cells suppress p53-mediated checkpoints and can progress through DNA replication.

1.3.2 DNA damage induced polyploidy

Polyploidy can also be induced in response to various stressors such as DNA damage. Several species have evolved to respond to threats to genetic integrity through polyploidization. *Arabidopsis* root tips, sepal cells, and leaves undergo endoreplication after induction of DSBs [55, 56]. In both mouse embryonic fibroblast and human mammary epithelial cells, damage to telomeres results in an increase in ploidy through endoreplication as well [48, 57, 58].

Changes in ploidy in response to genome instability resulting from DNA damage also occurs in the context of human cancers. Cancer cells that are deficient in p53 bypass G_1/S phase checkpoints in response to DNA damage, which results in mitotic catastrophe [41]. As a response, surviving cells undergo endoreduplication to become polyploid and suppress apoptosis (Fig2A) [43]. DNA repair factors and cell cycle checkpoint regulators can block DNA damage-induced polyploidy and mitotic catastrophe [46]. Further, type 1 insulin-like growth factor was demonstrated to work with the DDR protein DNA-PK to block polyploidization and multinucleation associated with mitotic errors in both cancerous and noncancerous human cells [44].

Chitikova and colleagues demonstrated in apoptosis-resistant, transformed human cells that X-Ray IR-induced polyploidy is accompanied by delayed recruitment

of cNHEJ protein 53BP1, which was sustained for several days following IR (Fig2A). These cells also undergo a reversible senescence [59]. As resistance to chemotherapy and radiation therapy is a prominent barrier to cancer treatments, several studies have investigated the protective mechanisms cancer cells employ to promote survival such as polyploidization. Extended exposure to the chemosensitizing agent (resveratrol (trans-3,4′,5-trihydroxystilbene) or RSV, results in polyploid induction in colon cancer cells. These polyploid cells resist damage by RSV-associated reactive oxygen species (ROS)-through partial DDR activation and senescence [45].

1.3.3 Polyploid DNA damage responses

While several studies investigating the connection between polyploidy and the DDR have focused on DNA damage-induced polyploidy, primarily in the context of cancer treatment resistance, comparatively less is known about how polyploid cells regulate DDRs compared to diploid cells. Here, I summarize the literature on primarily naturally occurring, noncancerous polyploid cells and how these cells respond to DNA damage.

Mehrotra *et. al.* investigated the effects of re-replication induced DNA damage (caused by aberrant replication origin licensing) on both mitotic and endocycling *Drosophila* follicle cells. Endocycling cells specifically suppressed apoptosis in response

to the genotoxic stress (Fig2A). It was identified that suppression of apoptosis was mediated through downregulation of pro-apoptotic genes at the *H99* locus [60]. Later studies revealed that a p53 isoform, p53B was sufficient to induce apoptosis in endocycling cells as a stronger activator of the *H99* locus compared to the p53A isoform through regulation of RNA pol II at apoptotic gene promoters [61]. Further, it was demonstrated that the endocycling program was responsible for mediating apoptotic suppression, as ectopic induction of polyploidy through *fzr*/*Cdh1* is sufficient to suppress apoptosis in response to IR [62].

Naturally occurring endocycled cells do experience DNA damage in response to genotoxic insults as demonstrated by Mehrotra *et. al.* and other groups. Furthermore, endocycled cells also have the ability to recruit DNA repair proteins [47, 60, 63-65]. A source of genomic instability that can lead to DNA damage in polyploid cells is the process of under-replication during S-phase. There are several studies performed in *Drosophila* tissues that document under-replication (UR) in endocycling cells [64, 65]. Specifically, in *Drosophila* polytene salivary glands, the degree of under-replication can vary depending on the chromatin environment and is driven primarily by the expression of the SNF2 family protein *SuUR, suppressor of underreplication.* This

incomplete replication likely occurs due to the fact that endocycling cells lack checkpoints normally found in diploid mitotically cycling cells [66].

Andreyeva and colleagues identified that under-replicated regions lead to recruitment of γH2Av (*Drosophila* variant of γH2Ax). This recruitment correlates with *SuUR* activity, as an increase or decrease in levels results in an increase or decrease in γH2Av, respectively [65]. Yarosh and Spradling further expanded on these findings using high-throughput sequencing. They identified extensive chromosome alterations at UR regions, likely through erroneous end-joining of broken DNA ends in *Drosophila* salivary glands and ovaries [64]. *Drosophila* salivary polytene chromosomes also recruit Mu2/MDC1 which colocalize with γH2Av at sites of DSBs. Furthermore, despite polytene chromosomes possessing a rigid physical structure, there is local chromatin relaxation and Arp2/3-relocalization of DSBs – likely to prevent erroneous recombination [67]. Under-replication is not specific to polyploid *Drosophila* salivary glands. Trophoblast giant cells in the mouse placenta have been also found to contain under-replicated regions [68]. Future studies investigating if DSBs are a general feature of all polyploid cells that have under-replicated portions of their genome will useful.

As a consequence of inactivating checkpoints, it remained possible that DNA repair mechanisms in polyploid cells may also be divergent from diploid, cycling cells.

The archaeon, *H. volcanii*, which is a naturally polyploid organism, accumulates DSBs and depends on conserved proteins Mre11 and Rad50 to delay potentially deleterious HR following DNA damage (Fig2A). These organisms primarily depend on alt-EJ and in the absence of both Mre11 and Rad50, recovery from DNA damage is significantly delayed [63]. Similarly, *Deinococcus radiodurans*, a radiosensitive, polyploid bacterium, is dependent on Mre11 and Rad50 homologs to repair excessive gamma-radiation induced DSBs. Interestingly, polymerase X (PolX) was also shown to be important for DSB repair in this system, however the effects of Mre11/Rad50 and PolX deletion were additive, suggesting that back up pathways exists in *D. radiodurans* to repair excessive DSBs [69].

In *Drosophila* follicle cells, Alexander e*t. al.* investigated a role for the alt-EJ gene *polQ,* in DSB repair at chorion genes, which are a discrete re-replicated region of the follicle cell genome. They showed that in response to DSBs that arise from rereplication, alt-EJ, cNHEJ, and HR all compete for repair. The DSB pathway of choice is also dictated by genomic locus underscoring the importance of cellular context in DSB repair pathway choice [70].

Additionally, our group identified that *Drosophila* rectal papillar cells, which undergo developmental endocycles and enter a programmed mitotic cell cycle days after, also possess non-canonical DDRs. As reported in previous studies, endocycled

papillar cells lack checkpoint features and suppress p53-mediated apoptosis in response to DNA damage. These cells depend on FA pathway proteins, namely Fancd2 and FancI, for survival following DNA damage (Fig2A) [47]. This thesis will expand on further findings related to how endocycled papillar cells regulate the DDR and can be found in Chapter 2.

Lastly, there may be differences in how polyploid cells regulate the DDR based on whether they are mono- or multinucleate cells (Fig2A). An example of these differences in that with both mononucleate, non-cancerous and cancerous cells, DNA damage does not result in a p53-mediated cell cycle arrest [41, 47, 60]. However, it was identified that multinucleate, human retinal pigment epithelial cells can arrest their cell cycle in the interphase following the first division after DNA damage. This response is also independent of p53 (Fig2A) [71]. Interestingly, these multinucleate cells also displayed delayed repair kinetics, similar to polyploid cells that are mononucleate [63, 71]. As mononucleate cells result from endocycling which leads to under-replicated regions of the genome, it is also more likely that DSBs would arise in this context and not with multinucleate cells. In some cases, multinucleated polyploid cells can actually lead to increased sensitivity to DNA damage. In *Drosophila* spermatogonia cysts, which are multinucleate cells, amplified DDRs via fusomes, allow coordination of cell death

across the entire cyst even when only a subset of nuclei contain DNA damage [72]. Taken together, these studies emphasize the importance of how polyploidy arises in influencing polyploid DDRs.

1.3.4 Polyploidy, DNA damage, and disease

Several studies thus far have made the connection that polyploidy results in genome instability, and that genome instability can also result in polyploidy. This reciprocal relationship has been explored in the context of understanding how polyploidy and DDRs can be investigated to identify cancer biology and reveal potential therapeutic applications.

Polyploidy and aneuploidy, defined as having an abnormal number of chromosomes based on the wild-type set, are both found frequently in cancer. Whole genome duplications were found to occur in 37% of all cancers [40, 73]. Aneuploidy can arise through erroneous polyploid mitosis in which whole or partial chromosomes are gained and lost through a variety of mechanisms detailed in Davoli and Lange, 2011 [40].

Mechanisms of polyploid DDRs in the context of cancer may not be so different than in naturally occurring polyploid cells. *In vivo* mouse models created from mouse embryonic fibroblast (MEFs) carrying mutations in the *FEN1* gene, which leads to

accumulation of SSB and DSBs, results in the formation of two distinct populations of cancer cells, one being mostly polyploid/aneuploid with increased proliferation and the other mostly diploid with decreased proliferation. The aneuploid cells show decreased expression of checkpoint proteins pATM/pChk1 compared to their diploid counterparts (Fig2A). Furthermore, these cells upregulate BRCA1 to repair SSBs and NHEJ machinery to repair DSBs, the latter of which leads to chromosomal rearrangements (Fig2A). An absence of a cell cycle arrest in this model suggests that polyploid cancer cells can uncouple DNA damage checkpoints from DNA repair. Suppression of apoptosis and senescence is also observed in these cells, mediated through regulation of *p21* (Fig2A). These DDR rewired polyploid cells are capable of promoting cancer progression *in vivo* [42].

Taken together these studies highlight the significance of understanding the context in which polyploidy can arise during cancer to understand how polyploid biology can be interpreted to identify cancer treatments [74].

1.4 Conclusion

In summary, organisms have evolved DDRs to preserve the integrity of genetic material. The conditions in which cells must employ DDRs will dictate repair pathway choice, cell cycle progression, and other related cellular processes. Here, I have

highlighted that cell cycle stage is critical to selecting which DNA repair pathway is most appropriate to avoid potentially deleterious consequences and genomic instability. Further, DNA damage can induce cell cycle alterations leading to changes in cell ploidy, which can also alter DNA damage responses. Increases in genome content are associated with DDR rewiring and can be used to buffer against effects of excessive DNA damage to avoid mitotic catastrophe and cell death. As polyploidy is common in various cancers, understanding the conditions in which polyploid cells overcome barriers to proliferation is paramount to developing stronger cancer therapies.

The remainder of this thesis will focus on polyploid DDRs in the context of cell cycle stage and DNA repair pathway choice. Chapter 2 contains published findings related to mitotic DNA damage responses in *Drosophila* rectal papillar cells. Chapter 3 will contain unpublished findings expanding on repair pathways identified to be important for polyploid cell survival following DSBs. Additionally, we have identified what is likely a separate pathway required for cell survival following DSBs that involves changes in chromatin organization. Finally, in Chapter 4, I will discuss what our findings thus far signify for understanding factors involved in DDRs in different contexts (i.e. cell cycle stage, extra DNA copies), what future directions should be

explored to address existing gaps in knowledge, and the significance of this work in understanding both basic cell biology and translational applications.

2. Persistent DNA Damage Signaling and DNA Polymerase Theta Promote Broken Chromosome Segregation

The following chapter includes published work from my first author paper, "Persistent DNA Damage Signaling and DNA Polymerase Theta Promote Broken Chromosome Segregation," in the Journal of Cell Biology. In this study, we show that cells with DNA breaks that persist into mitosis activate sustained DNA damage signaling, regulated by Fanconi Anemia proteins and the alternative end-joining repair protein DNA Polymerase Theta. This signaling enables broken chromosome segregation and prevents micronuclei. The majority of the work in this chapter was performed by me, with the following exceptions. Heidi Bretscher, PhD laid the foundational work for this study in her 2016 publication [47]. This work helped to establish the assays discussed in Fig3A-B, Fig 10A, and Fig11A. Additionally, H. Bretscher performed the experiments in Fig10B-C, Fig12A, Fig13A, and Fig14C. Erin Jezuit, MS performed the experiments and contributed to the data analysis in Fig7A-D, Fig8A-C',F and Fig9C-D, G. Korie Bush, PhD candidate, performed half the screen in Table 2 (Pre-Endocycle Phenotype) in collaboration with H. Bretscher. Lastly, Don Fox, PhD collaborated with me on the manuscript and figures.

2.1 Summary

Cycling cells must respond to DNA double-strand breaks (DSBs) to avoid genome instability. Mis-segregation of chromosomes with DSBs during mitosis results in micronuclei, aberrant structures linked to disease. How cells respond to DSBs during mitosis is incompletely understood. We previously showed that Drosophila papillar cells lack DSB checkpoints (as observed in many cancer cells). Here, we show that papillar cells still recruit early-acting repair machinery (Mre11 and RPA3) and the Fanconi Anemia (FA) protein Fancd2 to DSBs. These proteins persist as foci on DSBs as cells enter mitosis. Repair foci are resolved in a step-wise manner during mitosis. DSB repair kinetics depends on both monoubiquitination of Fancd2 and the alternative end-joining protein DNA Polymerase Theta. Disruption of either or both of these factors causes micronuclei after DNA damage, which disrupts intestinal organogenesis. This study

2.2 Introduction

Cells are constantly at risk for DNA damage from internal and external factors [9], and respond to such damage to maintain genome stability [2, 72]. DNA lesions trigger DNA damage response (DDR) checkpoints that result in cell cycle arrest, DNA repair, or apoptosis [4, 73]. DDR checkpoints primarily act in interphase but allow for

faithful chromosome segregation when damaged cells enter mitosis [3, 5]. If cell cycle checkpoints are inactivated or dysregulated, damaged DNA can persist into mitosis [14, 74]. One of the more problematic forms of persistent DNA damage for the mitotic cell are double-strand breaks (DSBs), which can lead to mis-segregation and subsequent loss of portions of the genome [75, 76]. DSBs generate acentric DNA, a DNA fragment that lacks canonical kinetochore-spindle attachments and is at risk of mis-segregating in mitosis which can lead to micronuclei, aberrant nuclear structures with a poorly-formed nuclear envelope [45, 77, 78].

However, acentric DNA can segregate properly in several organisms including yeast, Drosophila, and human cells [79]. In S. pombe, acentric DNA can segregate in mitosis by forming a neocentromere and by noncanonical DNA repair [80, 81]. In C. elegans, acentric meiotic chromosomes are thought to segregate by poleward microtubule-generated forces [82]. In Drosophila brain progenitors, acentric DNA can segregate poleward in mitosis using various mechanisms involving protein-based tethers, microtubule forces, nuclear envelope reformation and fusion, as well as the recruitment of early-acting repair proteins [36, 83-87]. Therefore, there are several proposed mechanisms for how acentric DNA properly segregates in mitosis under distinct conditions.

Despite the multiple mechanisms of acentric DNA segregation, questions still remain surrounding possible physical connections that might link the acentric fragment to segregating, centromeric DNA. More specifically, DNA damage signaling could potentially regulate such a linkage, or influence segregation of acentric DNA. We established Drosophila hindgut rectal papillar cells (hereafter: papillar cells) as an accessible model to understand cellular responses to damaged, acentric DNA that is present in mitosis [45]. We previously found that papillar cells inactivate DSB checkpoint responses at a specific developmental time point. At the second larval instar stage (L2), papillar cells undergo two rounds of endocycling [46, 88], where they replicate genome content without cell division (Fig3A, L2). During this stage, papillar cells do not arrest the cell cycle or undergo apoptosis in response to high levels of DNA damage (20 Gy X-ray Irradiation, IR), as in other endocycling cells [58, 60, 89]. Papillar cells do not respond to changes in p53 expression nor do they depend on the checkpoint kinases Chk1 and Chk2 following DNA damage [45]. Despite inactivating canonical DSB responses, several (5-6) days later during the early pupation stage, papillar cells leave a G_2-like state and enter a mitotic cell cycle (Fig3A, Early pupal, [52, 69, 70], As a consequence, papillar cells frequently enter mitosis with acentric DNA fragments (~12% of divisions; [45]. Despite papillar cell acentric DNA lacking obvious physical

connections, these fragments lag but ultimately segregate into daughter nuclei (Fig3A, mitotic). We identified that papillar cell acentric DNA segregation requires proteins from the Fanconi Anemia (FA) pathway, Fancd2 and FancI [45].

In this current study, we further investigate the mechanism of acentric DNA segregation to better understand the possible linkage of acentric fragments to centromeric DNA during mitosis. We find that despite lacking a canonical DDR, papillar cells recruit early-acting repair proteins from the MRN (Mre11) and RPA (RPA3) complexes as well as Fancd2 to DSBs. These proteins persist on damaged papillar chromosomes for days (5-6 days) following DSBs and remain present as these cells enter mitosis. During mitosis, repair protein kinetics are distinct, with Mre11 and Fancd2 leaving the DNA prior to RPA3. Further, we find that the alternative end-joining (alt-EJ) repair protein DNA Polymerase Theta (hereafter Pol Theta, encoded by the *polQ* gene), but not homologous recombination (HR) nor canonical homologous end-joining (cNEHJ), is required for RPA3 removal during mitosis, for acentric DNA segregation, and for micronuclei prevention. Finally, we show that *polQ* RNAi is epistatic to mutants lacking the conserved monoubiquitination site of Fancd2. The action of Mre11, Pol Theta, and monoubiquitinated Fancd2 are critical for intestinal organogenesis following DSBs. Our findings highlight a role for persistent DNA repair signaling, regulated by a

conserved alternative end-joining protein and monoubiquitinated Fancd2, on acentric DNA.

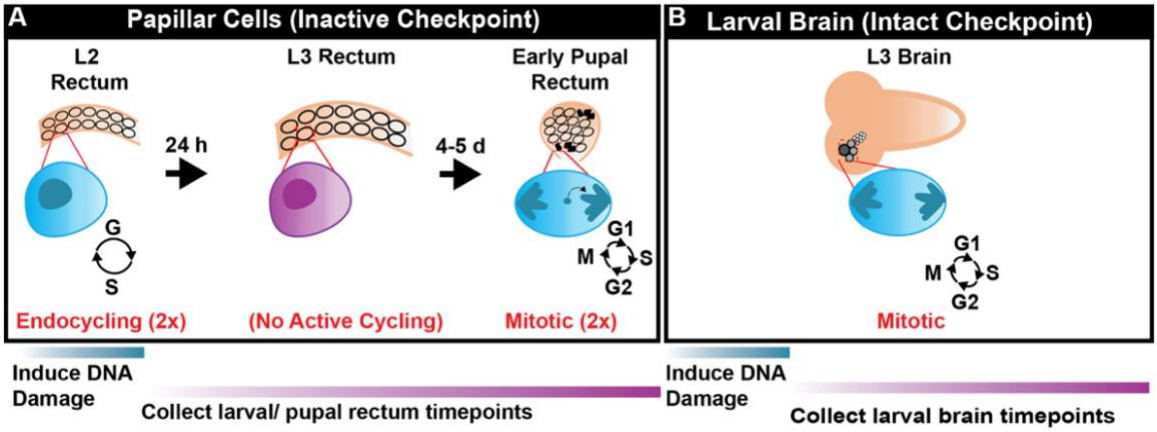

Figure 3: Drosophila rectal papillar cells and larval brain progenitors as a model to study inactive versus intact checkpoints.

(A) Schematic of the developing *Drosophila* rectum from the second larval instar (L2) stage to early pupation. (B) Schematic of the feeding third larval instar (L3) brain. Dark gray circles= neuroblasts, gray circles= ganglion mother cells, white circles= neurons. (See Results).

2.3 Results

2.3.1 Mre11 and RPA3 are recruited to damaged papillar chromosomes but are not resolved prior to mitosis

Although papillar cells lack apoptotic and cell cycle arrest responses to DNA damage, it remained possible that these cells activate DNA repair responses to segregate acentric DNA. To visualize DNA repair signaling dynamics, we investigated the

temporal recruitment of early-acting DNA damage repair proteins following DSBs. The highly conserved MRN (Mre11, Rad50, Nbs) complex is recruited immediately to DSBs and initiates downstream repair events [75-77]. We assayed localization of Mre11 over time using animals expressing ubi-*mre11-GFP* [38]. Using an established method to induce DSBs, we used the endonuclease, *hs-I-Cre*I, which creates DSBs in the rDNA of the Drosophila sex chromosomes, to increase the frequency of papillar cells with acentric DNA from 12% to up 90% [47, 78, 79].

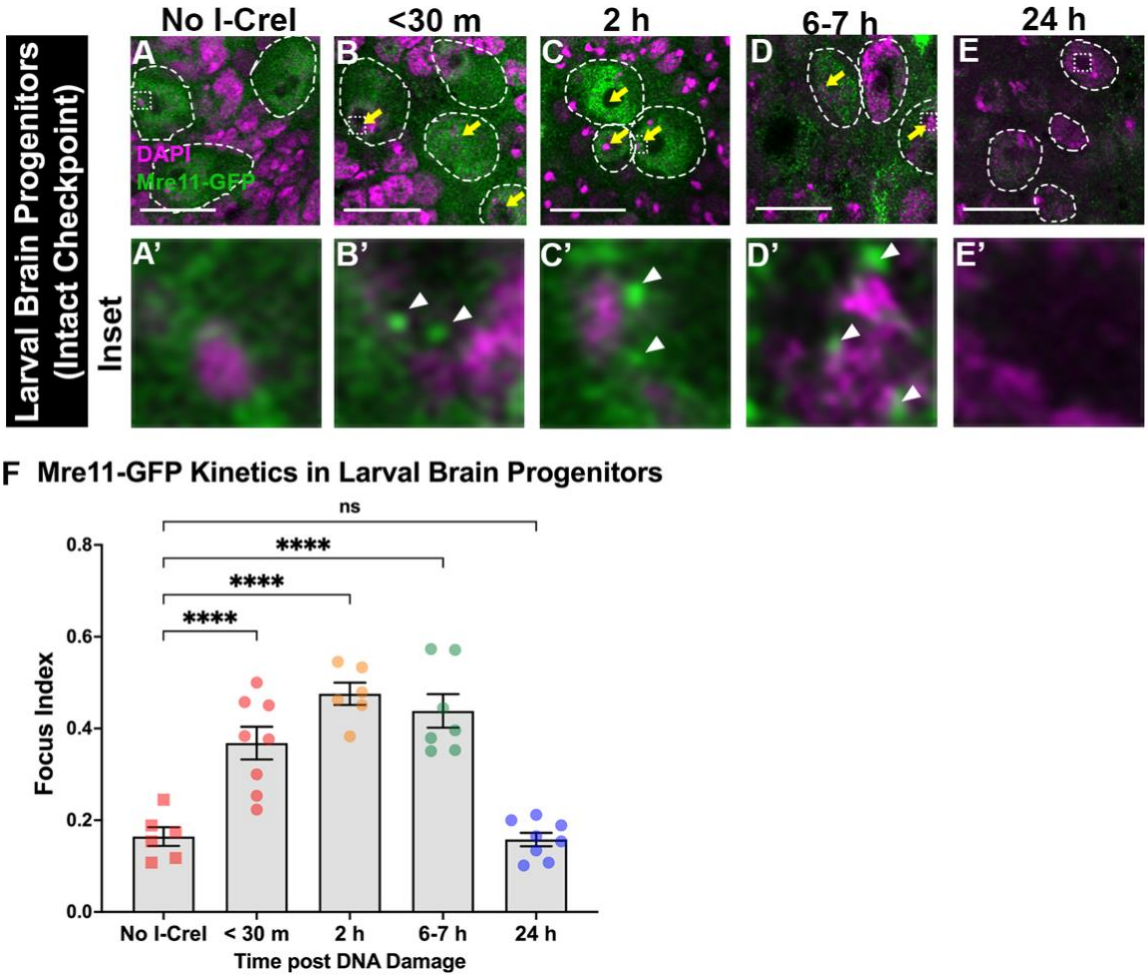

Figure 4: Mre11 is recruited to checkpoint intact *Drosophila* larval brain progenitors.

(A-E') Mre11-GFP localization over time +/- hs-I-CreI in larval brain progenitors. Time after break induction is indicated in minutes (m) or hours (h). Mre11, green; DNA (DAPI), magenta. Yellow arrows= Mre11+ foci. Hatched outlines= Nuclei. Hatched box= area magnified 10X in the corresponding inset below each panel. White arrowheads= enlarged foci. Scale bars= 10μm. (F) Quantification of Mre11+ foci kinetics in larval brain progenitors. Focus index is the frequency of cells with at least one focus. Each timepoint represents at least two biological replicates. Each data point represents a single animal (N). Statistical test: Ordinary one-way ANOVA, $p<0.0001$. See Methods for statistical notations.

As a control for mitotic cycling cells with an intact DSB response, we examined third larval instar (L3) stage brain progenitor cells (neuroblast and ganglion mother cells, Fig3B, [80-82]. In brain progenitors, Mre11+ foci are recruited shortly (<30 minutes, m) after *hs-I-Cre*I DSB induction (Fig4A, A' vs. B,B', F). These foci are mostly resolved 24 hours (h) after DNA damage, suggesting that repair is complete within this timeframe (Fig4B-E',F). Consistent with this idea, 24 h after DNA damage, we observe mitotic neural progenitors, suggesting that these cells begin to exit cell cycle arrest (not shown). Similar to our findings in brains, checkpoint-inactive papillar cells recruit Mre11+ foci <30 m after inducing DSBs (Fig5A, A' vs. B, B', F). However, these foci persist for much longer than in larval brain progenitors (Fig4B-E,F). During early pupation, several days after we induce DSBs, Mre11+ foci still persist on damaged papillar chromosomes. The long time-frame of Mre11 persistence corresponds with the 5-6 day (d) period between papillar cell endocycles and the first mitosis, which occurs 24 h after pupation onset (Fig3A, [47]). Thus, although an MRN component is promptly recruited to checkpoint-inactive papillar cells shortly after a DSB, this protein persists on broken DNA into mitosis.

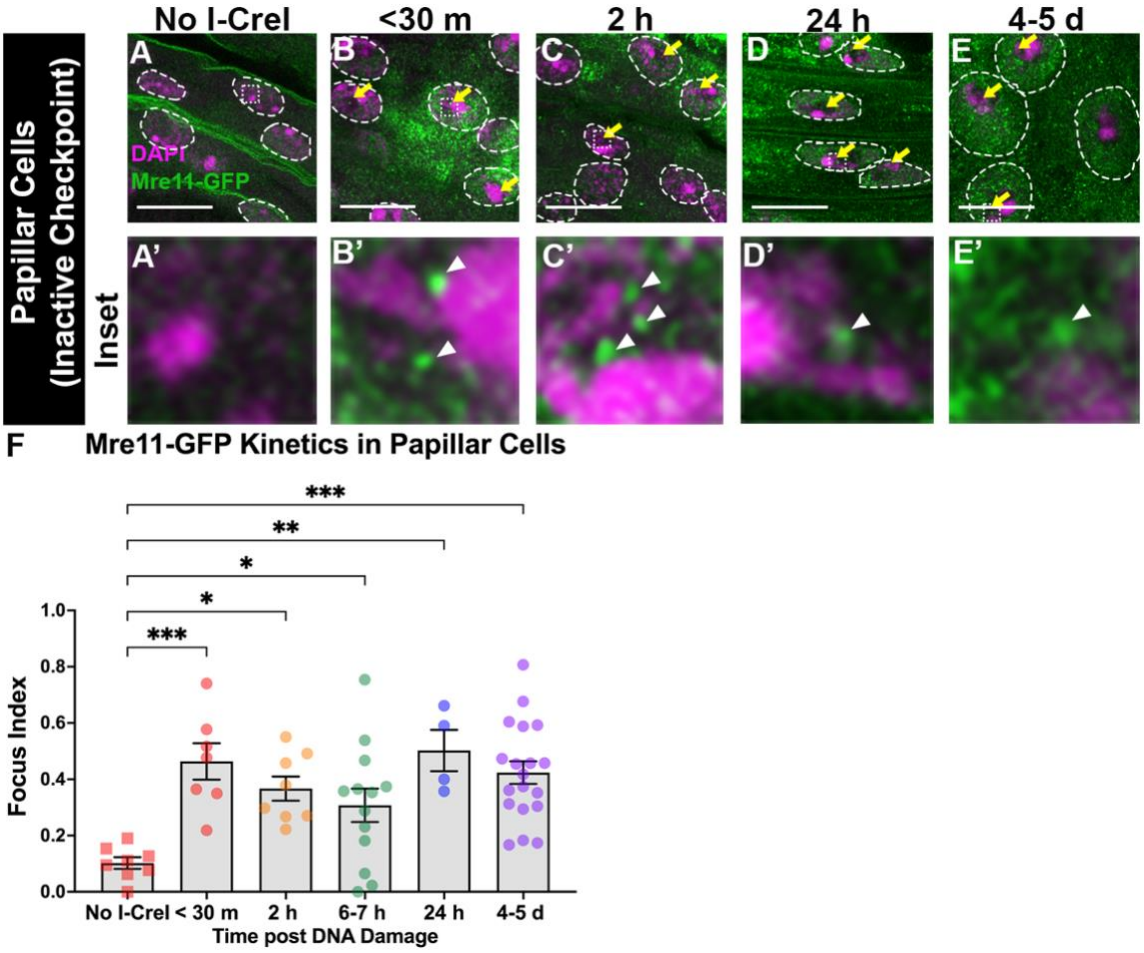

Figure 5: Mre11 is recruited to checkpoint inactivated papillar cells and persists for days.

(A-E′) Mre11-GFP localization over time in papillar cells +/- *hs-I-Cre*I. Labeling as in Fig4A-E′. (F) Quantification of Mre11+ foci kinetics in papillar cells. Each timepoint represents at least two biological replicates. Each data point represents a single animal (N). Statistical test: Ordinary one-way ANOVA, p=0.0002. See Methods for statistical notations.

We next investigated if Mre11 recruitment coincides with and recruits other markers of DSB repair. Mre11+ foci in both brain and papillar cells colocalizes with

gH2Av, a hallmark of DSB signaling (Fig6A-B'; 6C-D'). Mre11 and gH2Av do not always co-localize (Fig6E). Similar Mre11 kinetics have been observed in other studies and likely reflects dynamic repair signaling over time [83, 84]. MRN binds to either side of a DSB, then recruits downstream repair factors of different DSB repair pathways. MRN can also initiate DNA resection, in which 5' DNA ends are processed leaving 3' single-strand DNA overhangs. These 3' overhangs are coated by the heterotrimeric complex RPA, which prevents annealing of single-strand DNA [76, 77].

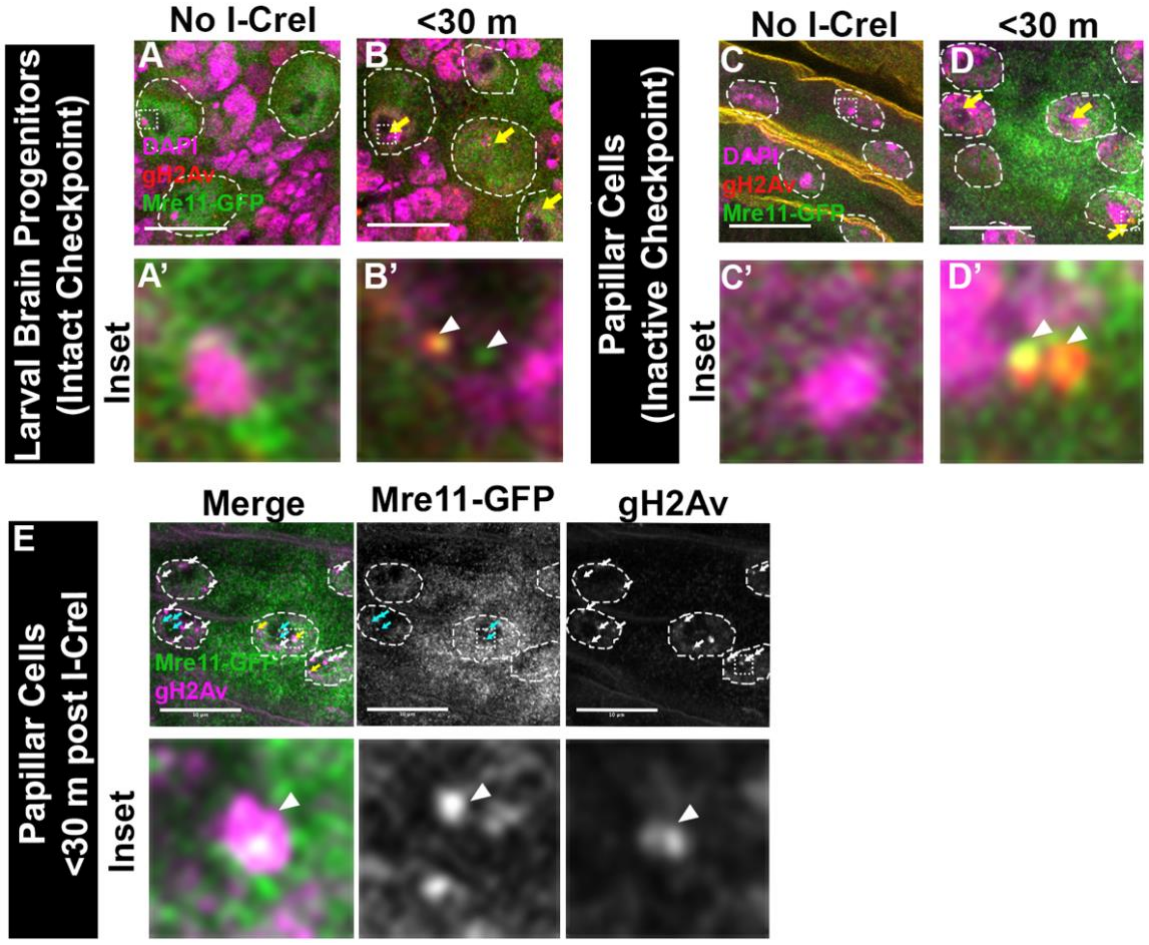

Figure 6: Mre11 colocalizes with gH2Av in larval brain progenitors and papillar cells after DSBs.

(A-B') Mre11-GFP co-localization with gH2Av in larval brain progenitors less than 30 m after +/- *hs-I-Cre*I. Time after break induction is indicated in minutes (m). Mre11+ foci are marked with yellow arrows. Nuclei are demarcated with white hatched outline. The hatched box highlights an area magnified 10X in the corresponding inset below each panel. Enlarged foci are marked with white arrowheads. (C-D') Mre11-GFP co-localization with gH2Av, in papillar cells less than 30 m after +/- *hs-I-Cre*I . Labeling as in A-B'. (E) Mre11+gH2Av+ (yellow arrows), Mre11+ (cyan arrows), and gH2Av+ (white arrows) foci in papillar cells less than 30 m after +*hs-I-Cre*I. Labeling as in A-B' except for the following: Mre11, green; gH2Av, magenta.

To determine if MRN recruits RPA in papillar cells after DNA damage, we used animals expressing ubi-*RPA3-GFP* [85]. Similar to Mre11, RPA3+ foci are present <30 m after *hs-I-Cre*I-induced DSBs in larval brain progenitors (Fig7A, A' vs. B,B',D). These foci are resolved 24 h after DNA damage (Fig7C, C', D). RPA3+ foci also appear in papillar cells <90 m after *hs-I-Cre*I-induced DSBs (Fig8A, A' vs. B, B', F). However, unlike in neural progenitors, RPA3 foci are not resolved by 24 h (Fig8C, C', F) and persist 4-5 d after DNA damage (Fig8D, D', F) similar to Mre11. Persistent RPA3 is not due to GFP tagging RPA3, as we observe similar persistent foci with an RPA antibody (Fig8G). Further, persistent RPA foci colocalize with gH2AV, indicating that foci represent sites of DSB signaling (Fig8G). We then determined if Mre11 recruits RPA3 to papillar DSBs. We examined *ubi-RPA3-GFP* in animals expressing UAS-*mre11* RNAi, which was expressed by the pan-hindgut driver *byn*>GAL4 [86]. RPA3+ foci are significantly decreased in *mre11* RNAi papillar cells (Fig8E, E', F). These data suggest that RPA3 is recruited to papillar chromosomes in an Mre11-depedendent manner in response to DSBs.

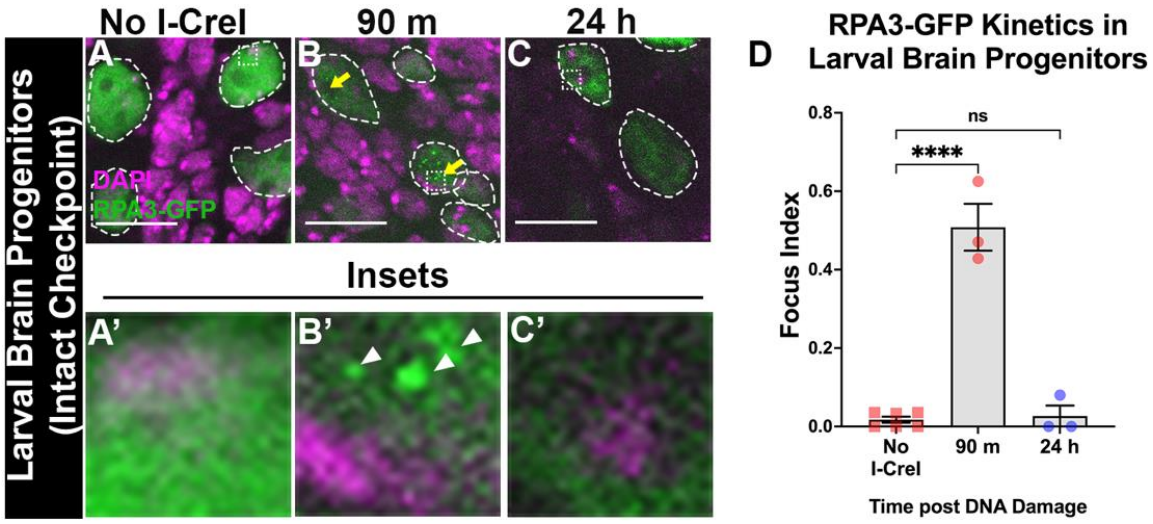

Figure 7: RPA3 is recruited to checkpoint intact *Drosophila* larval brain progenitors.

(A-C') RPA3-GFP localization over time +/- *hs-I-Cre*I in larval brain progenitors. Time after break induction is indicated in minutes (m) or hours (h). RPA3, green; DNA (DAPI), magenta. Yellow arrows= RPA3+ foci. Hatched outlines= Nuclei. Hatched box= area magnified 10X in the corresponding inset below each panel. White arrowheads= enlarged foci. Scale bars= 10μm. (D) Quantification of RPA3+ foci kinetics in larval brain progenitors. Each timepoint represents at least two biological replicates. Each data point represents a single animal (N). Statistical test: Ordinary one-way ANOVA, $p<0.0001$

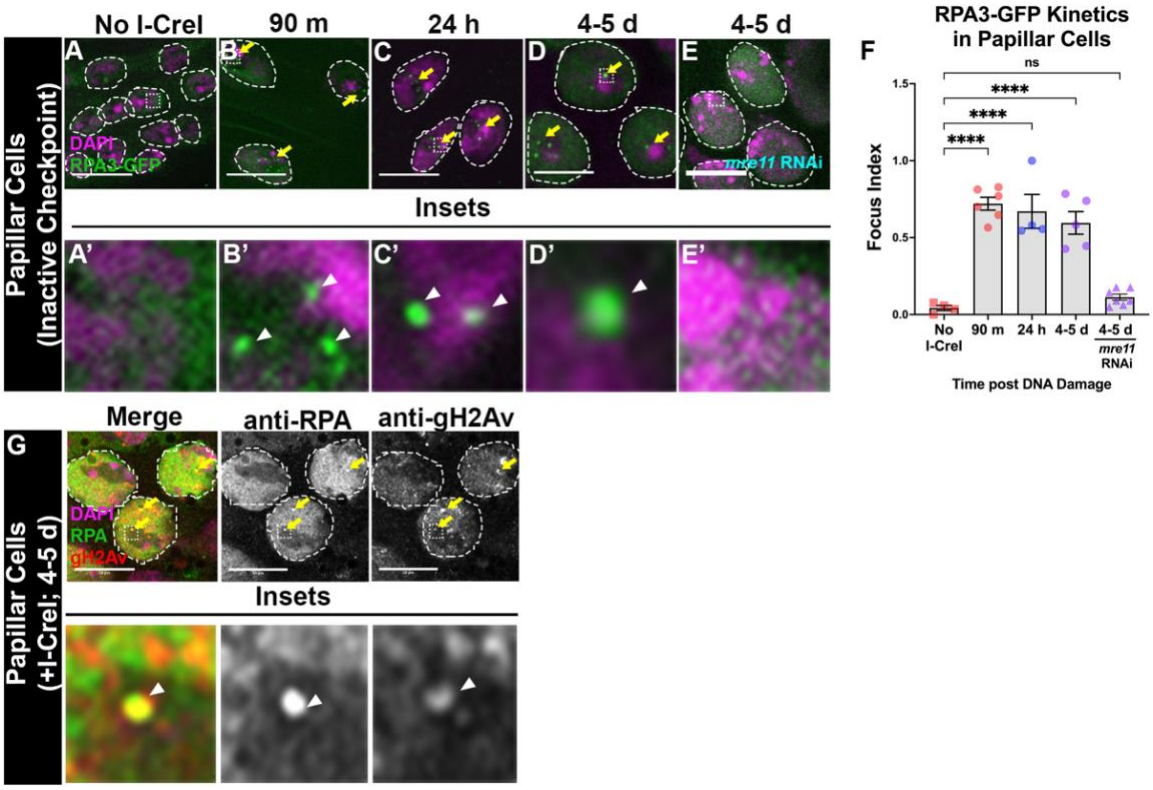

Figure 8: RPA3 is recruited to checkpoint inactive papillar cells and persists for days.

(A-E') RPA3-GFP localization over time in WT papillar cells (A-D') and *mre11* RNAi papillar cells (E,E') +/- *hs-I-Cre*I. Labeling as in Fig7A-C'. (F) Quantification of RPA3+ foci kinetics in papillar cells. Each timepoint represents at least two biological replicates. Each data point represents a single animal (N). Statistical test: Ordinary one-way ANOVA, $p<0.0001$. See Methods for statistical notations. (G) RPA+gH2Av+ foci recruitment to papillar cells 4-5 days after *hs-I-Cre*I. RPA, green; DNA (DAPI), magenta; gH2Av, red. Yellow arrows=RPA+gH2Av+ foci, Hatched outline= Nuclei. Hatched box= area magnified 10X in the corresponding inset below each panel. White arrowheads= enlarged foci.

Using other DSB strategies, we confirmed that RPA3 recruitment and persistence in papillar cells is not specific to *hs-I-Cre*I-induced DSBs in rDNA. Using IR (20 Gy) to

induce randomly located DSBs, persistent Mre11 and RPA3+ foci form on papillar cell DNA, compared to quickly resolved foci in larval brain progenitors (9A-D). *I-Cre*I targets repetitive heterochromatin and DSB responses can vary based on chromatin state [67, 78, 87]. We therefore tested if a single break in a defined euchromatic locus also recruits persistent RPA3 in papillar cells. We used CRISPR-Cas9 to generate DSBs at the *rosy (ry)* locus [88]. Using this method, we find that RPA3+ foci persist in papillar cells (Fig9E-F), similar to our results with *hs-I-Cre*I. Foci recruitment occurs both in the DAPI-bright heterochromatin and other nuclear sites (Fig9G). Overall, our results are consistent with immediate recruitment of Mre11, which recruits RPA3, after DSBs in papillar cells. Unlike checkpoint-intact neural progenitors, these repair markers persist on damaged DNA during a long interphase and continue into mitosis.

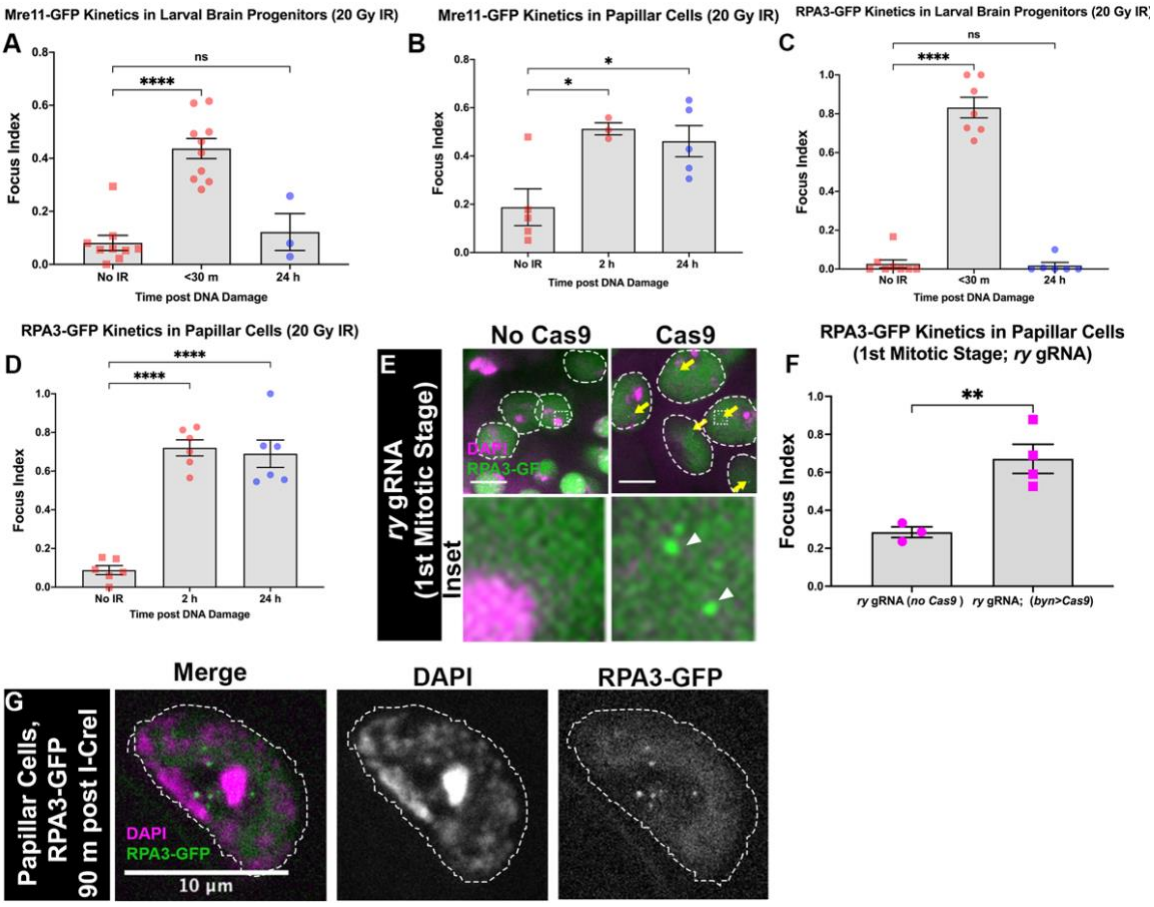

Figure 9: Mre11 and RPA3 is recruited to papillar cells with delayed kinetics after IR-induced DSBs.

(A) Mre11-GFP localization over time in larval brain progenitors +/- IR. Statistical test: Ordinary one-way ANOVA, p<0.0001. (B) Mre11-GFP localization over time in papillar cells +/- IR. Statistical test: Ordinary one-way ANOVA, p=0.0147. (C) RPA3-GFP localization over time in larval brain progenitors +/- IR. Statistical test: Ordinary one-way ANOVA, p<0.0001. (D) RPA3-GFP localization over time in papillar cells +/- IR. Statistical test: Ordinary one-way ANOVA, p<0.0001. (E) RPA3 recruitment to papillar cells +/- Cas9-induced DSBs using *ry* gRNA. RPA3+ foci are marked with yellow arrows. Nuclei are demarcated with white hatched outline. The hatched box highlights an area magnified 10X in the corresponding inset below each panel. Enlarged foci are marked with white arrowheads. (F) Quantification of RPA3-GFP foci recruitment in papillar cells +/- Cas9-induced DSBs using *ry* gRNA during the 1st mitotic stage.). Ordinary one-way ANOVA, p =0.0092. (A-D, F) Each condition has at least 2 biological replicates. Each data point represents a

single animal (N). See Methods for statistical notations. (G) RPA3-GFP recruitment to +*hs-I-Cre*I papillar cells after 90 m. Cells are enlarged and the channels are split to show recruitment of RPA3+ foci to DNA. DAPI (DNA), magenta; RPA3, green.

2.3.2 Mre11 is required for acentric DNA segregation and cell survival following DNA damage

To determine the function of persistent Mre11 following DSBs in papillar cells, we induced *hs-I-Cre*I during the L2 stage, when papillar cells are endocycling and suppressing canonical DNA damage checkpoints (Fig10A). Then, using *byn>GAL4* we expressed *UAS-mre11* RNAi in the fly hindgut (Fig10A). Following two rounds of mitoses during pupal development, four papillar structures made up of ~100 cells each are present in the adult animal [89, 90]. We previously found that *fancd2 RNAi* decreases adult papillar cell number after DSB induction, following failure to segregate acentric DNA. In contrast, no cell number reduction occurs in *p53* null mutants or in *chk1, chk2* double mutants [47]. Similar to our previous findings with *fancd2 RNAi*, *mre11 RNAi* adult animals contain a significantly reduced number of adult papillar cells and have aberrantly shaped papillae following *hs-I-Cre*I (Fig10B,C).

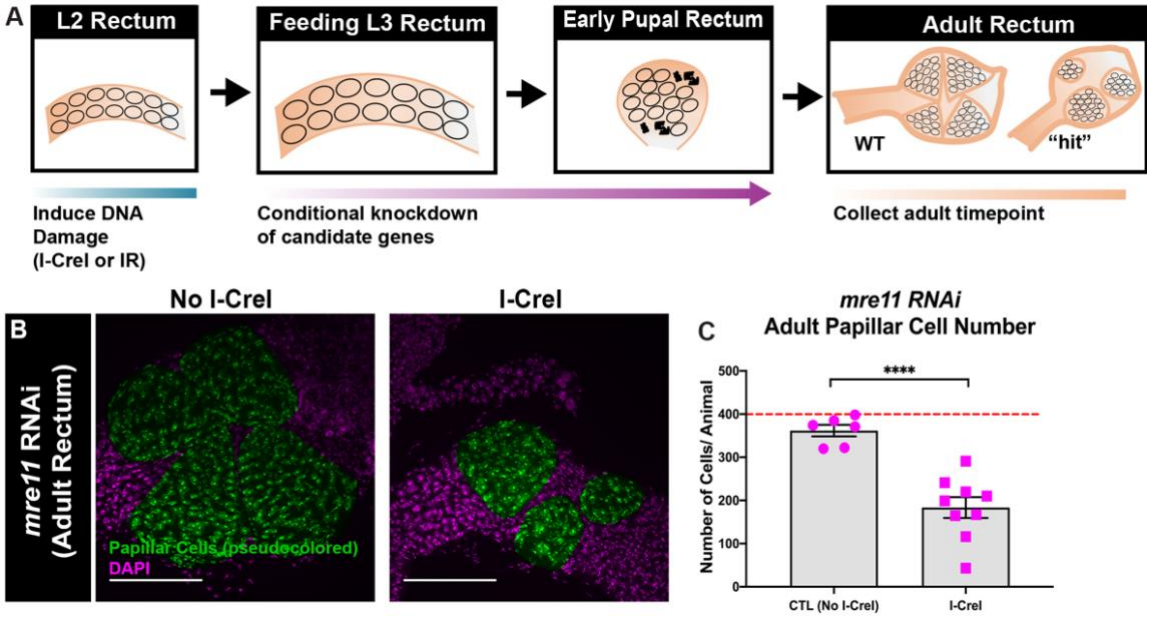

Figure 10: Mre11 is required for adult papillar cell survival following DSBs.

(A) Adult candidate screen assay for identifying regulators of acentric DNA segregation based on (Bretscher and Fox, 2016) (See Results) . (B) Adult rectums of *mre11* RNAi animals +/- *hs-I-Cre*I. Papillar cells (pseudo-colored), green; DNA (DAPI), magenta. Scale bars = 50μm (C) Quantification of adult papillar cell number in *mre11* RNAi expressing animals +/- *hs-I-Cre*I-induced DNA damage. Red dashed line= expected number of papillar cells in a WT adult. Each condition has at least 2 biological replicates. Each data point represents a single animal (N). Statistical test: Unpaired t-test, $p<0.0001$.

Using fixed and *in vivo* live imaging, we followed the fate of acentric DNA in the first mitosis following DSBs (Fig11A), using H2Av-GFP to label DNA and CenpC-Tomato to mark centromeres/kinetochores. Previously, we found that failed acentric DNA segregation in papillar cells leads to acentric micronuclei, as occurs in *fancd2 RNAi* animals [47]. Similarly, *mre11* RNAi results in an inability to properly segregate acentric

DNA during papillar cell mitosis, leading to an increase in acentric micronuclei (Fig11B-C). We note that, in addition to accumulating acentric micronuclei, *mre11* RNAi also increases anaphase bridges between centromere-containing chromosomes in both *hs-I-Cre*I (Fig11B, arrowheads) and no *hs-I-Cre*I animals (data not shown). This is likely due to the Mre11 function in telomere maintenance [76]. To focus on acentric DNA, we only counted micronuclei that lacked a Cenp-C signal, as acentric fragments do not express this marker. We conclude that Mre11 is required to properly segregate acentric DNA during mitosis, subsequent cell survival, and normal papillar organogenesis.

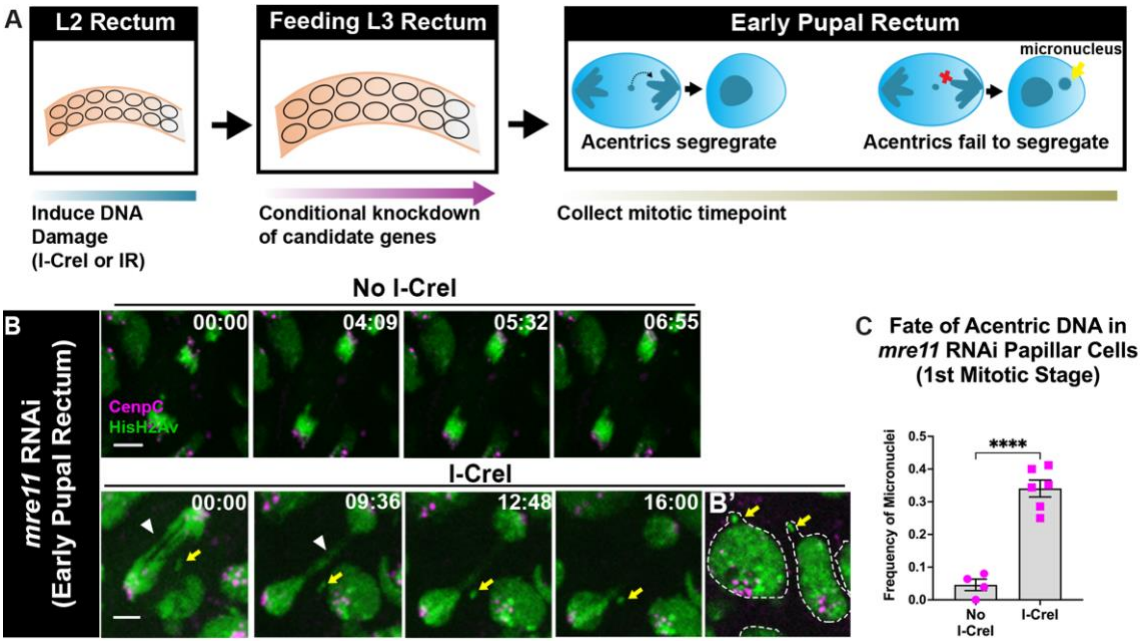

Figure 11: Mre11 is required for segregation of acentric DNA during mitosis.

(A) Pupal candidate screen assay for identifying regulators of acentric DNA segregation based on (Bretscher and Fox, 2016) (See Results) (B) Live imaging of papillar cell mitosis in mre11 RNAi animals +/- hs-I-CreI. HisH2Av, green; CenpC, magenta. Yellow arrow= acentric fragment, White arrowheads= chromatin bridge. Scale bars = 5μm. (B') Micronuclei-containing papillar cells following mitosis +hs-I-CreI in animals expressing mre11 RNAi. Hatched outline= nuclei. Labeling and scale as in B. (C) Quantification of the fate of acentric fragments in mre11 RNAi papillar cells +/- hs-I-CreI. Each condition has at least 2 biological replicates. Each data point represents a single animal (N). Statistical test: Unpaired t-test, $p<0.0001$. See Methods for statistical notations.

2.3.3 Mre11 and RPA3 have distinct localization patterns at DSBs during mitosis

As acentric fragments fail to properly incorporate during mitosis after mre*11* knockdown, we next examined Mre11 dynamics specifically in the first mitosis after DSBs. We live imaged rectums expressing *H2Av*-RFP and *mre11-GFP* during the early (24 h post puparium formation, PPF) pupal stage. Compared to papillar cells without *hs-I-Cre*I DSBs, Mre11+ foci persist on papillar chromosomes at a significantly higher frequency during early prophase (Fig12A [-17:00], B). After nuclear envelope breakdown (NEBD), Mre11+ foci are resolved (Fig12A [00:00],B). Therefore, Mre11+ foci are apparent at DSBs in <30 m, persist for days on broken papillar chromosomes until early mitosis, and are resolved by NEBD.

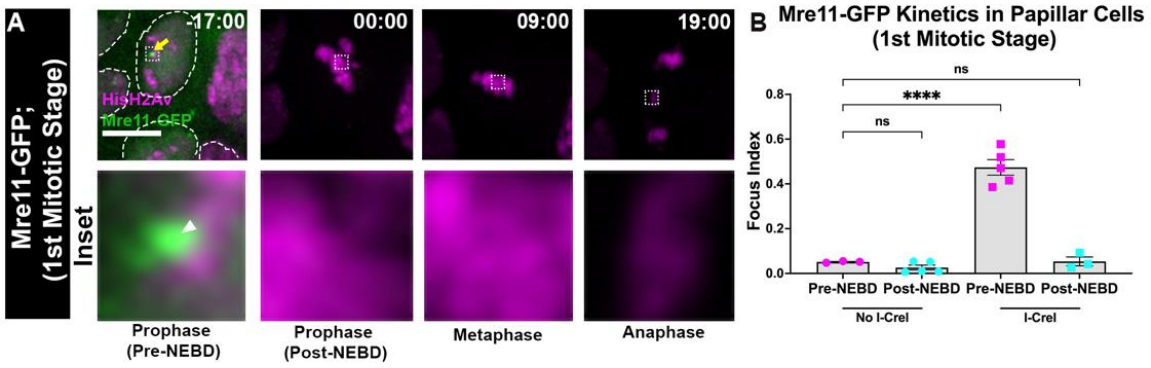

Figure 12: Mre11 foci persist into mitosis and are resolved prior to NEBD.

(A) Mre11-GFP localization in papillar cells during mitosis +/- *hs-I-Cre*I. Mre11, green; HisH2Av, magenta. Yellow arrows= Mre11+ foci. Hatched box= area magnified 10X in the corresponding inset below each panel. White arrowheads= enlarged foci. -17:00 – Hatched outline=Nuclei. Scale bars = 5μm. (B) Quantification of the focus index for Mre11 during papillar mitosis. Each timepoint represents at least two biological replicates. Each data point represents a single animal (N). Statistical test: Ordinary one-way ANOVA, $p<0.0001$.

As RPA3 is recruited downstream of Mre11 (Fig8E-F), we next examined RPA3 localization during the first mitosis after induced DSBs. We live imaged *H2Av*-RFP and *ubi-RPA3*-GFP in mitotic papillar cells. Similar to Mre11, RPA3+ foci are found on mitotic papillar chromosomes after *hs-I-Cre*I DSBs (Fig13A [-11:00], D). However, RPA3 differs from Mre11 in that *hs-I-Cre*I-induced RPA3+ foci are found at an increased level through prophase (Fig13A, B). Following prophase, the mean RPA3 focus index (the frequency in which a cell contains at least one RPA3 focus) decreases (Fig13B), though a subset of cells contain RPA3+ foci on lagging DNA fragments during anaphase (Fig13A, [25:00]). RPA3+ foci are mostly resolved by the following interphase after mitosis

(Fig13A, [40:00]). This gradual RPA3 loss beginning at metaphase may reflect the onset of repair between metaphase and the next interphase (See Discussion). We also assayed the focus intensity, which steadily decreases as cells progress through mitosis (Fig13A, C). We confirmed that similar kinetics are observed when monitoring localization of endogenous RPA (Fig13D, E). We conclude that Mre11 and RPA3+ foci persist into mitosis after DSBs. While Mre11+ foci are resolved before NEBD, RPA3+ foci continue to persist at high levels until metaphase, and then gradually decrease on broken papillar DNA, resolving fully by the following interphase.

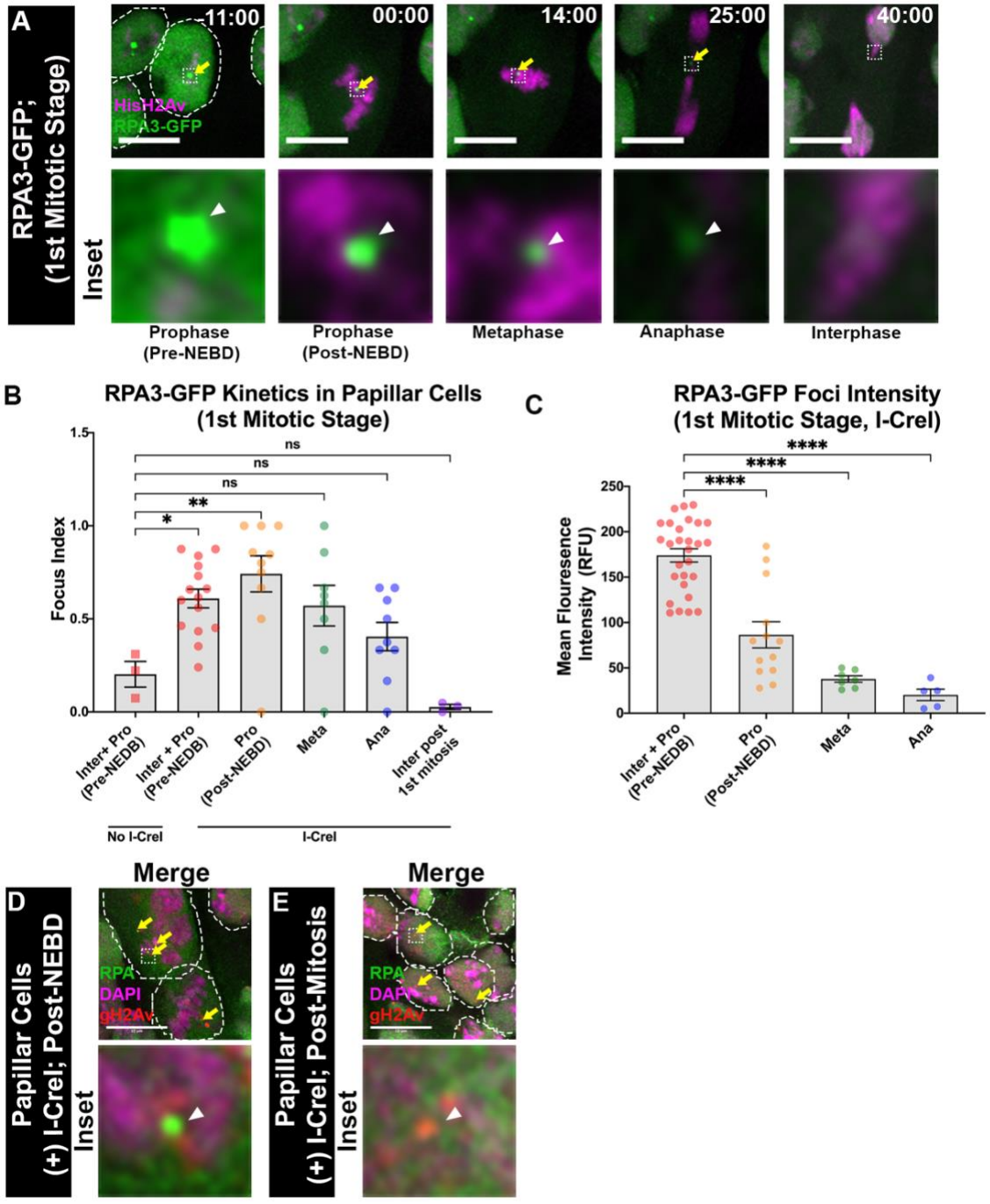

Figure 13: RPA foci persist into mitosis and have kinetics distinct from Mre11.

(A) RPA3-GFP localization in papillar cells during mitosis +/- hs-I-CreI. RPA3, green; HisH2Av, magenta. Labeling as in A. -11:00 - Hatched outline= nuclei. (B) Quantification of RPA3+ foci kinetics in papillar cells during mitosis +/- hs-I-CreI. Each timepoint represents at least two biological replicates. Each data point represents a single animal (N). Statistical test: Ordinary one-way ANOVA, p= 0.0003 (C) Quantification of RPA3+ foci intensity in papillar cells during mitosis after hs-I-CreI. Each timepoint represents at least two biological replicates. Each data point represents a single cell (N). RFU, relative fluorescence units. Statistical test: Ordinary one-way ANOVA, p<0.0001. See Methods for statistical notations. (D-E) RPA+gH2Av+ foci recruitment to papillar cells post-NEBD (F) and post the 1st mitotic division (D) +hs-I-CreI. DAPI (DNA), magenta; RPA, green; gH2Av, red. RPA+gH2Av+ foci are marked with yellow arrows. Nuclei are demarcated with white hatched outline. The hatched box highlights an area magnified 10X in the corresponding inset below each panel. Enlarged foci are marked with white arrowheads.

2.3.4 A candidate genetic screen identifies *polQ* as being required for acentric DNA segregation

The requirement for Mre11 and the dynamic mitotic localization of Mre11 and RPA3 suggested that these proteins might actively signal repair events to segregate acentric DNA. Based on our observations that Mre11 is required for RPA3 recruitment – likely due to DNA resection – we undertook a candidate genetic screen, with the hypothesis that other repair events occur downstream of RPA3 recruitment. Using adult papillar cell number after *hs-I-Cre*I DSBs as a readout to identify regulators of acentric DNA segregation during mitosis (Fig11A, [47], we screened 80 candidate genes that we hypothesized to be possibly important for acentric DNA segregation (Table 1). We chose candidate genes based either on their known function in DNA repair

Table 1: Results from candidate screen for acentric DNA segregation in papillar cells

Gene	Candidate Source/ Pathway[1]	Reagent Type	Reagent Source[2]	Pre-Endocycle Phenotype	Post-Endocycle Phenotype
14-3-3 epsilon	1	RNAi	3488	WT	
ald	1	RNAi	v101339	No HG	Lethal
atm	1	RNAi	108074	WT	
atm	1	RNAi	22502	WT	
blm	1	RNAi	1287	WT	
brwd3	1	RNAi	33421	No HG	DDI
cdc45l	1	RNAi	v110478	No HG	DDI
cdk8	1	RNAi	v107187	No HG	WT
CG9797	1	RNAi	v110498	No HG	No HG
csn1b	1	RNAi	v110477	No HG	
csn2	1	RNAi	33369	No HG	Hit
csn3	1	RNAi	v101516	No HG	DDI
csn4	1	RNAi	v103803	No HG	Lethal
csn5	1	RNAi	36073	No HG	Lethal
csn6	1	RNAi	41991	WT	WT
csn7	1	RNAi	33663	No HG	No HG
csn8	1	RNAi	33370	WT	
cul1	1	RNAi	v108558	Lethal	No HG
cul4	1	RNAi	50614	Lethal	No HG
cycc	1	RNAi	33753	Hit	DDI
ddb1	1	RNAi	41997	Lethal	Hit
ddx6	1	RNAi	38923	Lethal	No HG
e(bx)	1	RNAi	33658	Lethal	Hit
eif4g	1	RNAi	33049	Lethal	Lethal

[1] 1 – Genes selected based on findings of *91. Kondo, S. and N. Perrimon, A genome-wide RNAi screen identifies core components of the G_2-M DNA damage checkpoint. Science signaling, 2011. 4(154): p. rs1-rs1.*

[2] All stocks are from Bloomington Drosophila Stock Center and Vienna Drosophila Resource Center (stocks with 'v') unless otherwise noted

gfzf	1	RNAi	32399	WT	Lethal
kap-alpha3	1	RNAi	v106249	No HG	DDI
mbd-r2	1	RNAi	v110429	Lethal	Lethal
mcm7	1	RNAi	32867	No HG	
mcrs1	1	RNAi	v108017		Lethal
med17	1	RNAi	34664	Lethal	Hit
med4	1	RNAi	34697	Hit	DDI
not1	1	RNAi	32836		DDI
not2	1	RNAi	57549	Hit	WT
nsl1	1	RNAi	58328	Hit	
nsl2	1	RNAi	v108668	WT	WT
nsl3	1	RNAi	v108002	WT	
pont	1	RNAi	50972	WT	WT
pop2	1	RNAi	52947	Lethal	No HG
recq4	1	RNAi	v107718	No HG	
rept	1	RNAi	32415	Lethal	
rpa70	1	RNAi	v110368	Lethal	
rpb4	1	RNAi	v23308	No HG	
rpb5	1	RNAi	v105428	WT	
rpb8	1	RNAi	v106838	No HG	Lethal
rpII15	1	RNAi	v110724	Lethal	No HG
rpII18	1	RNAi	v105937	Lethal	WT
rpII215	1	RNAi	v110340	Lethal	Lethal
sf2	1	RNAi	32367		WT
skp1	1	RNAi	v46607	WT	
spt5	1	RNAi	34837	Lethal	No HG
su(var)2-10	1	RNAi	58067	Lethal	No HG
tango6	1	RNAi	33883	WT	WT
top2	1	RNAi	v30625	Lethal	Lethal
topors	1	RNAi	34671	WT	Hit
ubc9	1	RNAi	37506	WT	
wds	1	RNAi	32952	No HG	No HG
fancd2^{K595R}	FA	MUTANT	*this study*	Hit	
fancd2^{del}	FA	MUTANT	*this study*	Hit	

fanci	1; FA	RNAi	24654	Weak Hit	
fanci	1; FA	RNAi	24655	Weak Hit	
fancl	1; FA	RNAi	33050	WT	Hit
fancl	FA	RNAi	32025		Hit
fancm	FA	RNAi	33889		Hit
fancm	FA	RNAi	v104865		Hit
gen1	SSE	RNAi	42787		Hit
gen1	SSE	RNAi	v12626		Hit
mus81	SSE	RNAi	13285		Hit
mus81	SSE	RNAi	65012		Hit
mms4 RNAi	SSE	RNAi	64952		Hit
slx1	SSE	RNAi	32501		Hit
slx1	SSE	RNAi	34949		Hit
slx4	SSE	RNAi	34873		Hit
slx4	SSE	RNAi	34951		Hit
slx4	1; SSE	RNAi	v28932	WT	WT
rad54	HR	RNAi	31047		WT
rad54	HR	RNAi	31329		WT
rad51	HR	RNAi	38898		DDI
rad51	HR	RNAi	51926		DDI
brca2	HR	MUTANT	13272	WT	
ku70	NHEJ	RNAi	35819	WT	
ku70	NHEJ	RNAi	29594	Hit	
ku80	NHEJ	RNAi	27710	WT	
ku80	NHEJ	RNAi	62513	WT	
lig4	NHEJ	MUTANT	8519	WT	
lig4	NHEJ	MUTANT	8520	WT	
mre11	Resection	RNAi	50628	WT	
mre11	Resection	RNAi	39028	Hit	
nbs	Resection	RNAi	65971	Hit	

nbs	Resection	RNAi	v28216	Hit	
ctip	Resection	RNAi	36622	Hit	
ctip	Resection	RNAi	62005	Hit	
rad50	Resection	RNAi	v103394	WT	
polQ	alt-EJ	RNAi	58238		Hit
polQ	alt-EJ	RNAi	v104788		Hit
parp1	alt-EJ	RNAi	34888		DDI
parp1	alt-EJ	RNAi	57265		DDI
ercc1	alt-EJ	RNAi	36906		Hit
fen1	alt-EJ	RNAi	35764		Hit
xpf	alt-EJ	RNAi	55313		Hit
lig1	alt-EJ	RNAi	34564		DDI
lig1	alt-EJ	RNAi	52951		DDI

or their identification in a previous cell culture-based *Drosophila* screen for DSB-responsive genes (Table 1, [91]).

Most genes that we interrogated did not disrupt papillar organogenesis following DSBs. Interestingly, we did not identify a requirement for cNHEJ nor HR [5, 92, 93]. Specifically, knockdown of regulators of cNHEJ, *ku70, ku80,* and *lig4* [5, 94], did not consistently result in a DSB-specific decrease in papillar cell number (Table 1, 5/6 lines tested were not a hit). Furthermore, the requirement and recruitment of resection factors is inconsistent with cNHEJ, as this pathway does not require end resection [95]. Similarly, Rad51, which is required for HR [5, 93, 94], is not required for papillar cell survival after DSBs (Table 1; Fig14A-B). We do note that there is a significant decrease in

rad51 RNAi papillar cell number without *hs-I-Cre*I, suggesting that Rad51 plays a role in papillar organogenesis (Fig14A-B). Additionally, using an antibody for *Drosophila* Rad51, we find that Rad51 is not recruited until the interphase following the first mitosis, is independent of exogenous DNA damage, and depends on Rad51 function (Fig14C-D), validating that we efficiently knocked down Rad51.

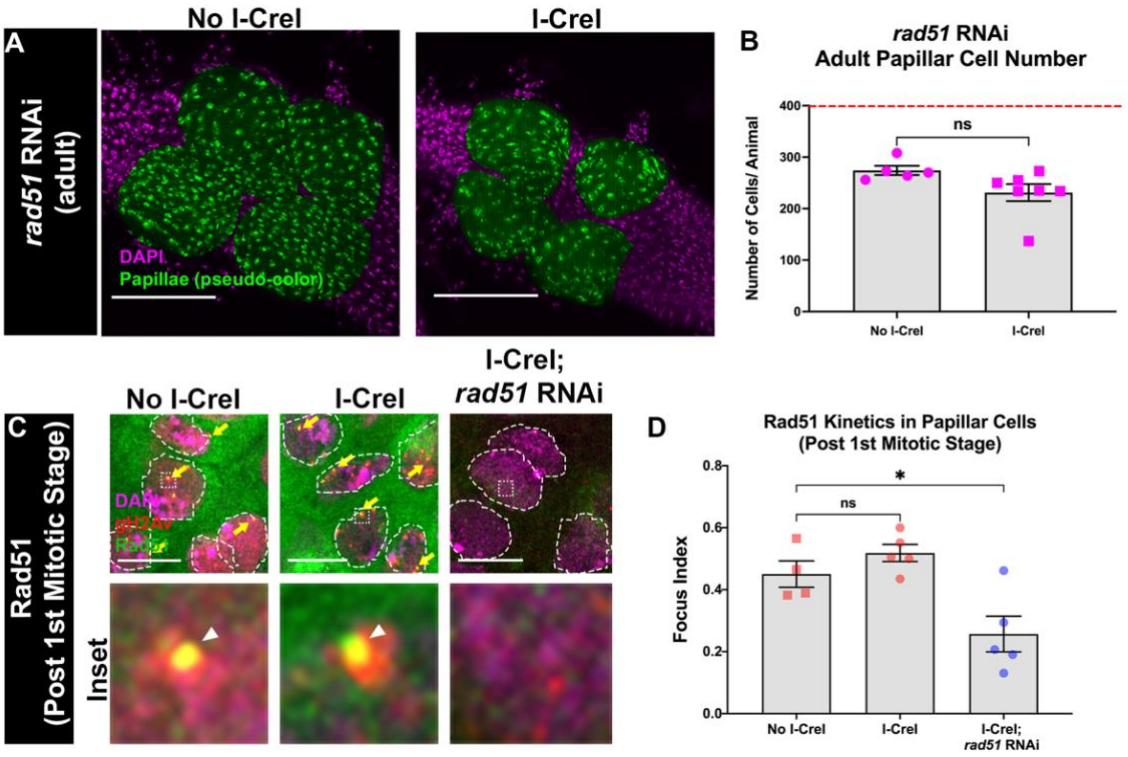

Figure 14: Rad51 is not required for cell survival following DSBs in papillar cells.

(A) Adult rectums of *rad51* RNAi animals +/- *hs-I-CreI*. Green= pseudo colored rectal papillae, magenta= DAPI (DNA). Scale bars = 100 μm (B) Quantification of adult papillar cell number in *rad51* RNAi animals +/- *hs-I-CreI*. Each condition has at least 2 biological replicates. Each data point represents a single animal (N). Red dashed line indicates the expected number of

papillar cells in a WT adult. Statistical test: Unpaired t-test, p=0.0702. (C) Rad51 recruitment to WT papillar cells +/- *hs-I-Cre*I and *rad51* RNAi papillar cells. Rad51+ foci are marked with yellow arrows. Nuclei are demarcated with white hatched outline. The hatched box highlights an area magnified 10X in the corresponding inset below each panel. Enlarged foci are marked with white arrowheads. (D) Quantification of Rad51 foci recruitment in papillar cells in +/- *hs-I-Cre*I and *rad51* RNAi papillar cells post the 1st mitotic stage. Each condition has at least 2 biological replicates. Each data point represents a single animal (N). Statistical test: Ordinary one-way ANOVA, p =0.0037.

Our screen also included regulators of other DSB repair pathways. In contrast to the lack of requirement for cNHEJ and HR, we identified the gene *DNA polymerase Q (polQ)* as a potential candidate for acentric DNA segregation in papillar cells. *polQ* encodes the Pol Theta protein, which is critical in alt-EJ which has also been described as microhomology-mediated end-joining (MMEJ) or Theta-mediated end-joining (TMEJ) [96-101]. Pol Theta recognizes microhomologies around a DSB and anneals homologous sequences together [96-100, 102]. We identified several other genes implicated in alt-EJ (Table 1, *ercc1, fen1, xpf*) as required for papillar cell survival following DSBs [102-105]. As Pol Theta is critical in several steps of alt-EJ [5, 88, 96-98, 100, 105, 106], our further analysis focused on *polQ.*

Knockdown of *polQ* using two independent RNAi lines results in both a *hs-I-Cre*I and IR- induced DSB-specific decrease in adult papillar cell number (Fig15A-F). To determine if the decrease in cell number coincides with an increase in acentric micronuclei, we observed mitotic stage papillar cells in pupae expressing UAS-*polQ*

RNAi. Acentric (CenpC-negative) micronuclei increase after *hs-I-Cre*I DSBs in animals expressing UAS-*polQ* RNAi (Fig16A,B). To determine the extent to which *polQ* knockdown affects RPA3+ foci, we visualized *ubi-RPA3-GFP* in the presence of *polQ* RNAi. RPA3+ foci are present both during and prior to mitosis on broken papillar chromosomes in animals with *polQ* RNAi. However, whereas RPA3+ foci are resolved by the following interphase after mitosis in WT animals (Fig8A [40:00], D), RPA3+ foci persist into the following interphase in animals expressing *polQ* RNAi (Fig16C,D). These data suggest that our candidate screen successfully identified the alt-EJ regulator *polQ* as required for DSB-dependent cell survival in papillar cells. *polQ* is responsible for proper acentric DNA segregation and micronuclei prevention during papillar mitosis, and for the removal of RPA3 by the following interphase.

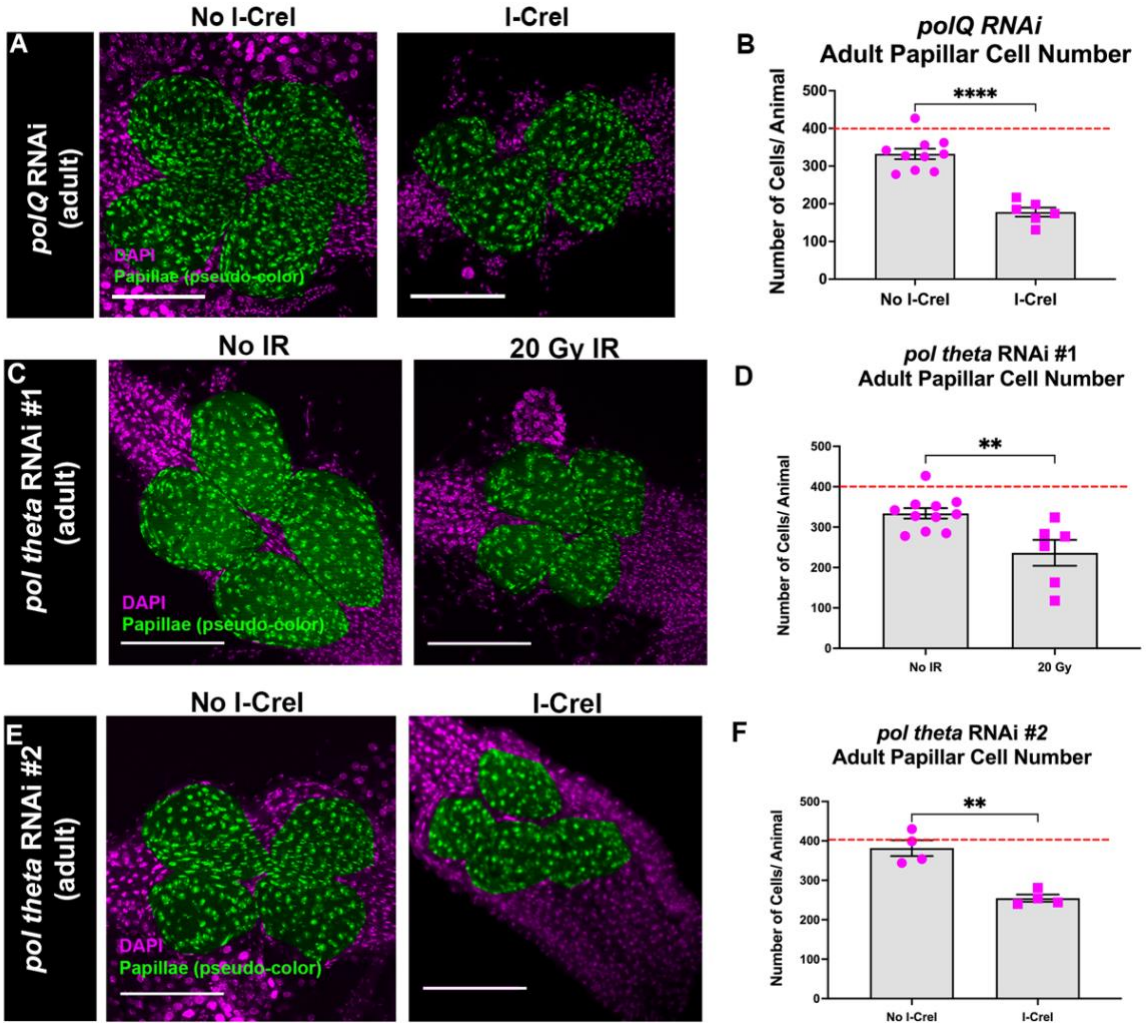

Figure 15: *polQ* is required for papillar cell survival following DSBs.

(A) Adult rectums of *polQ* RNAi animals +/- *hs-I-Cre*I. Papillar cells (pseudo-colored), green; DNA (DAPI), magenta. Scale bars = 50μm (B) Quantification of adult papillar cell number in *polQ* RNAi expressing animals +/- *hs-I-Cre*I. Statistical test: Unpaired t-test, p<0.0001. (C) Adult rectums of *polQ* RNAi animals +/- IR. Labeling as in A. (D) Quantification of adult papillar cell number in *polQ* RNAi animals +/- IR. Statistical test: Unpaired t-test, p=0.0043 (E) Adult rectums of *polQ* RNAi #2 (2nd RNAi line) animals +/- *hs-I-CreI*. Labeling as in A. (F) Quantification of adult papillar cell number in *polQ* RNAi #2 animals +/- *hs-I-CreI*. Statistical test: Unpaired t-test, p=0.0012. (B,D,F) Each condition has at least 2 biological replicates. Each data point represents a single animal

(N). Red dashed line indicates the expected number of papillar cells in a WT adult. See Methods for statistical notations.

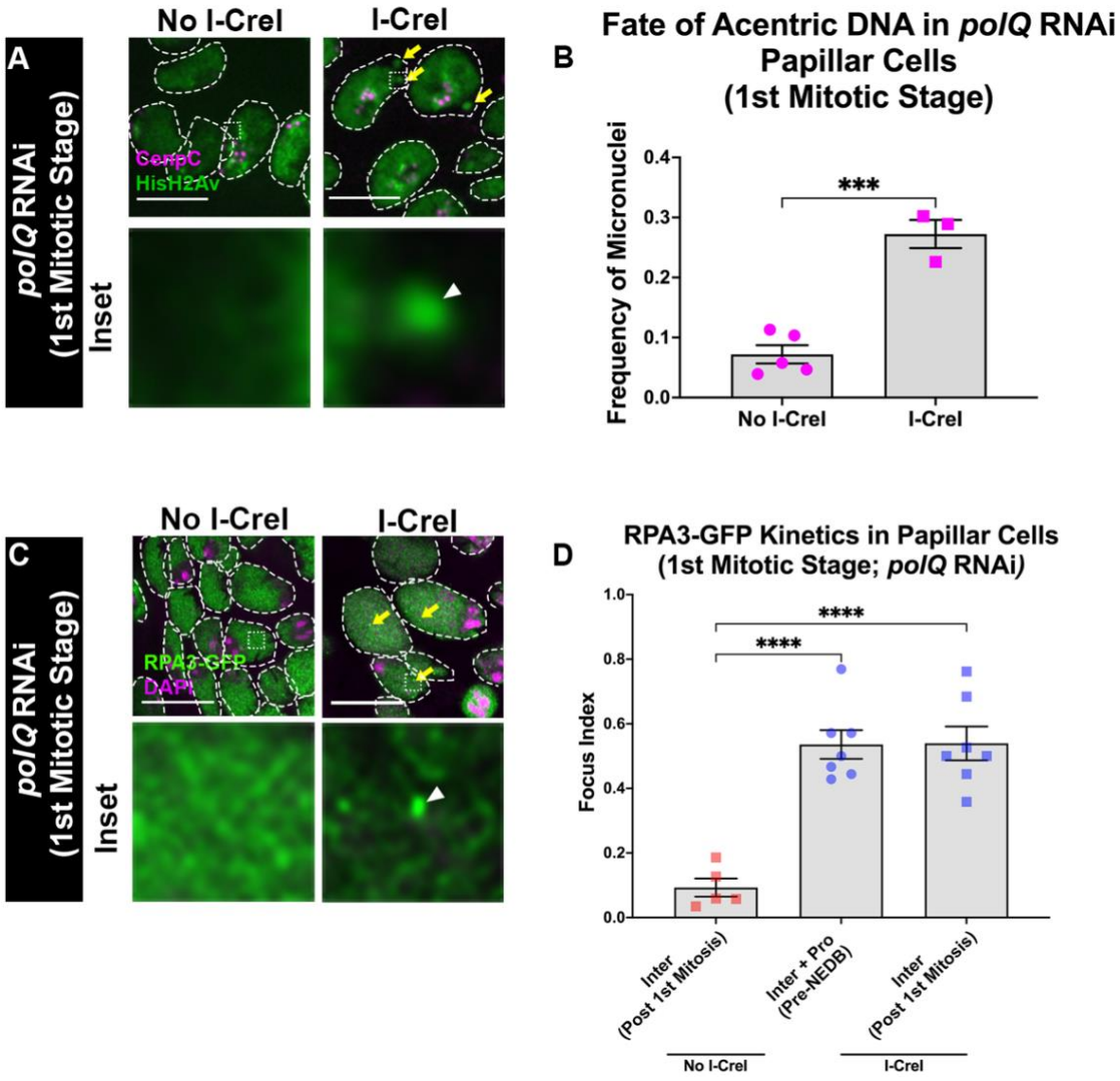

Figure 16: *polQ* is required for acentric DNA segregation and proper RPA3+ foci dynamics.

(A) Still images of live imaged rectums expressing *polQ* RNAi +/- *hs-I-Cre*I. HisH2Av, green; CenpC, magenta. Yellow arrows= micronuclei. Hatched outline= nuclei. Hatched box= area magnified 10X in the corresponding inset below each panel. White arrowhead= enlarged micronucleus. Scale bars = 10μm. (B) Quantification of the fate of acentric fragments in polQ RNAi papillar cells +/- *hs-I-Cre*I. Each condition has at least 2 biological replicates. Each data point represents a single animal (N). Statistical test: Unpaired t- test, p=0.0003 (C) RPA3-GFP localization in *polQ* RNAi papillar cells during mitosis +/- hs-I-CreI. RPA3, green; DAPI, magenta. Yellow arrows= RPA3+ foci. All other labeling as in A. (D) Quantification of RPA3+ foci kinetics in *polQ* RNAi papillar cells during mitosis +/- *hs-I-Cre*I. Each timepoint represents at least two biological replicates. Each data point represents a single animal (N). Ordinary one-way ANOVA, $p<0.0001$. See Methods for statistical notations.

2.3.5 Monoubiquitinated Fancd2 is required for micronuclei prevention and RPA3 removal

Our analysis of *polQ* RNAi papillar cells resembled our previous study of the FA pathway protein Fancd2. In animals expressing *UAS-fancd2* RNAi under the control of *byn*> Gal4, acentric fragments fail to properly incorporate into daughter papillar cell nuclei and instead form micronuclei [47]. This increase in micronuclei correlates with decreased papillar cell number and papillar organogenesis defects, the latter seen also in the Fancd2 binding partner, FancI.

Fancd2 forms a heterodimer with FancI and the recruitment and activation of these proteins frequently depends on monoubiquitination on conserved lysine residues in by the FA core complex (FancM and FancL in *Drosophila*, [107, 108]. To determine to what extent Fancd2 depends on its conserved monoubiquitination, we examined adult papillar cell number in FA core complex RNAi animals (Fig17A-D). Knockdown of both

FA core complex members, *fancm* and *fancl*, in the hindgut using multiple independent RNAi lines, results in a *hs-I-Cre*I-specific decrease in papillar cell number and associated defects in papillar organogenesis (Fig17A-D). In our previous study [47] we used a *fancm* partial deletion allele ($fancm^{del}$) in combination with a deficiency in the *fancm* region and observed an IR-dependent adult papillar cell phenotype but not a significant *hs-I-Cre*I-dependent phenotype. Here we instead find significant *hs-I-Cre*I-dependent papillar cell phenotypes for *fancm* with two separate RNAi lines. Taken together with our previous findings for FancI and Fancd2 [47], we conclude that the entire FA pathway is required in *Drosophila* papillar cells with DSBs.

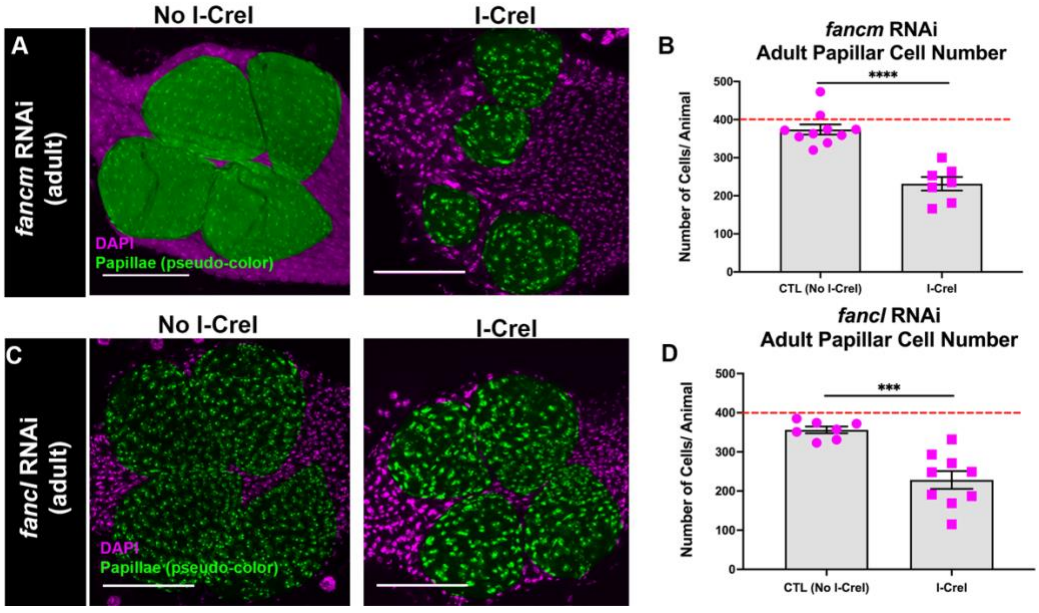

Figure 17: FA core complex members are required for papillar cell survival following DSBs.

(A) Adult rectums of *fancm* RNAi animals +/- *hs-I-CreI*. Green= pseudo colored rectal papillae, magenta= DAPI (DNA). Scale bars = 100 μm (B) Quantification of adult papillar cell number in *fancm* RNAi animals +/- *hs-I-CreI*. Each condition has at least 2 biological replicates. Each data point represents a single animal (N). Red dashed line indicates the expected number of papillar cells in a WT adult. Statistical test: Unpaired t-test, $p<0.0001$. (C) Adult rectums of *fancl* RNAi animals +/- *hs-I-CreI*. Labeling as in A. (D) Quantification of adult papillar cell number in *fancl* RNAi animals +/- *hs-I-CreI*. Each condition has at least 2 biological replicates. Each data point represents a single animal (N). Red dashed line indicates the expected number of papillar cells in a WT adult. Statistical test: Unpaired t-test, $p=0.0003$.

To further test if Fancd2 monoubiquitination is required for papillar cell survival after DSBs, we used two-step CRISPR-mediated homology-directed repair [109] to generate a fly where the conserved, endogenous monoubiquitination site for Fancd2, K595, is mutated to an arginine (*fancd2*^{K595R}, Fig18A). This mutation has been previously observed to disrupt monoubiquitination of *Drosophila* Fancd2 *in vitro* [108]. *fancd2*^{K595R} is the first animal model of a mutation in the endogenous conserved monoubiquitination site, and the first endogenous *fancd2* mutation of any kind in flies. *fancd2*^{K595R} homozygous animals are viable and fertile, enabling us to test a role for Fancd2 monoubiquitination in acentric DNA responses. *fancd2*^{K595R} animals have decreased adult papillar cell number after both *hs-I-Cre*I (Fig18B,C) and IR (Fig18D,E).

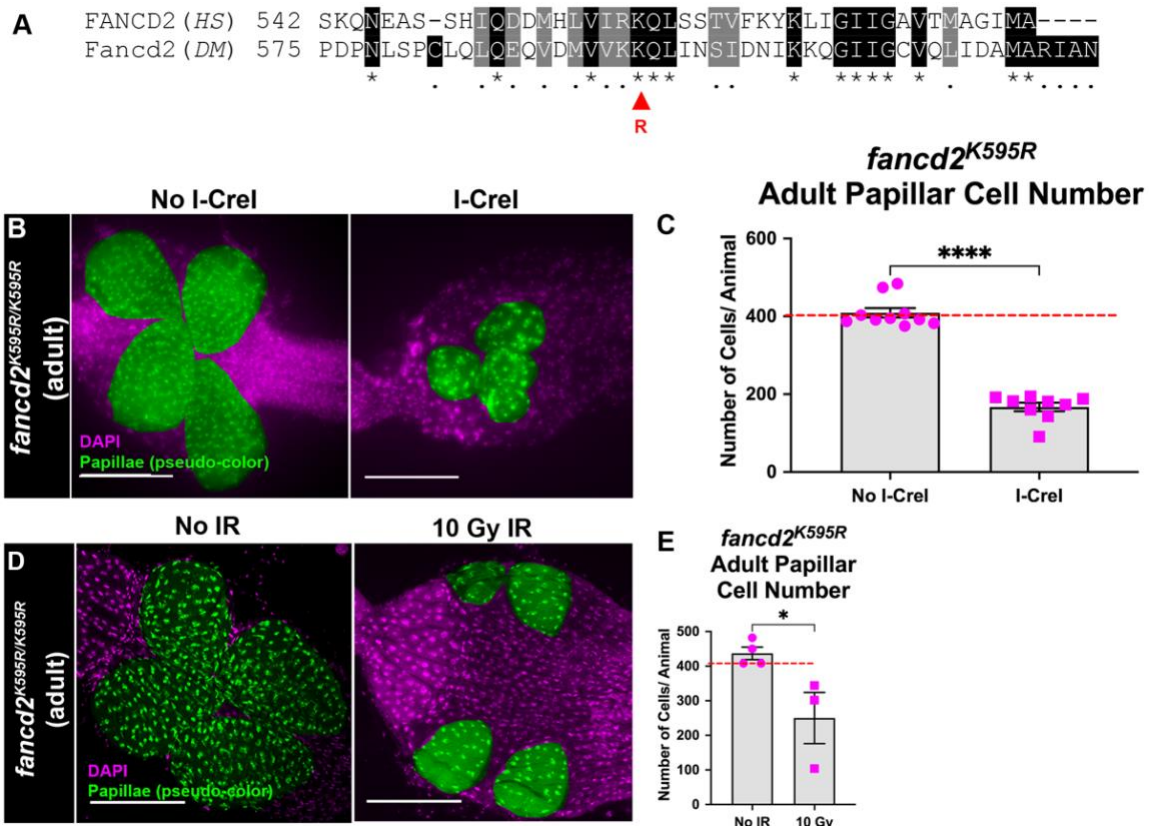

Figure 18: Monoubiquitinated Fancd2 is required for papillar cell survival following DSBs.

(A) Sequence alignment comparing the region of human (*HS*) FANCD2 protein sequence to *Drosophila* (*DM*) Fancd2 where the conserved monoubiquitination site is found. Asterisks and black shading= identical sequences, dots and gray shading= sequence similarities. Red arrowhead= the conserved monoubiquitinated lysine (K523 in humans; K595 in *Drosophila*). This site was mutated into an arginine (*fancd2*^{K595R}) using two-step CRISPR-mediated homology-directed repair (see Methods). (B) Adult rectums of *fancd2*^{K595R} animals +/- *hs-I-CreI*. Papillar cells (pseudo-colored), green; DNA (DAPI), magenta. (DNA). Scale bars = 50μm (C) Quantification of adult papillar cell number in *fancd2*^{K595R} animals +/- *hs-I-CreI*. Red dashed line= expected number of papillar cells in a WT adult. Each condition has at least 2 biological replicates. Each data point represents a single animal (N). Statistical test: Unpaired t-test, $p<0.0001$.

We then determined if Fancd2 monoubiquitination prevents micronuclei. To test this, we measured micronucleus frequency in response *hs-I-Cre*I DSBs. In *fancd2*^{K595R} animals, micronucleus frequency is significantly higher in cells with *hs-I-Cre*I DSBs compared to *fancd2*$^{K595R/+}$ animals (Fig19A,B). Our findings in previous and in this current study support a model where the FA core complex and monoubiquitination of the Fancd2-FancI heterodimer prevent micronuclei during mitosis with DSBs to promote cell survival.

We then examined if Fancd2 monoubiquitination impacts the dynamic localization of RPA3 after DSBs. To test this, we first visualized *ubi-RPA3-GFP* in animals expressing *fancd2* RNAi as in Fig16. *fancd2* RNAi papillar cells fail to remove RPA3 foci after mitosis following DSBs (Fig19C,D). We then visualized RPA3-GFP in *fancd2*^{K595R} animals. RPA3+ foci are recruited to papillar cells prior to mitosis in response to *hs-I-Cre*I DSBs in *fancd2*^{K595R} animals (Fig19F) and animals heterozygous for the K595R mutation (*fancd2*$^{K595R/+}$ Fig19G). However, DSBs increase the frequency of RPA3+ foci in *fancd2*^{K595R} animals following the first mitosis (Fig19E,F). This increased frequency following mitosis is not observed in either WT (Fig18A,B) or *fancd2*$^{K595R/+}$ animals (Fig19G). These findings suggest that, similar to Pol Theta, conserved Fancd2 monoubiquitination is required to displace RPA3+ foci during mitosis.

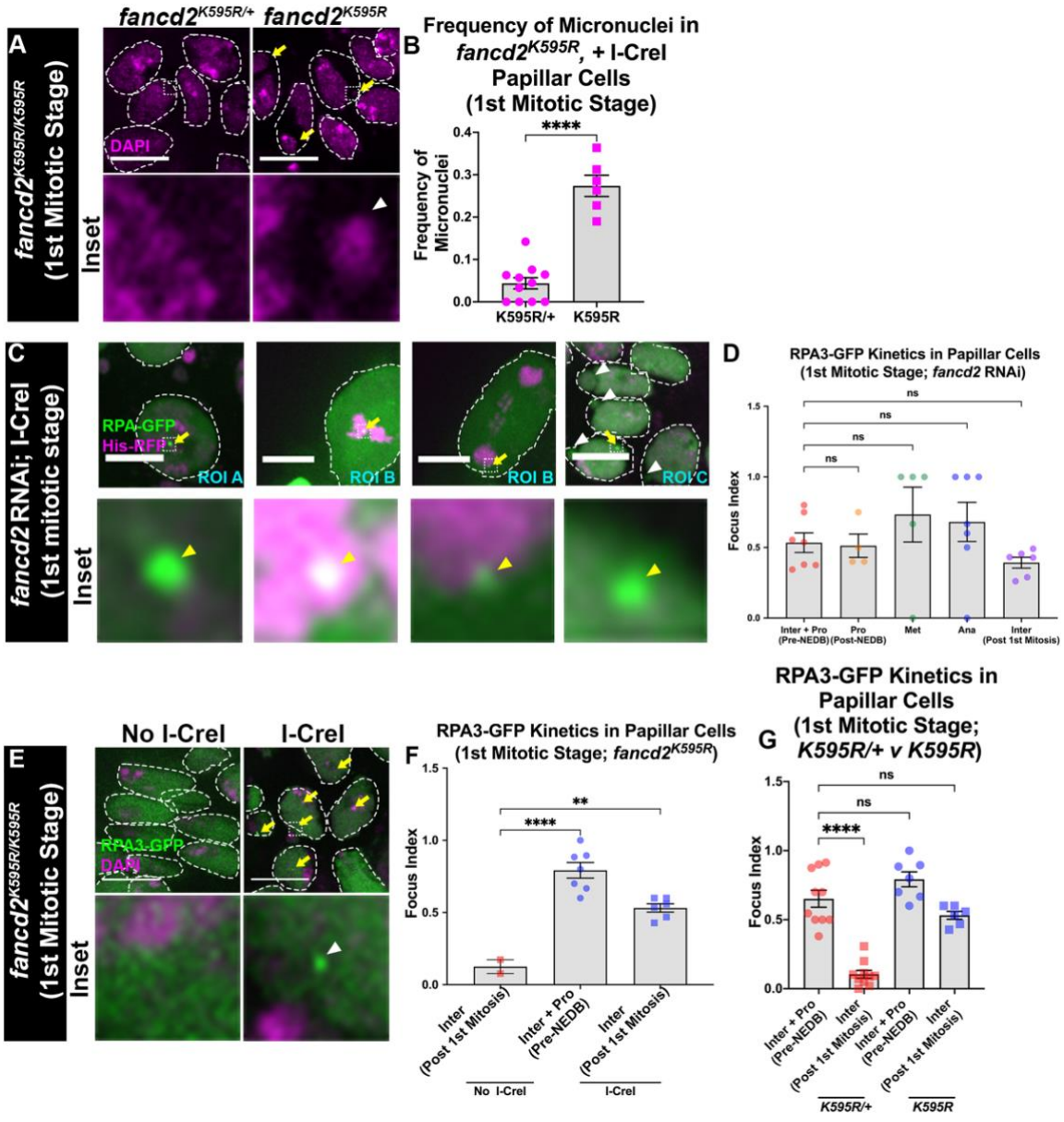

Figure 19: Monoubiquitinated Fancd2 is required for micronuclei prevention and proper RPA3 dynamics during mitosis.

(A) Mitotic stage *fancd2*^{K595R} animals +/- *hs-I-CreI*. DNA (DAPI), magenta. Yellow arrows= micronuclei. Hatched box= area magnified 10X in the corresponding inset below each panel. White

arrowhead= enlarged micronucleus. Hatched outline= nuclei. Scale bars = 10μm. (B) Quantification of the fate of acentric fragments with and without *hs-I-CreI*-induced DNA damage in *fancd2*^{K595R} papillar cells. Statistical test: Unpaired t-test, p<0.0001. (C) RPA3-GFP foci recruitment in *fancd2* RNAi expressing papillar cells +/- *hs-I-Cre*I. ROI=region of interest, letters indicate separate cells at a given timepoint for a single animal. RPA3+ foci are marked with yellow arrows. The hatched box highlights an area magnified 10X in the corresponding inset below each panel. Enlarged foci are marked with yellow arrowheads. Micronuclei are marked with white arrowheads. Nuclei are demarcated with white hatched outline. Scale bars = 10μm. (D) Quantification of RPA3-GFP foci recruitment in *fancd2* RNAi expressing papillar cells during mitosis +/- *hs-I-Cre*I. Statistical test: Ordinary one-way ANOVA, p-value=0.7076. (E) RPA3-GFP foci recruitment in *fancd2*^{K595R} animals +/- *hs-I-CreI*. Yellow arrows= RPA3+ foci. RPA3, green; DNA (DAPI), magenta. All other labelling as in A. (F) Quantification of RPA3+ foci kinetics in *fancd2*^{K595R} papillar cells during mitosis +/- *hs-I-Cre*I. Ordinary one-way ANOVA, p<0.0001. (B,D,F) Each condition has at least 2 biological replicates. Each data point represents a single animal (N). See Methods for statistical notations.

As monoubiquitinated Fancd2 is not required to recruit RPA3 immediately following DNA damage but is required for RPA3 foci resolution during mitosis, we next investigated the timing of Fancd2 arrival to papillar cells after DSBs. We examined animals expressing *Drosophila* Fancd2 tagged with GFP (Fancd2-GFP). Similar to RPA3 and Mre11, papillar cells recruit Fancd2+ foci <30 m after *hs-I-Cre*I DSBs (Fig20A). Fancd2+ foci persist into mitosis, but are resolved prior to NEBD, mirroring Mre11+ foci kinetics (Fig20A,B). Taken together, these data suggest that Fancd2 is recruited to RPA3-coated resected DNA shortly after a DSB and recruits downstream repair factors to promote the resolution of RPA3+ foci during mitosis.

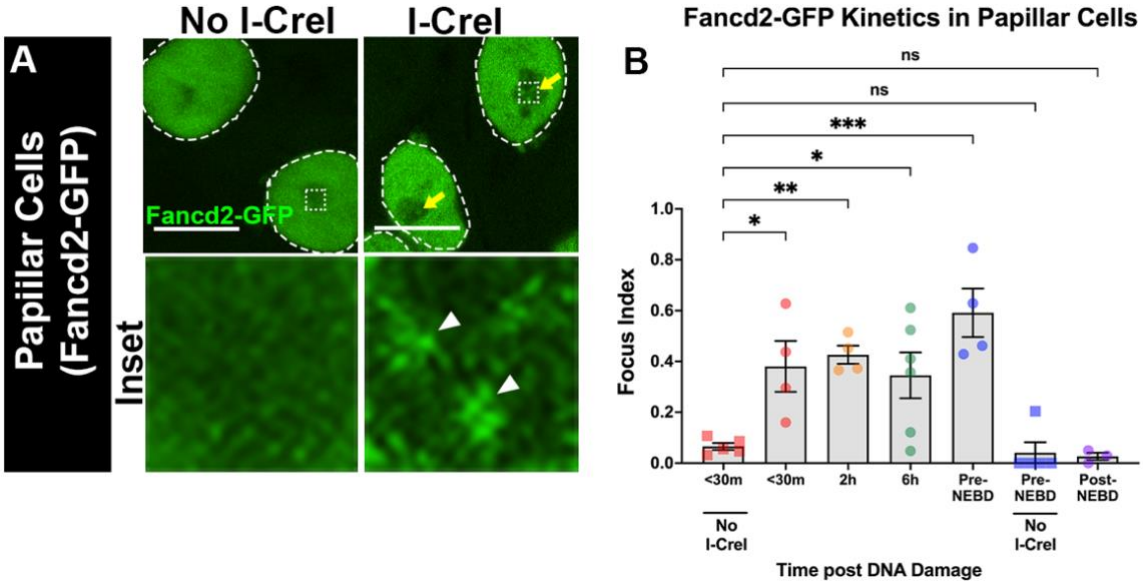

Figure 20: Fancd2+ foci are recruited to papillar cells and persists until NEBD after DSBs.

(A) Fancd2-GFP localization to papillar cells during mitosis +/- *hs-I-Cre*I. Fancd2, green. Yellow arrows= Fancd2+ foci. Yellow arrows= micronuclei. Hatched box= area magnified 10X in the corresponding inset below each panel. White arrowhead= enlarged micronucleus. Hatched outline= nuclei. Scale bars = 10μm. (B) Quantification of Fancd2+ foci recruitment in papillar cells +/- *hs-I-Cre*I from <30 m to the interphase following the first mitotic stage. Each condition has at least 2 biological replicates. Each data point represents a single animal (N). Statistical test: Ordinary one-way ANOVA, $p<0.0001$

2.3.6 *polQ* and *fancd2* mutants are epistatic during papillar cell mitosis with DSBs

Based on the observation that *polQ* and monoubiquitinated Fancd2 are both required for acentric DNA to be incorporated into daughter nuclei during mitosis, we next examined the genetic interaction between these two genes. To test at a genetic level

if *polQ* and monoubiquitinated Fancd2 work in concert to promote papillar cell survival following DNA damage, we knocked down *polQ* using UAS-*polQ* RNAi in fancd2K595R animals. After inducing hs-I-CreI DSBs in the endocycle, a significant decrease in adult papillar cell number occurs in fancd2K595R; *polQ* RNAi animals (Fig21A,B). However, we do not observe a significant difference in adult papillar cell number after DSBs in the double mutant animals compared to either single mutant.

We then determined the effect of fancd2K595R;*polQ* RNAi animals on micronuclei formation during mitosis in papillar cells with hs-I-CreI DSBs. The frequency of micronuclei in fancd2K595R;*polQ* RNAi animals increases after DSBs (Fig21C,D). Similar to our findings for adult papillar cell number, we do not observe a significant increase in micronuclei in fancd2K595R;*polQ* RNAi animals relative to either single gene disruption alone (fancd2K595R and *polQ* RNAi, Fig21D).

Lastly, we examined the ability of fancd2K595R;*polQ* RNAi animals to resolve RPA foci in mitosis. RPA+ gH2Av+ foci persist following mitosis in papillar cells specifically in response to hs-I-CreI DSBs (Fig21E,F). These findings are similar to what we observe in either single mutant. These data suggest that, during mitosis with DSBs, *polQ* and monoubiquitinated Fancd2 work in concert to resolve RPA3, prevent micronuclei, and promote papillar cell survival.

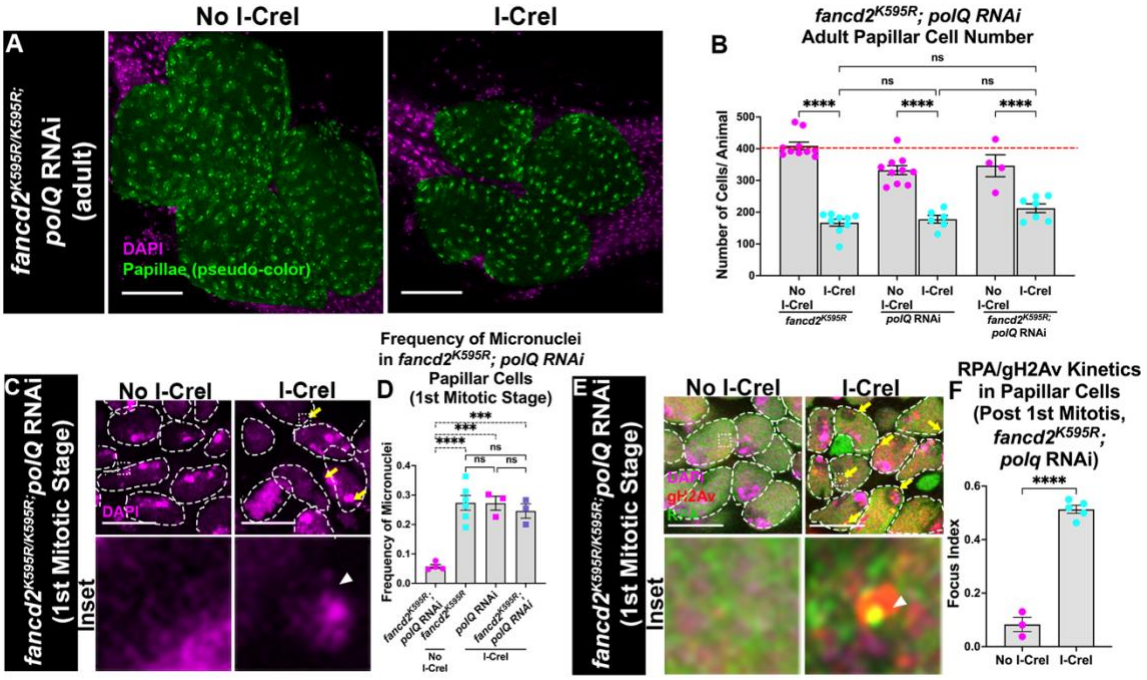

Figure 21: *polQ* and *fancd2* mutants are epistatic for micronuclei prevention during papillar cell mitosis.

(A) Adult rectums of *fancd2*^{K595R}*;polQ* RNAi animals +/- *hs-I-Cre*I. Papillar cells (pseudo-colored), green; DNA (DAPI), magenta. Scale bars = 50μm (B) Quantification of adult papillar cell number in *polQ* RNAi (data set from Fig. 5B), *fancd2*^{K595R} (data set from Fig. 6C), *fancd2*^{K595R}*;polQ* RNAi animals +/- *hs-I-Cre*I. Red dashed line= expected number of papillar cells in a WT adult. Each condition has at least 2 biological replicates. Each data point represents a single animal (N). Statistical test: Unpaired t-test, p<0.0001 (C) Mitotic stage *fancd2*^{K595R}*;polQ* RNAi animals +/- *hs-I-Cre*I. DNA (DAPI), magenta. Yellow arrows= micronuclei. Hatched box= area magnified 10X in the corresponding inset below each panel. White arrowhead= enlarged micronucleus. Hatched outline= nuclei. Scale bars = 10μm. (D) Quantification of the fate of acentric fragments in *fancd2*^{K595R}*;polQ* RNAi (+/- *hs-I-Cre*I) and *polQ* RNAi (+*hs-I-Cre*I) papillar cells. Each condition has at least 2 biological replicates. Each data point represents a single animal (N). Statistical test: Ordinary one-way ANOVA, p<0.0001. (E) RPA and gH2Av recruitment to *fancd2*^{K595R}*;polQ* RNAi papillar cells +/- *hs-I-Cre*I. DNA (DAPI), magenta; RPA, green; gamma H2Av, red . Yellow arrows= RPA+ gamma H2Av+ foci. All other labelling as in C. (F) Quantification of RPA+ gH2Av+ foci recruitment in *fancd2*^{K595R}*;polQ* RNAi papillar cells +/- *hs-I-Cre*I post the 1st mitotic stage. Each condition has at least 2 biological replicates. Each data point represents a single animal (N). Statistical test: Ordinary one-way ANOVA, p<0.0001.

2.4 Discussion

How DNA repair is regulated in the absence of a chk1/chk2/p53 checkpoint is incompletely understood. In this study, we find that checkpoint-inactive papillar cells still recruit early-acting repair proteins to DSBs (Fig22A).RPA3+ repair foci persist into mitosis (Fig22A) but are resolved by the following interphase (Fig22A). RPA3 removal is controlled by Fancd2 and Pol Theta (Fig22B). Failure to remove RPA3 correlates with acentric DNA failing to segregate into daughter nuclei, micronuclei, and intestinal organogenesis defects (Fig22B). Based on these findings, we propose that an alt-EJ repair intermediate links the acentric fragment to a broken, centromere containing chromosome during anaphase, preventing micronuclei and ensuring proper development (Fig22A, A').

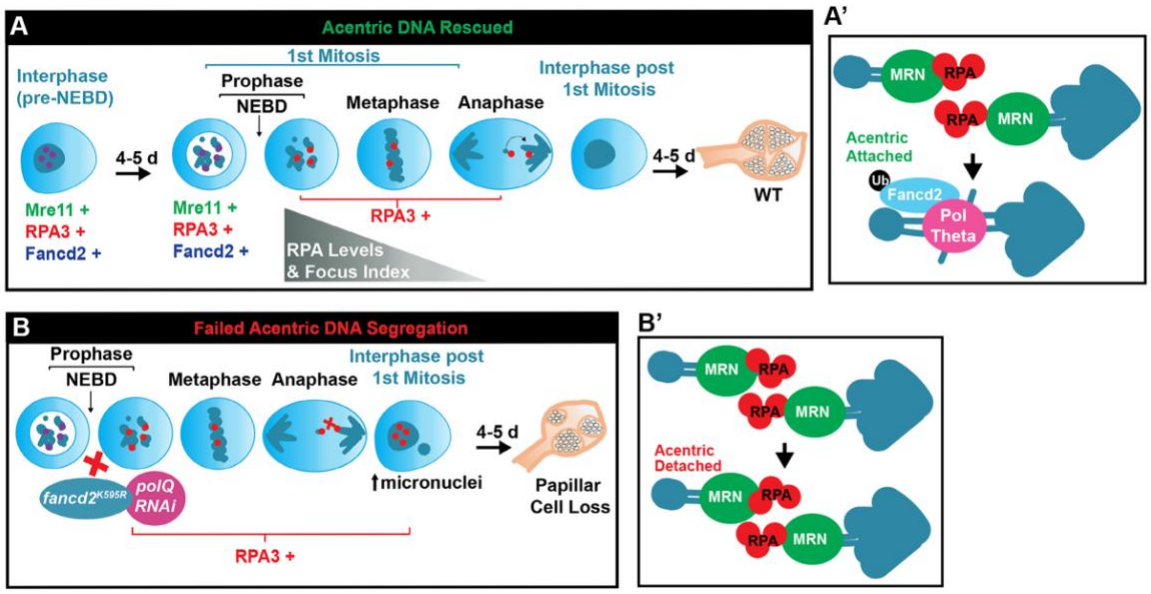

Figure 22: Model for acentric DNA segregation during mitosis.

(A-B') Proposed model for how Pol Theta and monoubiquitinated Fancd2 work in concert to promote acentric DNA segregation. Purple circles= Mre11+,RPA3+, and Fancd2+ foci; Red circles= RPA3+ foci (See Discussion).

2.4.1 A DNA repair intermediate promotes acentric DNA segregation

The recruitment of Mre11, RPA3, and Fancd2 to damaged papillar chromosomes mirrors previous findings, but there are also some distinctions. Following DSBs in checkpoint-inactive papillar cells (this study) and in damaged neuroblasts [38], Mre11 is recruited to DSBs, is dynamic during mitosis, and is required to recruit downstream proteins. While Landmann et al. observed Mre11 recruitment during later mitotic stages than we observe, we note that they induced DSBs in prometaphase, instead of prior to

mitosis as performed here. Indeed, timing of DSB induction influences DNA repair [92]. Also, in the Landmann study, the protein BubR1 is recruited to DSBs [38]. In contrast, our prior study [47] found that papillar cells do not recruit nor require BubR1 for acentric DNA segregation. Taken together, our work and findings in *Drosophila* neuroblasts highlight the importance of understanding the cellular context in which DSBs arise and how this influences DSB repair.

In mammalian cells, micronuclei and chromosomal aberrations are prevented by ultra-fine DNA bridges (UFBs), DNA and protein based linkages that need to be resolved during mitosis [110]. UFBs prevent micronuclei through resolution of replication and repair intermediates by FA proteins, BLM helicase, and RPA2. Similarly, we identified that BLM and Fancd2 are required for acentric DNA segregation in damaged papillar cells and here we observe Fancd2 and RPA3 recruitment to damaged papillar chromosomes during mitosis (Fig8A,B; Fig20A,B)[47]. We have not observed long RPA3-coated UFBs during mitosis, which we hypothesize to be because papillar cells engage in alt-EJ, which can displace RPA on short microhomology regions around a DSB. [2, 4, 5, 96-100, 111, 112]. Alt-EJ is a "back-up" pathway when major DSB repair pathways are unavailable [30] in some contexts, and is the preferred repair pathway in others [113], including during mitosis [114, 115]. We speculate that alt-EJ displaces RPA

during mitosis and promotes annealing of broken DNA ends by Pol Theta and monoubiquitinated Fancd2 (Fig22B').

2.4.2 Fancd2 monoubiquitination and Pol Theta work together to promote acentric DNA segregation

We find that Fancd2 monoubiquitination cooperates with Pol Theta to promote acentric DNA segregation. Monoubiquitinated Fancd2 and Pol Theta cooperate in other contexts [116, 117]. Additionally, mutants in Fancd2 and FEN1 (an implicated alt-EJ endonuclease and hit in our screen, (Table 1), are epistatic in the repair of chemotherapy-induced DNA damage [118]. Monoubiquitination of Fancd2 may recruit Pol Theta to resected, RPA coated-ssDNA to promote alt-EJ between acentric DNA and its centric partner, which pulls acentric DNA into daughter nuclei (Fig22A'). When Fancd2 monoubiquitination is disrupted and/or when *polQ* is knocked down, RPA-coated resected DNA persists and the acentric detaches from centromere containing chromosomes, causing micronuclei (Fig22B').

In addition to *polQ*, our candidate screen can identify additional acentric DNA segregation mechanisms. We identified several structure specific endonucleases (SSEs) which resolve replication and repair intermediates (Table 1) [119]. It was recently identified that in Drosophila, *polQ* and the SSEs, SLX4 and GEN1, process homologous recombination intermediates. *polQ* suppresses mitotic crossovers to prevent deleterious

loss of heterozygosity [88]. A similar *polQ*/SSE mechanism may also function in papillar cells.

2.4.3 Papillar cell acentric DNA segregation as a model for cancer cell biology and tumor resistance

We previously described characteristics of papillar cell biology that are similar to what is observed in cancer cells [90, 120]. Papillar cells are polyploid, as are over one-third of cancers [73]. Additionally, papillar cells resist multiple forms of DNA damage [47]. Similarly, some cancer cells that undergo genome duplication also resist various DNA damaging therapies such as chemotherapy drugs or irradiation [121-123]. One potential mechanism for how cancer cells and papillar cells tolerate high levels of DNA damage may be a dysregulated DDR [42, 47, 112]. As highlighted here, our findings are also relevant to preventing micronuclei, a prominent cancer feature [124]. Micronuclei can lead to deleterious chromosome rearrangements [125-127] [128, 129] and an inflammatory response linked to tumor formation and metastasis [130-132]. Our studies here on Pol Theta and Fancd2 add to the similarities between papillar cells and mechanisms that are relevant to cancer biology.

3. Expanding on mechanisms of acentric DNA segregation – insights from a papillar cell candidate screen

The following chapter includes unpublished work that aims to expand on our current knowledge of how acentric DNA fragments properly segregate during mitosis. This chapter will be divided into two main sections. The first section features unpublished work characterizing both the *fancd2*$^{K595R/K595R}$ CRISPR mutant and *Ubi-fancd2-GFP* transgenic animal developed for the study discussed in Chapter 2. Additionally I will introduce a new construct, *Ubi-fancd2*^{K595R}*-GFP,* which was made using identical methodology as *Ubi-fancd2-GFP* animals. The second section will focus on a novel complex implicated in acentric DNA segregation, CRL4^{CDT2}. The majority of the work in this chapter was performed by me, with the following exceptions. The survival analysis performed in Fig26B was conducted by Erin Jezuit, MS. Fig31A-B and the analysis of Cap-D2 localization in Fig32A-D was done by Don Fox, PhD. Lastly, the Co-IP experiment in Table 4 was performed in the laboratory of Greg Rogers, PhD by Daniel Buster at the University of Arizona.

3.1 Introduction

This introduction will also be divided into two parts for clarity. In the first half I will discuss in greater detail the role of the FA pathway in maintaining genome stability.

I will particularly focus on monoubiquitination of Fancd2 and how Fancd2 plays an important role in both replicating cells and in cells with DNA damage. The second half of this introduction will shift into discussing $CRL4^{CDT2}$, a novel complex that we have implicated to be involved in segregating acentric DNA.

3.1.1 The Fanconi Anemia pathway

The human Fanconi Anemia pathway is comprised of at least 22 complementation groups and was originally identified to be important in the repair of interstrand crosslinks (ICLs). The pathway is named after a rare genetic disorder, Fanconi Anemia, first identified by Guido Fanconi (1927). This disease is characterized by bone marrow failure and cancer predisposition[133]. FA patient cells fail to resolve DNA ICLs and are therefore sensitive to crosslinking agents such as cisplatin and mitomycin C [107, 134]. Furthermore, this pathway is at least partially conserved in organisms such as yeast (*S. cerevisiae*) and *C. elegans [134, 135]*. *Drosophila* also contain several FA complementation groups, many which are vital to FA pathway activation and with conserved residues important for FA protein function [5, 47, 108]. The conservation of critical FA proteins across various species emphasizes the importance of the pathway in maintaining genomic stability. This conservation has led to the creation

of strong genetic models, including in *Drosophila*, to shed light on FA pathway mechanisms, several which remain to be identified [107, 134].

The FA pathway involves a multi-protein complex, known as the FA core complex, that is recruited to sites of DNA damage. This complex functions as an E3 ubiquitin ligase that monoubiquitinates the proteins Fancd2 and FancI, which form a heterodimer [107, 134, 136]. Monoubiquitination of Fancd2 and FancI are thought to be the activating step of the pathway, and deubiquitination by the protein USP1 is required to deactivate the heterodimer and prevent further downstream recruitment of effector proteins [133] (Fig23A) . While the FA pathway was first identified to be involved in ICL repair, it is now understood that the FA pathway has several other functions including maintaining fork stability during replication stress, DSB repair independent of ICL repair, and mitotic progression [107].

3.1.1.1 The FA core complex

FancM, a translocase, participates in lesion recognition and can be recruited to chromatin through association with Fanconi Anemia-associated proteins (FAAP), MHF1 and MHF2 [136]. This complex can recruit other FA core complex members and together forms a FA core complex. This multi-protein complex functions as an E3 ubiquitin ligase, which monoubiquitinates the Fancd2 and FancI heterodimer. The ubiquitin

ligase, FancL, is responsible for directly monoubiquitinating Fancd2 and FancI [137]. Additionally, the FA core complex is activated through phosphorylation by ATR/Chk1, which initiates the FA pathway following DNA damage [133] .

3.1.1.2 The Fancd2 and FancI heterodimer

The Fancd2-FancI heterodimer is monoubiquitinated by the FA core complex, in which one proteins' monoubiquitination is dependent on the other. Further, Fancd2-FancI recruitment, which is also interdependent, occurs independently of the FA core complex recruitment [136]. Fancd2-FancI recruitment depends on the DNA damage sensor protein UHRF1 and is further monoubiquitinated through its association with proliferating cell nuclear antigen (PCNA) [107, 134, 136, 138]. Fancd2 and FancI then recruit downstream effector proteins that are involved in various replication, repair, and cell cycle processes [107]. Moreover, Fancd2 and FancI have been described to have roles independent of one another outside of the heterodimer [107, 134, 136, 139].

3.1.1.3 Fancd2 post-translational modifications

Fancd2 (as well as FancI) undergo several post-translational modifications during FA pathway activation [136, 140]. Fancd2 is phosphorylated by ATM at several residues following IR. This phosphorylation is important in cell cycle arrest following IR, but not required for Fancd2 monoubiquitination, recruitment to DNA damage sites,

and ICL repair. In contrast, ATR phosphorylates Fancd2 during replication stress, and this modification is required for monoubiquitination and repair of ICLs [140].

Fancd2 monoubiquitination by the FA core complex is required for Fancd2 foci formation and co-localization with downstream effector proteins following FA pathway activation during replication stress, ICL repair, and DSB repair. Monoubiquitination and foci formation are interdependent on one another, as abrogating one process disrupts the other. There has not been a report of Fancd2 polyubiquitination and how this process is inhibited has been hinted at since uncovering the Fancd2-FancI heterodimer crystal structure in mice [107, 134, 136, 140]. Both monoubiquitinated sites are within the heterodimer interface. It has been hypothesized that the association of Fancd2 and FancI through each other's ubiquitin moiety may prevent further ubiquitination to occur [140]. Additionally, deubiquitination of both proteins is required to halt to the FA pathway following complete repair. This process is carried out by USP1 and its binding partner UAF1 [134, 140]. Fancd2 is also SUMOylated, a post-translational modification that involves covalently attaching SUMO (small ubiquitin-like modifier) proteins to other proteins [141]. The SUMO E3 ligases, PIAS1 and PIAS4 are responsible for SUMOylation of the Fancd2-FancI heterodimer which leads do the deactivation of the FA pathway through resolution of Fancd2-FancI foci at repair sites [136].

3.1.1.4 The role of the FA pathway in ICL repair

ICLs are forms of DNA damage that result from endogenous or exogenous agents crosslinking DNA, creating a barrier to DNA replication, transcription, and cell cycle progression [107]. The FA pathway has been well-characterized to participate in ICL repair, as loss of FA genes leads to an impairment of this process [107, 133, 134, 136, 137]. ICL repair can be described to occur in various steps in which distinct FA proteins participate in repair [136, 137]. The first step involves recognition of the ICL through the FA core complex and the Fancd2-FancdI recruiter, UHRF1. Once the monoubiquitinated Fancd2-FancI heterodimer is recruited, downstream effector proteins, such as SSEs are recruited and participate in the next step of ICL repair which involves steps of NER. This results in the unhooking of the crosslink and generation of a DSB. The final step of ICL repair is DSB repair, which is thought to primarily involve HR, however under certain conditions, cNHEJ, SSA, or alt-EJ may also be used to complete repair [134, 136, 137, 142].

3.1.1.5 The role of the FA pathway in replication stress

The FA pathway also plays a role in replication stress independent of DNA damage. Fancd2 has been identified to be involved in replication restart and suppressing replication origin firing [139]. Additionally Fancd2 is involved in preventing ssDNA

accumulation and deleterious replication intermediates [107]. FancI has been identified to promote the recruitment of the FA core complex, suggesting that this protein can function upstream of this complex [107, 134]. Furthermore, in the case of less severe replication stress, FancI can function to activate dormant origin firing to ensure complex DNA replication [107]. Additionally, Fancd2 in conjunction with RNAse H1 prevents DNA-RNA hybrids during stalled replication [107]. Lastly, underreplication can result in the formation of UFBs that persist into mitosis. Fancd2 and FancI are recruited to these structures and are required for their resolution during cytokinesis [107, 134].

3.1.1.6 The role of the FA pathway in DSB repair

FA proteins also function in various DSB repair pathways, independent of the DSB intermediate produced during ICL repair. Indeed, several genes involved in HR are also FA complementation groups (BRCA1/2, BRIP1, PALB2, RAD51) [107, 136]. Furthermore, end-resection, which is required for HR, alt-EJ, and SSA, depends of Fancd2. Fancd2 is recruited following MRN-induced end resection, and Fancd2 is required for CtIP recruitment for further DNA processing [136]. SLX4, which is an SSE, is also an FA complementation group (P), and functions in the resolution of HR intermediates [107, 133, 134, 136, 137]. Fancd2 is also thought to inhibit cNHEJ. This is primarily through inhibiting Ku binding to DSB ends and is likely due to the role of

Fancd2 in end resection [136, 137, 142]. Lastly, Fancd2 was identified to be involved in alt-EJ repair. Not only have FA proteins that participate in NER, have been implicated in alt-EJ, but in some conditions, Fancd2 can promote recruitment of DNA polymerase Theta, a protein required for alt-EJ [94, 134] (See Chapter 2, Discussion).

3.1.2 CRL4^{CDT2}, an E3 ubiquitin ligase

Protein turnover by the ubiquitin-proteasome system is crucial for maintaining normal cell physiology [143]. As such, protein complexes known as E3-ubiquitin ligases function to carry out proteolysis during cellular processes [144]. One of the largest known families of E3 ubiquitin ligases, the Cullin RING E3 ubiquitin ligases (CRLs), function to maintain genome integrity by regulation of protein levels. One specific type of CRL, CRL4^{CDT2}, has emerged as a master regulator of the genome [143-145].

CRL4^{CDT2} is comprised of a multiprotein structure, similar to other E3 ubiquitin ligases. A scaffold protein known as CUL4 binds to the adaptor protein DDB1. DDB1 can bind multiple DCAF (DDB1- and CUL4- associated factors) that confer substrate specificity. The DCAF of CRL4^{CDT2}, is CDT2 which recruits specific proteins and facilitates the transfer of ubiquitin by bringing target proteins in contact with Roc1a, a CRL4 component which functions to recruit ubiquitin-charged E2 proteins (Fig28A) [143, 145].

$CRL4^{CDT2}$ is a unique E3 ubiquitin ligase in that is known to target proteins for destruction using a unique PCNA-dependent mechanism. $CRL4^{CDT2}$ binds to DNA-bound PCNA and ubiquitinates proteins also bound to PCNA [143-146]. A major function of $CRL4^{CDT2}$ is to control DNA replication by ensuring replication only occurs once per cell cycle through the regulation of various licensing factors. One well-characterized substrate of $CRL4^{CDT2}$ is CDT1, a licensing factor known to cause rereplication phenotypes when overexpressed [143-148]. Additionally, $CRL4^{CDT2}$ also regulates various forms of DNA repair including BER, NER, HR, and TLS [143, 147, 148].

3.1.2.1 Cullin-RING E3 ubiquitin ligases

Cullin-RING (Really Interesting New Gene) E3 ubiquitin ligases represent one of the largest classes of both RING and E3 ubiquitin ligases [149]. There are at least 7 known CRLs identified in mammals (Cul1-4A/B, 5, and 7) with diverse functions. CRLs all have similar structures, although assembly of these complexes may vary. Much of what is known about CRL structure and function is through studies of CRL1 (Skp1-Cul1-Fbox or SCF) E3 ubiquitin ligases which function during the cell cycle [149, 150].

Overall, CRLs are comprised of cullin scaffolds that assemble with bridging adaptor proteins that bind substrate receptor proteins. These substrate receptor proteins confer specificity to target proteins [149, 150]. Additionally, CRLs contain RING finger

proteins that bind E2 enzymes. CRLs recognize proteins for degradation through unique sequences termed "degrons" which proteins that are degraded by various CRLs often contain. CRLs also are regulated by post-translational modifications [151]. Neddylation, the process of transferring Nedd8, a ubiquitin-like protein, to CRLs is crucial for initiating the appropriate conformational change to ensure proper function. As such, this modification must be regulated to ensure that CRL-mediated proteolysis is controlled. This is carried out through deneddylation by a structure known as the COP9-sginalosome [149-151]. Further, a protein known as CAND1, participates in substrate receptor exchange as an additional regulation of CRLs [149, 150]. As CRLs control several major cellular processes, these complexes are often hijacked during diseases and viral infection. As such, CRLs are an attractive candidate for therapeutic treatments, an alternative to the cytotoxicity that results from targeting all proteolysis through the proteasome [149-151].

3.1.2.2 The role of the COP9 signalosome (CSN) in regulating CRLs

The COP9 signalosome (CSN) is a multiprotein complex that was first identified in *Arabidopsis*, and then later in humans [152]. CSN is highly conserved from yeast (*S. pombe* and *S. cerevisiae*) to plants to humans and is thought to be crucial for development in these organisms [152-154]. The first key that CSN regulated proteolysis was the

observation that the CSN structure resembled the 26S proteasome lid [152, 153, 155]. CSN is comprised of 8 subunits (1-8) which all have different functions within the complex. The most conserved subunits identified are CSN2 and CSN5, with CSN5 being the most studied subunit to date [152, 155]. Studies on the SCF E3 ubiquitin ligase revealed that CSN binds directly to CRLs and regulates proteolysis through deneddylation [153]. Specifically, the CSN5 subunit was found to have metalloprotease activity and is dependent on the CSN complex for properly cleavage of the Nedd8 moiety [152, 153, 155]. Interestingly, other CSN subunits have function outside of the 8-protein complex and can form subcomplexes that function independently, mainly in cell cycle progression [152].

3.1.2.3 The role of $CRL4^{CDT2}$ in regulating the genome integrity

$CRL4^{CDT2}$ plays a crucial role in maintaining genome integrity through regulating the cell cycle and the DDR [143-145]. There have been several identified substrates of $CRL4^{CDT2}$ and this number is constantly growing [143]. The most well-described substrate, CDT1, functions in DNA replication and as such $CRL4^{CDT2}$ degradation ensures that the genome is duplicated once per cell cycle. Other targets of $CRL4^{CDT2}$ also function during licensing such as cdc6 and Set8. Additionally, $CRL4^{CDT2}$ targets proteins that regulate cell cycle checkpoints, such as p21 and Chk1 kinase [143-145].

As $CRL4^{CDT2}$ often interacts with its targets through DNA-bound PCNA, a consensus sequence known as the PIP box is needed for both $CRL4^{CDT2}$ interaction with PCNA as well as the interaction of all target proteins [144, 145]. The canonical PIP box contains a Q with a hydrophobic residue two amino acids downstream, and two aromatic resides another two amino acids downstream (QxxΨxxϑϑ). A majority of $CRL4^{CDT2}$ targets are marked for destruction through a unique motif located within the PIP box known as a PIP degron. A PIP degron contains a TD domain buried within the PIP box that confers high affinity binding to PCNA. The second part of the PIP degron is a basic residue for amino acids downstream of the PIP box (QxxΨTDϑϑxxxB) [144, 145]. There are a few exceptions to this, including with Chk1, where $CRL4^{CDT2}$ can target proteins for degradation without PCNA and in the absence of a PIP degron [143, 156].

Further, CDT2 has been found to be upregulated in numerous cancers [143, 146, 157]. An "addiction" to CDT2 was identified in a number of cancer cell lines, with CDT1 knockdown resulting in a partial rescue [157]. Of note, CDT1 knockdown cannot rescue G_2/M arrest that results from *cdt2* inhibition, suggesting that other mechanisms of CDT2 overexpression can promote tumorigenesis [146]. CDT2 overexpression in cancer is correlated with poor prognosis and chemo-resistance. As such, drugs that target $CRL4^{CDT2}$ have been developed with promising results [143, 146, 157]. Developing

improved therapeutics to target this complex is of great interest particularly in recurrent cancers that have become resistant to previous treatments.

3.1.3 Introduction summary

The above introduction details current literature on both the FA pathway and the $CRL4^{CDT2}$ complex and their respective roles in safeguarding the genome. Proteins from both the FA and the $CRL4^{CDT2}$ complex have been identified as hits in our candidate screen for regulators of acentric DNA segregation. The remainder of this chapter will discuss reagents that were generated to study the role of Fancd2 in acentric DNA segregation, the $CRL4^{CDT2}$ complex and its role in acentric DNA segregation, and proposed mechanisms for how these two pathways/complexes may be working together or in parallel to promote acentric DNA segregation during mitosis.

3.2 Results

3.2.1 Generation of a Fancd2 monoubiquitination mutant using CRIPSR Homology Directed-Repair

We previously identified that Fancd2 was required for acentric DNA segregation and papillar cell survival following DNA damage [47]. To test on a molecular level whether Fancd2 monoubiquitination was required for acentric DNA segregation, we used CRIPSR-mediated homology directed repair (HDR) to generate a point mutation in the endogenous Fancd2 locus at the conserved monoubiquitination site (K595) (Fig23A').

This was carried out using two-step HDR in which during the first step, two pairs of gRNAs that target sites flanking a 490 bp region (Fig23C) were used:

FANCD2 gRNA1F: GTCGTGGGGCGATGATTTGTCAC

FANCD2 gRNA1R AAACGTGACAAATCATCGCCCCA

and

FANCD2 gRNA2F: GTCGTACGCACCGAGGCATCAAT

FANCD2 gRNA2R: AAACATTGATGCCTCGGTGCGTA

This region contained the K595 site and after DSBs induced by Cas9 to these sites, the breaks were repaired with a homologous donor cassette containing matching homology arms to the endogenous sequence, as well as a GFP tag. The resulting intermediate animal contained a Fancd2 truncation deletion at 2106-2595 bp with a GFP insertion. This intermediate does not function as a reporter of Fancd2 localization as the GFP tag is not in frame and is translated separately. Hereafter, we refer to this intermediate line as "*fancd2* deletion." The last step involved generating two additional pairs of gRNAs:

FANCD2 gRNA3F: GTCGCCAAATCTTCGTACAGGTG

FANCD2 gRNA3R: AAACCACCTGTACGAAGATTTGG

and

FANCD2 gRNA4F: GTCGAATCACAAGCTCTGTAAAT

FANCD2 gRNA4R: AAACATTTACAGAGCTTGTGATT

These gRNAs were targeted to delete the GFP cassette and replace it with a Fancd2 sequence containing the K595R deletion. The homology arms contained mutations in the PAM site to prevent Cas9-induced DSBs in the repair template (Fig23B). The final Fancd2^{K595R} mutation was checked using PCR to confirm loss of GFP. There were four independent lines generated from the intermediate line that showed GFP loss after expression of the second set of gRNAs. To confirm that the endogenous Fancd2 indeed contained the K595R mutation, primers were designed around the 490 bp region that was deleted to create the final mutants (Fig23C). We confirmed that our primers amplified a 490 bp region in all of the four GFP-negative lines. Further, our PCR conditions were such that the same primers did not amplify a 490 bp region in the Fancd2-deletion line (Fig23D). As additional controls, we used these primers to amplify the 490 bp region in w^{1118} flies and in flies heterozygous for a *fancd2* deficiency. As expected, we see a clear 490 bp band after PCR with w^{1118} DNA and a fainter band in with Fancd2 deficiency DNA (Fig23D).

We sent the resulting amplified DNA of the 4 lines for DNA sequencing and confirmed that ¾ of the lines contained the K595R mutation (lines #2-2, #4-3, and #1-3)

(Fig23E). The #5-2 line did not contain a K595R mutation but instead contained a D644E mutation (Fig23F). Interestingly, this residue is conserved in humans (D604E) despite Fancd2 having only 23% identity across *Drosophila* and humans. In conclusion, we successfully generated 3 confirmed endogenous *fancd2*^{K595R} mutant lines, a Fancd2-deletion, and a novel *fancd2*^{D644E} mutant line.

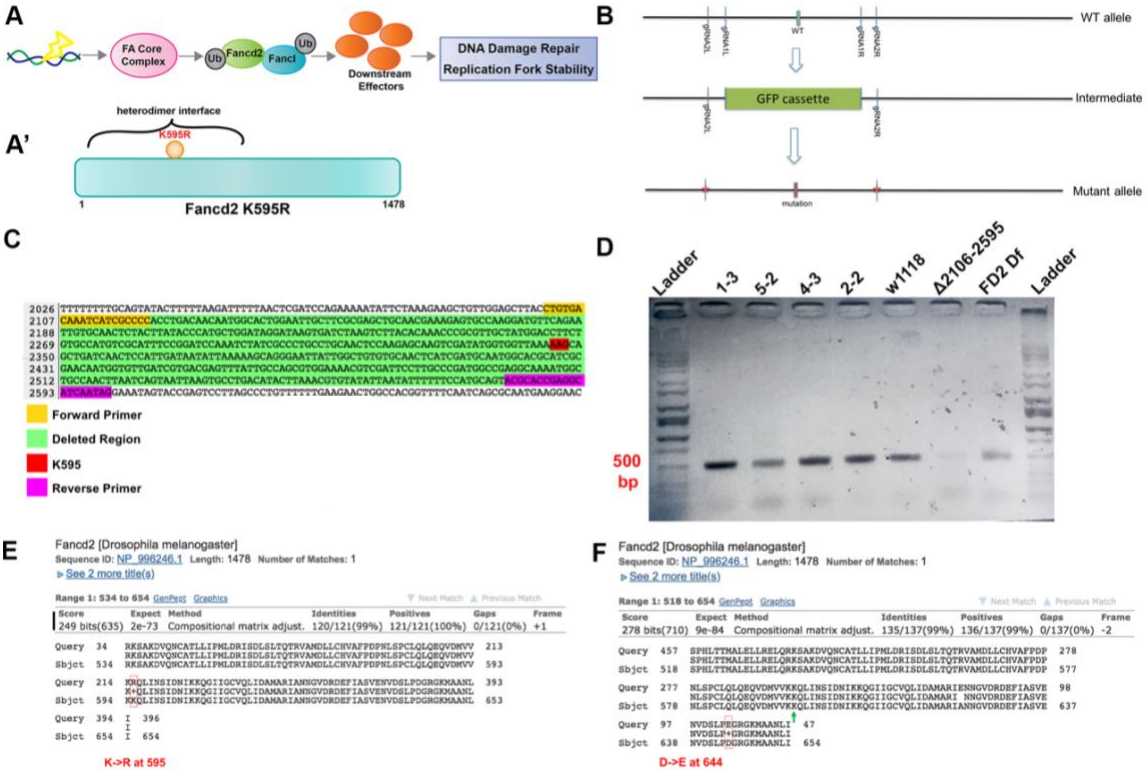

Figure 23: Generation of a Fancd2 monoubiquitination mutant

(A) Schematic of the FA pathway (See Introduction) (A') Schematic of Fancd2 protein with mutated monoubiquitination residue (K595R) (B) Two-step CRISPR homology-director repair scheme used to generate *fancd2*^{K595R} animals (See Results)(C) Portion of Fancd2 nucleotide CDS with deleted region (green) from step 1 of the *fancd2*^{K595R} construction. Primers forward, yellow; reverse,

magenta) were designed to amplify this 490 bp region for DNA sequencing to confirm the K595R mutation (red). (D) Gel electrophoresis of 490 bp region of Fancd2 amplified from primers generated in C. From left to right – Hi-Lo Ladder, line #1-3, line #5-2, line #4-3, line #2-2, w118, Fancd2 deletion, Fancd2 deficiency, Hi-Lo Ladder. The 500 bp band is labeled in red (E) Sequence alignment from NCBI BLAST for *fancd2*^{K595R} #1-3 line (representative of lines #4-3 and #2-2) (Query) to *Drosophila* Fancd2 (Subject). (F) Sequence alignment from NCBI BLAST for *fancd2*^{D644E} (line #5-2) (Query) to *Drosophila* Fancd2 (Subject). For E-F, point mutation indicated by red box and notation.

3.2.2 Characterization of whole fly and tissue-specific phenotypes in *fancd2*^{K595R} *animals*

We then sought out to characterize the *fancd2*^{K595R} mutant animals (Table 2). All three lines and the *fancd2*-deletion line were homozygous viable. Every line with the exception of #4-3, were also homozygous fertile, allowing us to generate additional fly stocks using these mutants. We suspect that #4-3 may contain additional second site mutations. We then measured the ratio of homozygous to heterozygous progeny that eclosed from heterozygous parents for each line. We found that with the exception of line #1-3, all lines had an overrepresentation of heterozygous mutants that eclosed compared to homozygous mutants (Table 2). Additionally, we used *hs-I-Cre*I and 20 Gy of X-Ray irradiation (IR) during the second larval instar stage to see if these animals displayed an DSB-specific decrease in papillar cell number, similar to *fancd2* RNAi animals. Indeed, of the lines tested, there was a DSB-specific decrease in papillar cell number.

Table 2: *fancd2*^{K595R} CRISPR mutant features

Line	Homozygous Viability	Homozygous Fertility	Ratio of Progeny (Homozygous: Heterozygous)	I-CreI Rectum Phenotype (Induced 2nd Instar)	X-Ray Rectum Phenotype (Induced in 2nd Instar)
#2-2	Yes	Yes	0.553605504	Not Tested	Not Tested
#4-3	Yes	No	0.295555556	Yes	Not Tested
#1-3	Yes	Yes	1.531400966	Yes	Yes
Δ2106-2595-GFP	Yes	Yes	0.803383283	Yes	Yes

We also observed that a subset of *fancd2*^{K595R} adults have necrotic eye spots in the absence of exogenous DSBs (Fig24A). Additionally, we investigated whether the previously uncharacterized *fancd2*^{D644E} mutants had a DSB-specific decrease in papillar cell number. Interestingly, we do observe a DNA damage-specific decrease in these mutants similar to the *fancd2*^{K595R} mutants (Fig24B-C). This is striking, considering this is a previously uncharacterized point mutation in a conserved residue (See Discussion for Analysis).

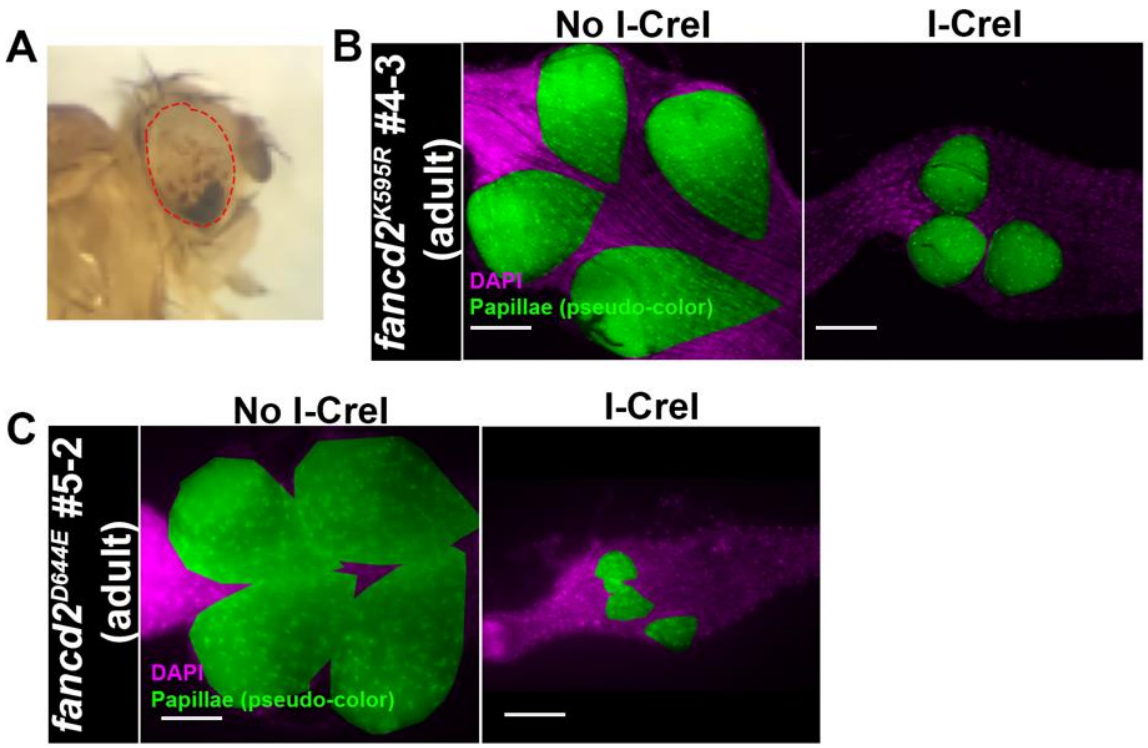

Figure 24: Fancd2^{K595R} tissue-specific and whole fly phenotypes

(A) Adult fly with necrotic eye spots from *fancd2*^{K595R} mutant. Red hatched outline – eye. (B) Adult rectums of *fancd2*^{K595R} (line *#4-3*) animals +/- *hs-I-CreI*. Papillar cells (pseudo-colored), green; DNA (DAPI), magenta. (DNA). Scale bars = 50μm. (C) Adult rectums of *fancd2*^{D644E} (line *#52*) animals +/- *hs-I-CreI*. Labeling as in B.

An outstanding question from our previous study in the role of monoubiquitinated Fancd2 on promoting acentric DNA segregation (See Chapter 2), was whether monoubiquitinated Fancd2 regulated Mre11 foci removal similarly to RPA3 during mitosis. To test this, we generated flies containing both the *fancd2*^{K595R} mutation and *ubi-mre11-GFP*. Using *hs-I-Cre*I to induce DSBs during the second larval

instar stage, we observed that Mre11 foci persist in papillar cells following the first mitosis (Fig25A-B). This is in contrast to what we observe in WT animals, which clear Mre11 foci prior to NEBD (Fig25B). We conclude that monoubiquitinated Fancd2 is required for both RPA3 and Mre11 foci removal following DSBs.

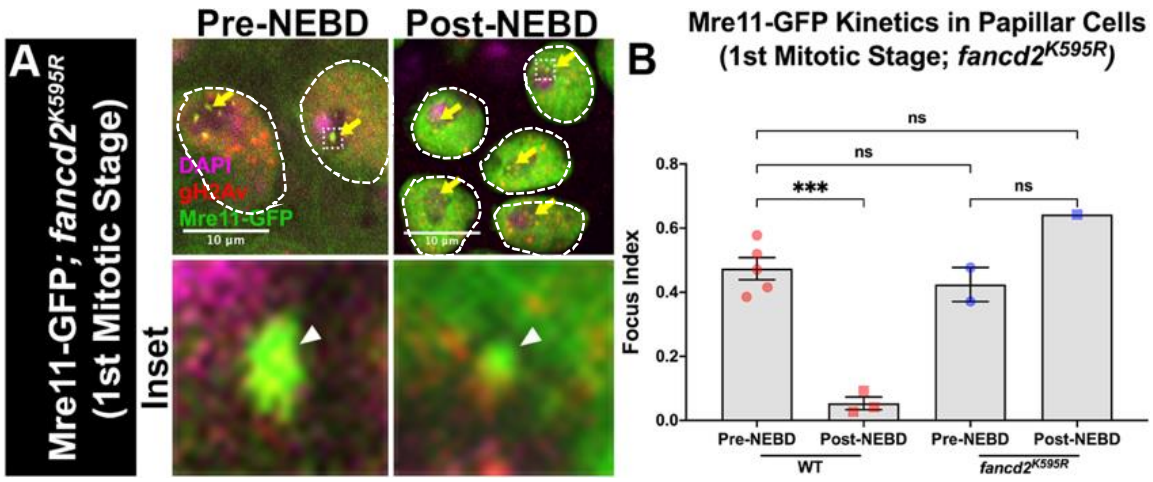

Figure 25: Fancd2^{K595R} is required for Mre11 foci removal during mitosis

(A) Mre11 and gH2Av recruitment to *fancd2*^{K595R} papillar cells +/- *hs-I-Cre*I. DNA (DAPI), magenta; Mre11, green; gamma H2Av, red . Yellow arrows= Mre11+ gamma H2Av+ foci. Hatched box= area magnified 10X in the corresponding inset below each panel. White arrowhead= enlarged micronucleus. Hatched outline= nuclei. Scale bars = 10µm. (F) Quantification of Mre11+ gH2Av+ foci recruitment in *fancd2*^{K595R} papillar cells +*hs-I-Cre*I pre- and post- the 1st mitotic stage. WT data from experiment performed in Fig12B. Each data point represents a single animal (N). Statistical test: Ordinary one-way ANOVA, p=0.0002. See Methods for statistical notations.

3.2.3 Generation of Fancd2-GFP WT and Fancd2-GFP K595R transgenic animals

To study the localization and other protein dynamics of Fancd2, we used a pBID vector (Amgen) to generate animals expressing GFP-tagged Fancd2. We cloned full length Fancd2 as well as Fancd2 with a K595R mutation into the PBID vector with a codon optimized eGFP sequence at the N-terminus. This fusion protein is under the expression of a *ubi* promoter contained within the vector. This construct, which contained attB sites allowing for phiC31-mediated integration, was injected into flies expressing attP40 landing sites (Fig26A). Animals with successful integration were then selected and used to generate various fly stocks (Fig26B-B').

To characterize the GFP-Fancd2 WT and K595R flies, we investigated both tissue-specific and whole fly phenotypes. Using 20 Gy IR, we tested to see if GFP-Fancd2 WT expression had an effect on survival to adulthood in $fancd2^{K595R}$ animals. Indeed, we observed an increase in the percent of animals that survived to adulthood in GFP-Fancd2 WT; $fancd2^{K595R}$ animals compared to $fancd2^{K595R}$ animals alone (Fig26C). Next, we tested to see if GFP-Fancd2 WT could similarly rescue survival in Fancd2-deletion mutants. We find that in both animals with GFP-Fancd2 WT, Fancd2-deletion and with the Fancd2-deletion alone, *hs-I-Cre*I- induced DSBs resulted in high pupal lethality with a majority of animals dying as pharate adults (meaning they die near the end of

pupation- data not shown). We then determined if GFP-Fancd2 WT animals could rescue Fancd2-deletion rectum phenotypes following DSBs. Intriguingly, we find that with GFP-Fancd2 WT animals, there is still a significant decrease in adult papillar cell number following DSBs (Fig26D-E). These findings suggest that GFP-Fancd2 can rescue K595R, but not deletion, mutants in Fancd2.

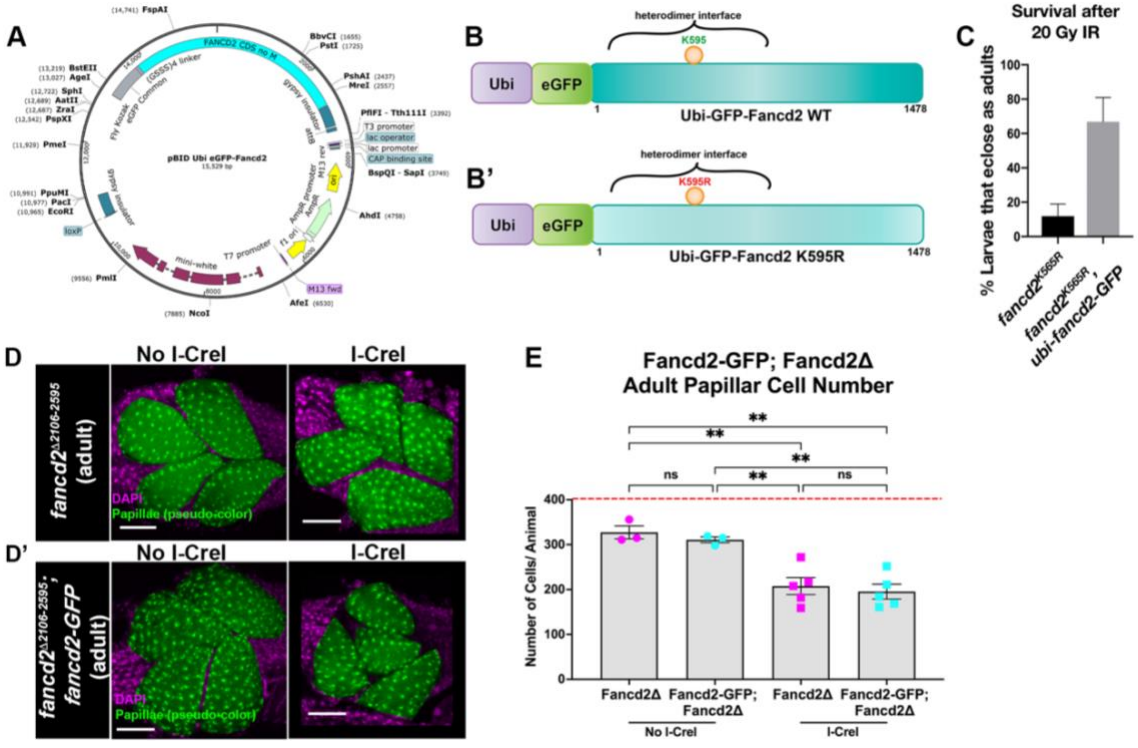

Figure 26: Generation of GFP-tagged Fancd2 WT and K595R animals

(A) Sequence map of pBID vector with Ubi-eGFP-Fancd2 cloned inside. (B-B') Schematics of GFP-Fancd2 transgenic constructs generated in A. with WT monoubiquitination reside (B) and the K595R point mutation (B') (C) Quantification of the percent survival of flies that eclose as adults

in *fancd2*^{K595R} mutants with and without *Ubi-Fancd2-GFP*. (D-D′) Adult rectums of Fancd2 deletion animals +/- hs-I-CreI with (D′) and without (D) *Ubi-Fancd2-GFP* . Papillar cells (pseudo-colored), green; DNA (DAPI), magenta. (DNA). Scale bars = 50μm. (E). Quantification of adult papillar cell number in Fancd2 deletion animals +/- *Ubi-Fancd2-GFP* animals +/- *hs-I-Cre*I. Red dashed line= expected number of papillar cells in a WT adult. Each condition has at least 2 biological replicates. Each data point represents a single animal (N). Statistical test: Ordinary one-way ANOVA, p=0.0002. See Methods for statistical notations.

3.2.4 Characterization of tissue-specific and whole-fly phenotypes in Fancd2-GFP WT and Fancd2-GFP K595R transgenic animals

We then sought to determine GFP-Fancd2 WT localization in various *Drosophila* tissues. We find that GFP-Fancd2 WT displays pan-nuclear expression even in the absence of exogenous DNA damage in the adult midgut *(small intestine), the developing (L3) brain, and in the developing (L3) rectum (See Chapter 2). We specifically observe an increase in GFP-Fancd2 WT expression in polyploid enterocytes (ECs) in the midgut (Fig27A). This is likely due to the constant cycling of cells in the midgut during turnover. Fancd2 plays a major role in S-phase and it is likely that cells that frequently enter S-phase (endocycling cells) would have increased expression [107, 134, 142]. Additionally, neural brain progenitors also contain pan-nuclear GFP-Fancd2 WT expression (Fig27B).

Lastly, GFP-Fancd2 WT displays pan-nuclear expression in papillar cells at both the larval (endocycle) and pupal (mitosis) stage (Fig27C-D). Further, to test if IR caused persistent GFP-Fancd2 WT foci, similar to what was observed with *hs-I-Cre*I (Chapter 2,

Fig20A-B), we live-imaged animals expressing both GFP-Fancd2 WT and GFP-Fancd2 K595R after 20 Gy IR during the second larval instar stage. We observed persistent Fancd2 foci in 20 Gy IR GFP-Fancd2 WT but not in 20 Gy IR GFP-Fancd2 K595R flies nor in 0 Gy IR GFP-Fancd2 WT flies (Fig27D). These data suggest that similar to our *fancd2*^{K595R} mutants, our GFP-Fancd2 K595R flies also fail to properly localize DNA repair foci following DSBs in papillar cells. Overall, our results suggest that GFP-Fancd2 is a useful model to study ubiquitination-dependent recruitment of Fancd2 in response to DSBs.

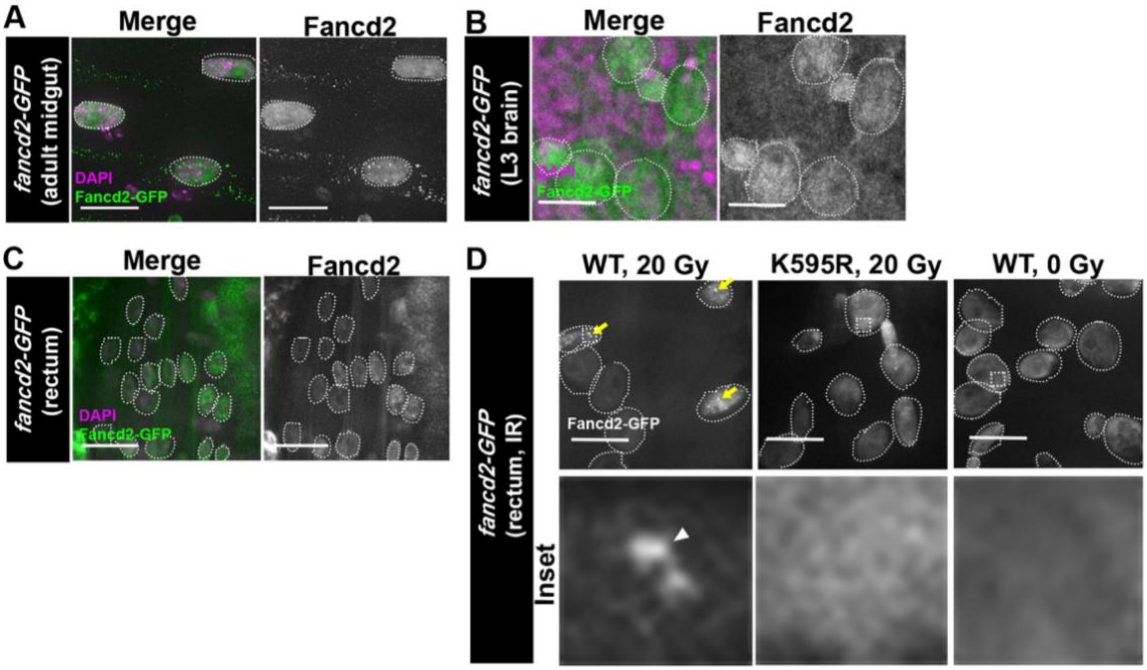

Figure 27: Fancd2-GFP localization in tissues

(A) Ubi-Fancd2-GFP expression in the adult midgut. Enterocytes are outlined with white hatched lines. DAPI, magenta, Fancd2-GFP, green. Scale bars = 10μm (B) Ubi-Fancd2-GFP expression in the L3 brain. Neuroblasts and ganglion mother cells are outlined with white hatched lines. All other labeling as in A. (C) Ubi-Fancd2-GFP expression in the L3 rectum. Papillar cells are outlined with white hatched lines. All other labeling as in A. (D) Ubi-Fancd2-GFP (WT and K595R) expression in the 1st mitotic stage rectum after IR. . Papillar cells are outlined with white hatched lines. Fancd2-GFP, gray. Yellow arrows= Fancd2+ foci. Hatched box= area magnified 10X in the corresponding inset below each panel. White arrowhead= enlarged micronucleus. Scale bars = 10μm.

3.2.5 CRL4^{CDT2} is required for papillar cell survival following DSBs

As mentioned in **Chapter 2**, we developed an assay for a candidate screen to identify novel genes that are required for acentric DNA segregation (Table 1). A majority of these genes were not a hit, however we did identify several genes that code proteins for the CRL4^{CDT2} E3 ubiquitin ligase. Using identical methodology as in Chapter 2, Fig10A, we used RNAi to knockdown genes identified to be required for the G_2/M phase arrest in *Drosophila* cells [91]. One of the genes that displayed a *hs-I-Cre*I-specific decrease in adult papillar cell number when knocked down was *ddb1. ddb1* encodes the protein DDB1 which is the adaptor protein for CRL4^{CDT2}. As a follow-up, we knocked down all the genes that encode the protein components of the CRL4^{CDT2} E3 ubiquitin ligase (*cul4*, *ddb1*, *cdt2*, *roc1a*) using multiple RNAi fly lines and quantified differences in adult papillar cell number. Similar to what we observed in our initial screen with *ddb1* knockdown, knocking down all components of the CRL4^{CDT2} complex resulted in a *hs-I-*

*Cre*I-specific decrease in adult papillar cell number (Fig28B-I). We thus concluded that $CRL4^{CDT2}$ is required for cell survival following DSBs in checkpoint-inactive papillar cells.

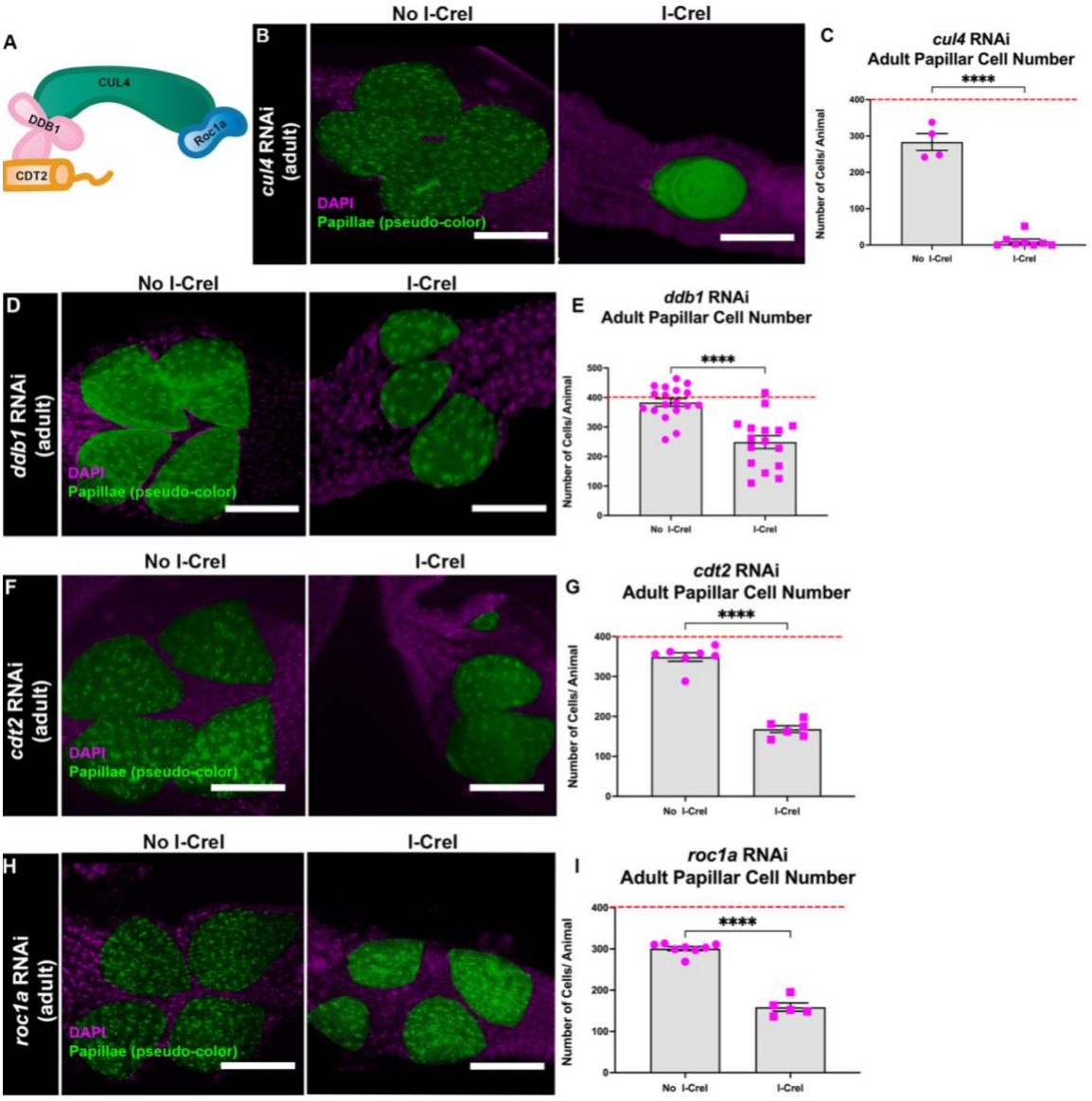

Figure 28: The CRL4^{CDT2} complex is required for adult papillar cell survival following DSBs

(A) Schematic of the CRL4^{CDT2} E3 ubiquitin ligase (B, D, F, H) Adult rectums of *cul4* (B), *ddb1* (D), *cdt2* (F), and *roc1a* (H) RNAi animals +/- hs-I-CreI. Papillar cells (pseudo-colored), green; DNA (DAPI), magenta. Scale bars = 50μm (C,E,G,I) Quantification of adult papillar cell

number in *cul4* (C), *ddb1* (E), *cdt2* (G), and *roc1a* (I) RNAi expressing animals +/- hs-I-CreI. Statistical test: Unpaired t-test, $p<0.0001$. See Methods for statistical notations.

3.2.6 *cdt2* is required for acentric DNA segregation during mitosis

After identifying that $CRL4^{CDT2}$ is required for adult papillar cell survival following DSBs, we then used methodology identical to Chapter 2, Fig11A, to investigate if $CRL4^{CDT2}$ was also required for acentric DNA fragment segregation. As the *cdt2* gene encodes the substrate recognizing protein that confers specificity of the $CRL4^{CDT2}$ complex, we knocked down *cdt2* using RNAi in animals expressing *byn>uas-CenpC-Tomato; HisH2Av-GFP; Moesin-GFP (*cell membrane marker). We then live imaged the animals during the mitotic stage during early pupal development and traced the fate of acentric fragments during mitosis. *cdt2* knock down did not induce significant DSBs on its own, as the no *hs-I-Cre*I controls did not show a significant amount of both acentric fragments and micronuclei (Fig29A). This is likely because we knocked down *cdt2* following the endocycle and prior to the next S-phase so any DSBs present during mitosis caused by rereplication phenotypes typically observed in $CRL4^{CDT2}$ mutants were not observed using our methods [158]. There was, however, a significant increase in the frequency of acentric DNA that mis-segregated into a micronucleus after *hs-I-Cre*I-induced DSBs (Fig29A-B). These data support the conclusion that $CRL4^{CDT2}$ is required

for micronuclei prevention when DSBs are present during mitosis and is thus a novel complex identified to be involved in acentric DNA segregation.

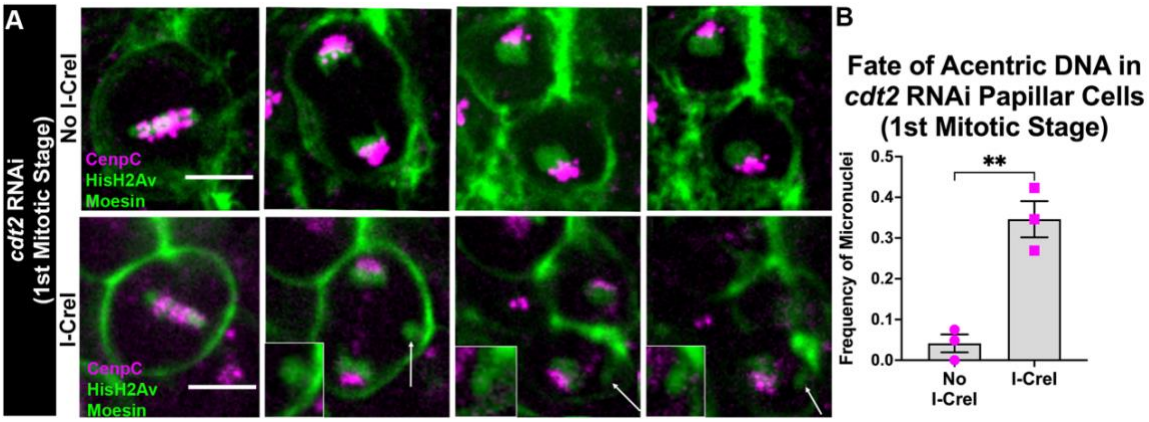

Figure 29: *cdt2* is required for acentric DNA segregation during mitosis

(A) Live imaging of papillar cell mitosis in *cdt2* RNAi animals +/- hs-I-CreI. HisH2Av, green; Moesin, green; CenpC, magenta. white arrow= acentric fragment, Scale bars = 5μm. Micronuclei enlarged 2x in inset (B) Quantification of the fate of acentric fragments in *cdt2* RNAi papillar cells +/- hs-I-CreI. Each condition has at least 2 biological replicates. Each data point represents a single animal (N). Statistical test: Unpaired t-test, p=0.0035. See Methods for statistical notations.

3.2.7 CSN subunits interact with Cdt2-GFP after IR in S2 cells

$CRL4^{CDT2}$ functions by targeting proteins for degradation during S-phase and the G_2/M phase checkpoint [159]. It has been hypothesized that several targets of $CRL4^{CDT2}$ have yet to be identified [143]. While $CRL4^{CDT2}$ targets are hypothesized to contain PIP box motifs and PIP degrons, increasing evidence suggests that not all targets conform to this requirement [156, 160]. It is thus important take unbiased approaches to identify

potential targets of $CRL4^{CDT2}$. We were specifically interested in identifying novel targets of $CRL4^{CDT2}$ following DSBs and not targets required for normal cycling cells. To identify novel targets of $CRL4^{CDT2}$ following DSBs, we cloned an eGFP-tag at the N-terminus of full-length *Drosophila* Cdt2 (Cdt2-GFP) into a PMT vector for expression in *Drosophila* S2 cells. With collaborators at U. Arizona, we then performed a Co-IP using an anti-GFP antibody in cells with and without X-Ray IR. Resulting IPs were then run on a mass spectrometer to identify interacting proteins.

Our analysis focused exclusively on peptides that interacted with Cdt2-GFP following IR. We successfully identified 480 proteins that interacted with Cdt2-GFP after IR-induced DNA damage (Table 3). Notable features of these proteins is that several members of the CSN were identified to interact with Cdt2-GFP (csn4 and csn7). This is consistent with our findings that *csn2*, which was a gene in our initial candidate screen, was also identified as a hit, having an DSB-specific decrease in adult papillar cell number (Fig30A-B). We thus conclude that the CSN is likely important in regulating $CRL4^{CDT2}$ following DSBs and possibly in acentric fragment segregation during mitosis.

Table 3: List of 480 proteins that interact with Cdt2-GFP following IR

Gene Symbol	Annotation
RpL10Ab	60S ribosomal protein L10a-2 OS=Drosophila melanogaster OX=7227 GN=RpL10Ab PE=1 SV=2
RpL13	60S ribosomal protein L13 OS=Drosophila melanogaster OX=7227 GN=RpL13 PE=1 SV=1
eEF1beta	Probable elongation factor 1-beta OS=Drosophila melanogaster OX=7227 GN=eEF1beta PE=1 SV=3
Lam	Lamin Dm0 OS=Drosophila melanogaster OX=7227 GN=Lam PE=1 SV=4
RpL9	60S ribosomal protein L9 OS=Drosophila melanogaster OX=7227 GN=RpL9 PE=1 SV=2
RpL10	60S ribosomal protein L10 OS=Drosophila melanogaster OX=7227 GN=RpL10 PE=1 SV=1
Hsp27	Heat shock protein 27 OS=Drosophila melanogaster OX=7227 GN=Hsp27 PE=1 SV=2
Prx2540-1	LD11278p OS=Drosophila melanogaster OX=7227 GN=Prx2540-1 PE=2 SV=1
Echs1	CG6543, isoform A OS=Drosophila melanogaster OX=7227 GN=Echs1 PE=1 SV=1
Prosalpha1	Proteasome subunit alpha type-6 OS=Drosophila melanogaster OX=7227 GN=Prosalpha1 PE=1 SV=2
BEST:LD29996	GH21273p OS=Drosophila melanogaster OX=7227 GN=BEST:LD29996 PE=1 SV=1
NHP2	H/ACA ribonucleoprotein complex subunit 2-like protein OS=Drosophila melanogaster OX=7227 GN=NHP2 PE=1 SV=1

Vha26	V-type proton ATPase subunit E OS=Drosophila melanogaster OX=7227 GN=Vha26 PE=2 SV=1
gag	Gag protein (Fragment) OS=Drosophila melanogaster OX=7227 GN=gag PE=4 SV=1
RpS11	40S ribosomal protein S11 OS=Drosophila melanogaster OX=7227 GN=RpS11 PE=1 SV=1
Ostgamma	GH11935p OS=Drosophila melanogaster OX=7227 GN=Ostgamma PE=1 SV=1
CG6084	Uncharacterized protein, isoform D OS=Drosophila melanogaster OX=7227 GN=CG6084 PE=1 SV=1
TFAM	LD40493p OS=Drosophila melanogaster OX=7227 GN=TFAM PE=1 SV=1
Su(var)205	Heterochromatin protein 1 OS=Drosophila melanogaster OX=7227 GN=Su(var)205 PE=1 SV=2
ATPsyngamma	ATP synthase subunit gamma, mitochondrial OS=Drosophila melanogaster OX=7227 GN=ATPsyngamma PE=2 SV=2
CG3689	Uncharacterized protein, isoform C OS=Drosophila melanogaster OX=7227 GN=CG3689 PE=1 SV=1
SrpRbeta	GM04779p OS=Drosophila melanogaster OX=7227 GN=SrpRbeta PE=1 SV=2
mRpS22	GH07821p OS=Drosophila melanogaster OX=7227 GN=mRpS22 PE=1 SV=1
Chd64	Transgelin OS=Drosophila melanogaster OX=7227 GN=Chd64 PE=1 SV=1

CG7477	RE59232p OS=Drosophila melanogaster OX=7227 GN=CG7477 PE=1 SV=2
SsRbeta	Translocon-associated protein subunit beta OS=Drosophila melanogaster OX=7227 GN=SsRbeta PE=1 SV=2
RpS9	40S ribosomal protein S9 OS=Drosophila melanogaster OX=7227 GN=RpS9 PE=1 SV=2
Prosalpha4	Proteasome subunit alpha type-7-1 OS=Drosophila melanogaster OX=7227 GN=Prosalpha4 PE=1 SV=2
RpL26	GEO07453p1 OS=Drosophila melanogaster OX=7227 GN=RpL26 PE=1 SV=1
RpS5a	40S ribosomal protein S5a OS=Drosophila melanogaster OX=7227 GN=RpS5a PE=1 SV=1
qkr58E-3	LD46502p OS=Drosophila melanogaster OX=7227 GN=qkr58E-3 PE=2 SV=1
mip40	LD06557p OS=Drosophila melanogaster OX=7227 GN=mip40 PE=1 SV=1
RpL27A	60S ribosomal protein L27a OS=Drosophila melanogaster OX=7227 GN=RpL27A PE=1 SV=2
FK506-bp1	39 kDa FK506-binding nuclear protein OS=Drosophila melanogaster OX=7227 GN=FK506-bp1 PE=1 SV=2
CG	Uncharacterized protein, isoform A OS=Drosophila melanogaster OX=7227 GN=CG 7834 PE=1 SV=1
26-29-p	26-29kD-proteinase OS=Drosophila melanogaster OX=7227 GN=26-29-p PE=1 SV=1
zfh1	Zinc finger protein 1 OS=Drosophila melanogaster OX=7227 GN=zfh1 PE=1 SV=2
Sc2-RA	FI06688p (Fragment) OS=Drosophila melanogaster OX=7227 GN=Sc2-RA PE=2 SV=1
Pdhb	Pyruvate dehydrogenase E1 component subunit beta OS=Drosophila melanogaster OX=7227 GN=Pdhb PE=1 SV=1
Dic1	BcDNA.GH02431 OS=Drosophila melanogaster OX=7227 GN=Dic1 PE=1 SV=1
ACSL1	LD09909p OS=Drosophila melanogaster OX=7227 GN=ACSL1 PE=1 SV=1

CG6087	RH51633p OS=Drosophila melanogaster OX=7227 GN=CG6087 PE=1 SV=1
CG9273	CG9273 protein OS=Drosophila melanogaster OX=7227 GN=CG9273 PE=4 SV=1
eIF3f1	Eukaryotic translation initiation factor 3 subunit F-1 OS=Drosophila melanogaster OX=7227 GN=eIF3f1 PE=2 SV=1
Rpn6	26S proteasome non-ATPase regulatory subunit 11 OS=Drosophila melanogaster OX=7227 GN=Rpn6 PE=1 SV=1
Scox	AT19154p OS=Drosophila melanogaster OX=7227 GN=Scox PE=1 SV=1
mgr	Prefoldin subunit 3 OS=Drosophila melanogaster OX=7227 GN=mgr PE=1 SV=3
Gtp-bp	Signal recognition particle receptor subunit alpha homolog OS=Drosophila melanogaster OX=7227 GN=Gtp-bp PE=1 SV=2
Pglym78	Phosphoglycerate mutase OS=Drosophila melanogaster OX=7227 GN=Pglym78 PE=1 SV=2
CG40813	Uncharacterized protein OS=Drosophila melanogaster OX=7227 GN=CG40813 PE=4 SV=2
eIF6	Eukaryotic translation initiation factor 6 OS=Drosophila melanogaster OX=7227 GN=eIF6 PE=2 SV=3
BEST:CK00496	Uncharacterized protein, isoform A OS=Drosophila melanogaster OX=7227 GN=BEST:CK00496 PE=1 SV=1
Prosbeta7	Proteasome subunit beta type-4 OS=Drosophila melanogaster OX=7227 GN=Prosbeta7 PE=2 SV=1
RpS7	40S ribosomal protein S7 OS=Drosophila melanogaster OX=7227 GN=RpS7 PE=1 SV=1
Arf79F	ADP-ribosylation factor 1 OS=Drosophila melanogaster OX=7227 GN=Arf79F PE=1 SV=2
	IP11827p (Fragment) OS=Drosophila melanogaster OX=7227 PE=2 SV=1

scu	3-hydroxyacyl-CoA dehydrogenase type-2 OS=Drosophila melanogaster OX=7227 GN=scu PE=1 SV=1
mask	Ankyrin repeat and KH domain-containing protein mask OS=Drosophila melanogaster OX=7227 GN=mask PE=1 SV=2
	RE14563p OS=Drosophila melanogaster OX=7227 PE=2 SV=1
mRpS26	Probable 28S ribosomal protein S26, mitochondrial OS=Drosophila melanogaster OX=7227 GN=mRpS26 PE=2 SV=1
hyd	E3 ubiquitin-protein ligase hyd OS=Drosophila melanogaster OX=7227 GN=hyd PE=1 SV=3
CG3995	Uncharacterized protein OS=Drosophila melanogaster OX=7227 GN=CG3995 PE=1 SV=1
Act88F	Actin, indirect flight muscle OS=Drosophila melanogaster OX=7227 GN=Act88F PE=1 SV=1
Cp190	Centrosome-associated zinc finger protein CP190 OS=Drosophila melanogaster OX=7227 GN=Cp190 PE=1 SV=2
mspo	M-spondin OS=Drosophila melanogaster OX=7227 GN=mspo PE=2 SV=1
mRpS5	Mitochondrial ribosomal protein S5, isoform A OS=Drosophila melanogaster OX=7227 GN=mRpS5 PE=1 SV=1
Dmel\CG5728	LD41803p OS=Drosophila melanogaster OX=7227 GN=Dmel\CG5728 PE=1 SV=2
Dmel21.3	LD37169p OS=Drosophila melanogaster OX=7227 GN=Dmel21.3 PE=1 SV=1
Sra-1	Cytoplasmic FMR1-interacting protein OS=Drosophila melanogaster OX=7227 GN=Sra-1 PE=1 SV=1
CG3902	GH07925p OS=Drosophila melanogaster OX=7227 GN=CG3902 PE=2 SV=1
CG3364	GH17623p OS=Drosophila melanogaster OX=7227 GN=CG3364 PE=2 SV=1

abs	ATP-dependent RNA helicase abstrakt OS=Drosophila melanogaster OX=7227 GN=abs PE=1 SV=1
CtBP	C-terminal-binding protein OS=Drosophila melanogaster OX=7227 GN=CtBP PE=1 SV=3
RpL18	60S ribosomal protein L18 OS=Drosophila melanogaster OX=7227 GN=RpL18 PE=1 SV=1
Rcc1	Regulator of chromosome condensation OS=Drosophila melanogaster OX=7227 GN=Rcc1 PE=1 SV=2
mRpL45	Probable 39S ribosomal protein L45, mitochondrial OS=Drosophila melanogaster OX=7227 GN=mRpL45 PE=2 SV=1
l(2)37Cc	Protein l(2)37Cc OS=Drosophila melanogaster OX=7227 GN=l(2)37Cc PE=2 SV=2
RpL13A	60S ribosomal protein L13a OS=Drosophila melanogaster OX=7227 GN=RpL13A PE=1 SV=1
CG30349-RA	FI03455p OS=Drosophila melanogaster OX=7227 GN=CG30349-RA PE=1 SV=1
SkpA	GEO01111p1 OS=Drosophila melanogaster OX=7227 GN=SkpA PE=1 SV=1
Kr-h2	Krueppel homolog 2 OS=Drosophila melanogaster OX=7227 GN=Kr-h2 PE=1 SV=1
CG2982	Bifunctional lysine-specific demethylase and histidyl-hydroxylase NO66 OS=Drosophila melanogaster OX=7227 GN=CG2982 PE=1 SV=1
Pfdn5	Probable prefoldin subunit 5 OS=Drosophila melanogaster OX=7227 GN=Pfdn5 PE=2 SV=1
EloB	Elongin B OS=Drosophila melanogaster OX=7227 GN=EloB PE=1 SV=1
CG9273	CG9273 protein (Fragment) OS=Drosophila melanogaster OX=7227 GN=CG9273 PE=4 SV=1
mRpS9	Mitochondrial ribosomal protein S9 OS=Drosophila melanogaster OX=7227 GN=mRpS9 PE=1 SV=1
FeCh	Ferrochelatase, mitochondrial OS=Drosophila melanogaster OX=7227 GN=FeCh PE=2 SV=1

Neos	Neosin, isoform A OS=Drosophila melanogaster OX=7227 GN=Neos PE=2 SV=1
zip	Myosin heavy chain, non-muscle OS=Drosophila melanogaster OX=7227 GN=zip PE=1 SV=2
Prosalpha7	Proteasome subunit alpha type-3 OS=Drosophila melanogaster OX=7227 GN=Prosalpha7 PE=1 SV=1
Clc	Clathrin light chain OS=Drosophila melanogaster OX=7227 GN=Clc PE=2 SV=1
pyd	Polychaetoid, isoform A OS=Drosophila melanogaster OX=7227 GN=pyd PE=1 SV=3
CG13638	LD35157p OS=Drosophila melanogaster OX=7227 GN=CG13638 PE=1 SV=1
Mtor	Nucleoprotein TPR OS=Drosophila melanogaster OX=7227 GN=Mtor PE=1 SV=1
porin	Voltage-dependent anion-selective channel OS=Drosophila melanogaster OX=7227 GN=porin PE=1 SV=3
Hexo2	Beta-hexosaminidase OS=Drosophila melanogaster OX=7227 GN=Hexo2 PE=1 SV=1
ics	LD43891p OS=Drosophila melanogaster OX=7227 GN=ics PE=2 SV=1
DHRS4	SD02021p OS=Drosophila melanogaster OX=7227 GN=DHRS4 PE=1 SV=1
CG11005	LD44221p OS=Drosophila melanogaster OX=7227 GN=CG11005 PE=1 SV=1
regucalcin	Regucalcin homologue OS=Drosophila melanogaster OX=7227 GN=regucalcin PE=1 SV=1
CG17544	Acyl-coenzyme A oxidase OS=Drosophila melanogaster OX=7227 GN=CG17544 PE=2 SV=1
RpII215	DNA-directed RNA polymerase II subunit RPB1 OS=Drosophila melanogaster OX=7227 GN=RpII215 PE=3 SV=4
Dis3	Dis3, isoform A OS=Drosophila melanogaster OX=7227 GN=Dis3 PE=1 SV=1
Hsp22	Heat shock protein 22 OS=Drosophila melanogaster OX=7227 GN=Hsp22 PE=1 SV=4

EndoGI	Endonuclease G inhibitor, isoform A OS=Drosophila melanogaster OX=7227 GN=EndoGI PE=1 SV=1
Dmel\CG5028	RH49423p OS=Drosophila melanogaster OX=7227 GN=Dmel\CG5028 PE=1 SV=1
Karybeta3	SD05186p OS=Drosophila melanogaster OX=7227 GN=Karybeta3 PE=2 SV=1
Ugt	UDP-glucose:glycoprotein glucosyltransferase OS=Drosophila melanogaster OX=7227 GN=Ugt PE=1 SV=2
Rpb5	RE34924p OS=Drosophila melanogaster OX=7227 GN=Rpb5 PE=1 SV=1
AIMP3	RH09246p OS=Drosophila melanogaster OX=7227 GN=AIMP3 PE=1 SV=1
Got2-RA	Aspartate aminotransferase (Fragment) OS=Drosophila melanogaster OX=7227 GN=Got2-RA PE=2 SV=1
Prosalpha3	Proteasome subunit alpha type-4 OS=Drosophila melanogaster OX=7227 GN=Prosalpha3 PE=1 SV=2
yip2	Yippee interacting protein 2 (Fragment) OS=Drosophila melanogaster OX=7227 GN=yip2 PE=2 SV=1
SdhB	Succinate dehydrogenase [ubiquinone] iron-sulfur subunit, mitochondrial OS=Drosophila melanogaster OX=7227 GN=SdhB PE=2 SV=2
SF1	LD36095p OS=Drosophila melanogaster OX=7227 GN=SF1 PE=1 SV=3
bur-RA	MIP06849p OS=Drosophila melanogaster OX=7227 GN=bur-RA PE=2 SV=1
128up	GTP-binding protein 128up OS=Drosophila melanogaster OX=7227 GN=128up PE=2 SV=2
CG3817	RRP15-like protein OS=Drosophila melanogaster OX=7227 GN=CG3817 PE=1 SV=1
CG13096	Ribosomal L1 domain-containing protein CG13096 OS=Drosophila melanogaster OX=7227 GN=CG13096 PE=1 SV=1

HP1b	FI06908p OS=Drosophila melanogaster OX=7227 GN=HP1b PE=1 SV=1
mRpS29	DAP3 OS=Drosophila melanogaster OX=7227 GN=mRpS29 PE=4 SV=1
Cam	Calmodulin OS=Drosophila melanogaster OX=7227 GN=Cam PE=1 SV=2
mRpL2-RA	FI07257p (Fragment) OS=Drosophila melanogaster OX=7227 GN=mRpL2-RA PE=2 SV=1
GstO3	Glutathione S transferase O3 OS=Drosophila melanogaster OX=7227 GN=GstO3 PE=1 SV=1
snf	U1 small nuclear ribonucleoprotein A OS=Drosophila melanogaster OX=7227 GN=snf PE=1 SV=1
PHGPx	Glutathione peroxidase OS=Drosophila melanogaster OX=7227 GN=PHGPx PE=1 SV=1
CG3259-RA	IP21508p OS=Drosophila melanogaster OX=7227 GN=CG3259-RA PE=2 SV=1
Sgt	LD24721p OS=Drosophila melanogaster OX=7227 GN=Sgt PE=1 SV=1
vir	Protein virilizer OS=Drosophila melanogaster OX=7227 GN=vir PE=1 SV=1
gfzf	GST-containing FLYWCH zinc-finger protein OS=Drosophila melanogaster OX=7227 GN=gfzf PE=1 SV=1
nclb	Periodic tryptophan protein 1 homolog OS=Drosophila melanogaster OX=7227 GN=nclb PE=1 SV=1
Dmel\CG3756	LP03982p OS=Drosophila melanogaster OX=7227 GN=Dmel\CG3756 PE=1 SV=1
CG15735	Protein LSM12 homolog A OS=Drosophila melanogaster OX=7227 GN=CG15735 PE=2 SV=2
nudC	Nuclear migration protein NudC OS=Drosophila melanogaster OX=7227 GN=nudC PE=1 SV=2
Dscam1	Down syndrome cell adhesion molecule 1, isoform T OS=Drosophila melanogaster OX=7227 GN=Dscam1 PE=1 SV=1

l(2)k09913	Lethal (2) k09913, isoform D OS=Drosophila melanogaster OX=7227 GN=l(2)k09913 PE=1 SV=1
CG10824-RA	RT10112p (Fragment) OS=Drosophila melanogaster OX=7227 GN=CG10824-RA PE=2 SV=1
Mat89Ba	Nucleolar protein 6 OS=Drosophila melanogaster OX=7227 GN=Mat89Ba PE=1 SV=1
bai	Transmembrane emp24 domain-containing protein bai OS=Drosophila melanogaster OX=7227 GN=bai PE=2 SV=1
eIF1A	Eukaryotic translation initiation factor 1A, isoform A OS=Drosophila melanogaster OX=7227 GN=eIF1A PE=1 SV=1
Dmel\CG6767	Uncharacterized protein, isoform C OS=Drosophila melanogaster OX=7227 GN=Dmel\CG6767 PE=1 SV=1
beag	Beag OS=Drosophila melanogaster OX=7227 GN=beag PE=1 SV=1
CG18592	LD31822p OS=Drosophila melanogaster OX=7227 GN=CG18592 PE=1 SV=2
CG6388	Probable tRNA (guanine(26)-N(2))-dimethyltransferase OS=Drosophila melanogaster OX=7227 GN=CG6388 PE=2 SV=1
CG10166	Probable dolichol-phosphate mannosyltransferase OS=Drosophila melanogaster OX=7227 GN=CG10166 PE=3 SV=1
Vha68-1	V-type proton ATPase catalytic subunit A isoform 1 OS=Drosophila melanogaster OX=7227 GN=Vha68-1 PE=2 SV=2
rhea	Rhea, isoform B OS=Drosophila melanogaster OX=7227 GN=rhea PE=1 SV=1
CG9281	GM14873p OS=Drosophila melanogaster OX=7227 GN=CG9281 PE=2 SV=1
fl(2)d	Pre-mRNA-splicing regulator female-lethal(2)D OS=Drosophila melanogaster OX=7227 GN=fl(2)d PE=1 SV=2
Fdh	Alcohol dehydrogenase class-3 OS=Drosophila melanogaster OX=7227 GN=Fdh PE=1 SV=3

Cdep	Chondrocyte-derived ezrin-like domain containing protein, isoform E OS=Drosophila melanogaster OX=7227 GN=Cdep PE=1 SV=1
CG8778	CG8778 OS=Drosophila melanogaster OX=7227 GN=CG8778 PE=1 SV=1
thoc6	THO complex subunit 6 OS=Drosophila melanogaster OX=7227 GN=thoc6 PE=1 SV=1
mRpL39	39S ribosomal protein L39, mitochondrial OS=Drosophila melanogaster OX=7227 GN=mRpL39 PE=2 SV=2
pix	Pixie, isoform A OS=Drosophila melanogaster OX=7227 GN=pix PE=1 SV=1
Dmel\CG9674	Uncharacterized protein, isoform E OS=Drosophila melanogaster OX=7227 GN=Dmel\CG9674 PE=1 SV=1
lid	Lysine-specific demethylase lid OS=Drosophila melanogaster OX=7227 GN=lid PE=1 SV=1
spoon	RE73736p OS=Drosophila melanogaster OX=7227 GN=spoon PE=1 SV=1
CG3662	LD11211p OS=Drosophila melanogaster OX=7227 GN=CG3662 PE=2 SV=1
	IP20089p OS=Drosophila melanogaster OX=7227 PE=2 SV=1
CG8414	Polynucleotide 5'-hydroxyl-kinase NOL9 OS=Drosophila melanogaster OX=7227 GN=CG8414 PE=2 SV=1
Rab4-RB	FI09101p (Fragment) OS=Drosophila melanogaster OX=7227 GN=Rab4-RB PE=2 SV=1
Dmel\CG5746	RH13835p OS=Drosophila melanogaster OX=7227 GN=Dmel\CG5746 PE=2 SV=1
ncm	Pre-mRNA-splicing factor CWC22 homolog OS=Drosophila melanogaster OX=7227 GN=ncm PE=1 SV=3
sea	LD46175p OS=Drosophila melanogaster OX=7227 GN=sea PE=1 SV=1
prod	PROD (Fragment) OS=Drosophila melanogaster OX=7227 GN=prod PE=4 SV=1

Vps28	Vacuolar protein sorting-associated protein 28 homolog OS=Drosophila melanogaster OX=7227 GN=Vps28 PE=1 SV=1
Stim	Stromal interaction molecule homolog OS=Drosophila melanogaster OX=7227 GN=Stim PE=1 SV=1
RpII140	DNA-directed RNA polymerase II subunit RPB2 OS=Drosophila melanogaster OX=7227 GN=RpII140 PE=2 SV=2
dre4	FACT complex subunit spt16 OS=Drosophila melanogaster OX=7227 GN=dre4 PE=1 SV=2
CG1129	Mannose-1-phosphate guanyltransferase beta OS=Drosophila melanogaster OX=7227 GN=CG1129 PE=1 SV=1
Prosbeta6	Proteasome subunit beta type-1 OS=Drosophila melanogaster OX=7227 GN=Prosbeta6 PE=2 SV=2
BEST:LD38280	LD02975p OS=Drosophila melanogaster OX=7227 GN=BEST:LD38280 PE=1 SV=1
Sec24CD	LP05220p OS=Drosophila melanogaster OX=7227 GN=Sec24CD PE=1 SV=2
Fim	FI20019p1 OS=Drosophila melanogaster OX=7227 GN=Fim PE=1 SV=1
CG6686	GH14426p OS=Drosophila melanogaster OX=7227 GN=CG6686 PE=2 SV=1
SMC2	Structural maintenance of chromosomes protein OS=Drosophila melanogaster OX=7227 GN=SMC2 PE=1 SV=1
Arp3	Actin-related protein 3 OS=Drosophila melanogaster OX=7227 GN=Arp3 PE=2 SV=3
CG5792	IP16022p OS=Drosophila melanogaster OX=7227 GN=CG5792 PE=2 SV=1
Rpd3	Histone deacetylase Rpd3 OS=Drosophila melanogaster OX=7227 GN=Rpd3 PE=1 SV=2
Rrp40	RE44908p OS=Drosophila melanogaster OX=7227 GN=Rrp40 PE=1 SV=1
Ubc12	Nedd8-conjugating enzyme Ubc12 OS=Drosophila melanogaster OX=7227 GN=Ubc12 PE=1 SV=1

CG4882	CG4882, isoform A OS=Drosophila melanogaster OX=7227 GN=CG4882 PE=1 SV=1
pea	ATP-dependent RNA helicase DHX8 OS=Drosophila melanogaster OX=7227 GN=pea PE=1 SV=1
Trap1	Hsp90-related protein TRAP1 OS=Drosophila melanogaster OX=7227 GN=Trap1 PE=2 SV=1
CG5854	RH40150p OS=Drosophila melanogaster OX=7227 GN=CG5854 PE=2 SV=1
Mitofilin	MICOS complex subunit Mic60 OS=Drosophila melanogaster OX=7227 GN=Mitofilin PE=1 SV=4
AOX1	Aldehyde oxidase 1 OS=Drosophila melanogaster OX=7227 GN=AOX1 PE=1 SV=1
CG5174	CG5174, isoform M OS=Drosophila melanogaster OX=7227 GN=CG5174 PE=1 SV=2
Arf102F	ADP-ribosylation factor 2 OS=Drosophila melanogaster OX=7227 GN=Arf102F PE=2 SV=2
trsn	GM27569p OS=Drosophila melanogaster OX=7227 GN=trsn PE=1 SV=1
pyd	TamA OS=Drosophila melanogaster OX=7227 GN=pyd PE=2 SV=1
woc	LD44304p OS=Drosophila melanogaster OX=7227 GN=woc PE=2 SV=1
cpb	F-actin-capping protein subunit beta OS=Drosophila melanogaster OX=7227 GN=cpb PE=2 SV=1
ND-75	NADH-ubiquinone oxidoreductase 75 kDa subunit, mitochondrial OS=Drosophila melanogaster OX=7227 GN=ND-75 PE=2 SV=3
Dmel\CG2931	RE50009p OS=Drosophila melanogaster OX=7227 GN=Dmel\CG2931 PE=1 SV=1
Rrp46	GM01970p OS=Drosophila melanogaster OX=7227 GN=Rrp46 PE=2 SV=1
CG5181	SOSS complex subunit B homolog OS=Drosophila melanogaster OX=7227 GN=CG5181 PE=2 SV=1
eIF2Bbeta	EG:100G10.3 protein OS=Drosophila melanogaster OX=7227 GN=eIF2Bbeta PE=1 SV=1

Sym	Symplekin OS=Drosophila melanogaster OX=7227 GN=Sym PE=1 SV=1
CSN7	COP9 signalosome complex subunit 7 OS=Drosophila melanogaster OX=7227 GN=CSN7 PE=1 SV=2
BcDNA:GH06032	Cation-transporting ATPase OS=Drosophila melanogaster OX=7227 GN=BcDNA:GH06032 PE=1 SV=1
rush	Pleckstrin homology domain-containing family F member 1 homolog OS=Drosophila melanogaster OX=7227 GN=rush PE=1 SV=1
Atg16	Autophagy-related 16, isoform C OS=Drosophila melanogaster OX=7227 GN=Atg16 PE=1 SV=1
ifc	Des-1 protein OS=Drosophila melanogaster OX=7227 GN=ifc PE=1 SV=1
nesd	Protein nessun dorma OS=Drosophila melanogaster OX=7227 GN=nesd PE=1 SV=1
mRpL43	Mitochondrial ribosomal protein L43 OS=Drosophila melanogaster OX=7227 GN=mRpL43 PE=1 SV=1
mRpL24	Probable 39S ribosomal protein L24, mitochondrial OS=Drosophila melanogaster OX=7227 GN=mRpL24 PE=2 SV=1
Dmel\CG6833	GH21710p OS=Drosophila melanogaster OX=7227 GN=Dmel\CG6833 PE=1 SV=1
mRpS10	28S ribosomal protein S10, mitochondrial OS=Drosophila melanogaster OX=7227 GN=mRpS10 PE=2 SV=2
Arp2	Actin-related protein 2 OS=Drosophila melanogaster OX=7227 GN=Arp2 PE=2 SV=3
CG17266	Peptidyl-prolyl cis-trans isomerase OS=Drosophila melanogaster OX=7227 GN=CG17266 PE=1 SV=1
24643014	Uncharacterized protein, isoform G OS=Drosophila melanogaster OX=7227 GN=24643014 PE=1 SV=3
CG16917	RE10350p OS=Drosophila melanogaster OX=7227 GN=CG16917 PE=1 SV=1
Mtr4	L.2.35Df OS=Drosophila melanogaster OX=7227 GN=Mtr4 PE=1 SV=1

Rpn12	26S proteasome regulatory complex subunit p30 OS=Drosophila melanogaster OX=7227 GN=Rpn12 PE=1 SV=1
Dmel\CG1416	LD43819p OS=Drosophila melanogaster OX=7227 GN=Dmel\CG1416 PE=1 SV=2
woc	Without children, isoform E OS=Drosophila melanogaster OX=7227 GN=woc PE=1 SV=1
CG6183	GH09427p OS=Drosophila melanogaster OX=7227 GN=CG6183 PE=2 SV=1
CkIIbeta	Casein kinase II subunit beta OS=Drosophila melanogaster OX=7227 GN=CkIIbeta PE=2 SV=2
CG17202	c-Myc-binding protein homolog OS=Drosophila melanogaster OX=7227 GN=CG17202 PE=2 SV=2
CG9436	CG9436 OS=Drosophila melanogaster OX=7227 GN=CG9436 PE=1 SV=1
BEST:GH25183	MIP21654p OS=Drosophila melanogaster OX=7227 GN=BEST:GH25183 PE=1 SV=1
mRpS34	Mitochondrial ribosomal protein S34 OS=Drosophila melanogaster OX=7227 GN=mRpS34 PE=1 SV=2
BcDNA:GH04978	BcDNA.GH04978 OS=Drosophila melanogaster OX=7227 GN=BcDNA:GH04978 PE=1 SV=1
poly	MIP09035p OS=Drosophila melanogaster OX=7227 GN=poly PE=1 SV=1
Rpn8	26S proteasome non-ATPase regulatory subunit 7 OS=Drosophila melanogaster OX=7227 GN=Rpn8 PE=1 SV=6
gag	Nucleic-acid-binding protein from mobile element jockey OS=Drosophila melanogaster OX=7227 GN=gag PE=4 SV=1
Idh	Isocitrate dehydrogenase [NADP] OS=Drosophila melanogaster OX=7227 GN=Idh PE=1 SV=2
swm	Zinc finger protein swm OS=Drosophila melanogaster OX=7227 GN=swm PE=1 SV=1
Arc42	Arc42 OS=Drosophila melanogaster OX=7227 GN=Arc42 PE=1 SV=1

CG7800-RA	FI02011p OS=Drosophila melanogaster OX=7227 GN=CG7800-RA PE=1 SV=2
Dmel\CG11811	GH06691p OS=Drosophila melanogaster OX=7227 GN=Dmel\CG11811 PE=1 SV=1
Bacc	Bacchus OS=Drosophila melanogaster OX=7227 GN=Bacc PE=2 SV=1
l(1)G0193	Lethal (1) G0193, isoform B OS=Drosophila melanogaster OX=7227 GN=l(1)G0193 PE=1 SV=1
sip1	Septin-interacting protein 1 OS=Drosophila melanogaster OX=7227 GN=sip1 PE=1 SV=1
tacc	Transforming acidic coiled-coil protein, isoform L OS=Drosophila melanogaster OX=7227 GN=tacc PE=1 SV=1
LBR	Lamin-B receptor OS=Drosophila melanogaster OX=7227 GN=LBR PE=1 SV=1
Sep1	Septin-1 OS=Drosophila melanogaster OX=7227 GN=Sep1 PE=1 SV=1
mRpL12	CG5012 (Fragment) OS=Drosophila melanogaster OX=7227 GN=mRpL12 PE=4 SV=1
Sf3a2	LD47455p OS=Drosophila melanogaster OX=7227 GN=Sf3a2 PE=1 SV=1
HP1c	Heterochromatin protein 1c OS=Drosophila melanogaster OX=7227 GN=HP1c PE=1 SV=1
Pvr	FI18308p1 OS=Drosophila melanogaster OX=7227 GN=Pvr PE=1 SV=1
CG5589	Uncharacterized protein OS=Drosophila melanogaster OX=7227 GN=CG5589 PE=3 SV=1
Rap1	Ras-related protein Rap1 OS=Drosophila melanogaster OX=7227 GN=Rap1 PE=2 SV=2
CG10131	GH23990p OS=Drosophila melanogaster OX=7227 GN=CG10131 PE=2 SV=1
Spt6	Transcription elongation factor SPT6 OS=Drosophila melanogaster OX=7227 GN=Spt6 PE=1 SV=1
mEFTu2	AT01345p OS=Drosophila melanogaster OX=7227 GN=mEFTu2 PE=1 SV=1

CT9894	EG:25E8.1 protein OS=Drosophila melanogaster OX=7227 GN=CT9894 PE=1 SV=1
Kcmf1	E3 ubiquitin-protein ligase Kcmf1 OS=Drosophila melanogaster OX=7227 GN=Kcmf1 PE=1 SV=1
Rhau	GH12763p OS=Drosophila melanogaster OX=7227 GN=Rhau PE=1 SV=1
Khc	Kinesin heavy chain OS=Drosophila melanogaster OX=7227 GN=Khc PE=1 SV=2
Apc	APC-like, isoform A OS=Drosophila melanogaster OX=7227 GN=Apc PE=4 SV=1
Cpsf73	Cleavage and polyadenylation specificity factor 73 OS=Drosophila melanogaster OX=7227 GN=Cpsf73 PE=1 SV=2
CG6094	CG6094-PA OS=Drosophila melanogaster OX=7227 GN=CG6094 PE=4 SV=1
whd	LD31742p OS=Drosophila melanogaster OX=7227 GN=whd PE=1 SV=1
CG3884-RB	IP19903p OS=Drosophila melanogaster OX=7227 GN=CG3884-RB PE=1 SV=1
Prosbeta3	Proteasome subunit beta type-3 OS=Drosophila melanogaster OX=7227 GN=Prosbeta3 PE=1 SV=1
Dmel\CG6028	GH23390p OS=Drosophila melanogaster OX=7227 GN=Dmel\CG6028 PE=1 SV=1
SNF4Agamma	IP17340p OS=Drosophila melanogaster OX=7227 GN=SNF4Agamma PE=2 SV=1
Ago2	Argonaute-2 (Fragment) OS=Drosophila melanogaster OX=7227 GN=Ago2 PE=2 SV=1
Sirt1	NAD-dependent histone deacetylase sirtuin-1 OS=Drosophila melanogaster OX=7227 GN=Sirt1 PE=1 SV=1
fat-spondin	Fat-spondin OS=Drosophila melanogaster OX=7227 GN=fat-spondin PE=1 SV=1
CG5862	DDRGK domain-containing protein 1 OS=Drosophila melanogaster OX=7227 GN=CG5862 PE=2 SV=1
FASN1	Fatty acid synthase 1, isoform A OS=Drosophila melanogaster OX=7227 GN=FASN1 PE=1 SV=1

Dak1	RH52725p (Fragment) OS=Drosophila melanogaster OX=7227 GN=Dak1 PE=2 SV=1
SREBP	LP12374p OS=Drosophila melanogaster OX=7227 GN=SREBP PE=1 SV=1
CG3527	Ribosomal RNA small subunit methyltransferase NEP1 OS=Drosophila melanogaster OX=7227 GN=CG3527 PE=3 SV=2
CG2159	GH16843p OS=Drosophila melanogaster OX=7227 GN=CG2159 PE=2 SV=1
Dhpr	Dihydropteridine reductase OS=Drosophila melanogaster OX=7227 GN=Dhpr PE=1 SV=1
Ppt1	Palmitoyl-protein thioesterase 1 OS=Drosophila melanogaster OX=7227 GN=Ppt1 PE=2 SV=2
Fkbp14	Peptidylprolyl isomerase OS=Drosophila melanogaster OX=7227 GN=Fkbp14 PE=1 SV=1
Nup214	Nuclear pore complex protein Nup214 OS=Drosophila melanogaster OX=7227 GN=Nup214 PE=1 SV=2
Prosbeta1	Proteasome subunit beta type OS=Drosophila melanogaster OX=7227 GN=Prosbeta1 PE=2 SV=1
CG2852-RA	Peptidyl-prolyl cis-trans isomerase OS=Drosophila melanogaster OX=7227 GN=CG2852-RA PE=2 SV=1
CG33542	CG33542 (Fragment) OS=Drosophila melanogaster OX=7227 GN=CG33542 PE=4 SV=1
DCP1	Decapping protein 1, isoform A OS=Drosophila melanogaster OX=7227 GN=DCP1 PE=1 SV=1
CG9521	Uncharacterized protein OS=Drosophila melanogaster OX=7227 GN=CG9521 PE=1 SV=1
Atpalpha	Sodium/potassium-transporting ATPase subunit alpha OS=Drosophila melanogaster OX=7227 GN=Atpalpha PE=1 SV=3
BEST:CK02656	RE02452p OS=Drosophila melanogaster OX=7227 GN=BEST:CK02656 PE=2 SV=1
mEFTs	Elongation factor Ts, mitochondrial OS=Drosophila melanogaster OX=7227 GN=mEFTs PE=2 SV=1
REG	LD45860p OS=Drosophila melanogaster OX=7227 GN=REG PE=1 SV=1

Dmel\CG4901	RE48269p OS=Drosophila melanogaster OX=7227 GN=Dmel\CG4901 PE=1 SV=2
l(2)gl	Lethal(2) giant larvae protein OS=Drosophila melanogaster OX=7227 GN=l(2)gl PE=1 SV=2
Dhc64C	Dynein heavy chain, cytoplasmic OS=Drosophila melanogaster OX=7227 GN=Dhc64C PE=2 SV=2
CG11498-RA	MIP13816p OS=Drosophila melanogaster OX=7227 GN=CG11498-RA PE=2 SV=3
RpL27	60S ribosomal protein L27 OS=Drosophila melanogaster OX=7227 GN=RpL27 PE=1 SV=1
Dmel\CG12301	LD31322p OS=Drosophila melanogaster OX=7227 GN=Dmel\CG12301 PE=1 SV=2
Cap-G	SD10043p OS=Drosophila melanogaster OX=7227 GN=Cap-G PE=2 SV=1
su(sable)	Protein suppressor of sable OS=Drosophila melanogaster OX=7227 GN=su(sable) PE=1 SV=2
Rrp1	Recombination repair protein 1 OS=Drosophila melanogaster OX=7227 GN=Rrp1 PE=1 SV=2
Prx2540-1	1-cys peroxiredoxin DPx-2540-1 OS=Drosophila melanogaster OX=7227 GN=Prx2540-1 PE=2 SV=1
Flacc	Fl(2)d-associated complex component OS=Drosophila melanogaster OX=7227 GN=Flacc PE=1 SV=1
Dmel\CG1582	GH07148p OS=Drosophila melanogaster OX=7227 GN=Dmel\CG1582 PE=1 SV=2
Rpn2	26S proteasome non-ATPase regulatory subunit 1 OS=Drosophila melanogaster OX=7227 GN=Rpn2 PE=1 SV=1
Ten-m	Teneurin-m OS=Drosophila melanogaster OX=7227 GN=Ten-m PE=1 SV=2
CG32563	Uncharacterized protein, isoform A OS=Drosophila melanogaster OX=7227 GN=CG32563 PE=4 SV=2
Dmel\CG10907	RE08109p OS=Drosophila melanogaster OX=7227 GN=Dmel\CG10907 PE=2 SV=1
Fpps	Farnesyl pyrophosphate synthase OS=Drosophila melanogaster OX=7227 GN=Fpps PE=1 SV=1

sqh	Myosin regulatory light chain sqh OS=Drosophila melanogaster OX=7227 GN=sqh PE=1 SV=1
CG5877	Uncharacterized protein, isoform B OS=Drosophila melanogaster OX=7227 GN=CG5877 PE=4 SV=2
RhoGAPp190	Rho GTPase-activating protein 190 OS=Drosophila melanogaster OX=7227 GN=RhoGAPp190 PE=1 SV=2
154229_at	LD24105p OS=Drosophila melanogaster OX=7227 GN=154229_at PE=1 SV=1
CG4887	RH03791p OS=Drosophila melanogaster OX=7227 GN=CG4887 PE=2 SV=1
CG1681	CG1681 (Fragment) OS=Drosophila melanogaster OX=7227 GN=CG1681 PE=4 SV=1
CG12112-RA	RE16061p1 OS=Drosophila melanogaster OX=7227 GN=CG12112-RA PE=1 SV=2
BcDNA:GH07921	LD27033p OS=Drosophila melanogaster OX=7227 GN=BcDNA:GH07921 PE=1 SV=1
pnut	Protein peanut OS=Drosophila melanogaster OX=7227 GN=pnut PE=1 SV=2
faf	Probable ubiquitin carboxyl-terminal hydrolase FAF OS=Drosophila melanogaster OX=7227 GN=faf PE=1 SV=2
UQCR-C1	GH01077p OS=Drosophila melanogaster OX=7227 GN=UQCR-C1 PE=1 SV=2
CG17078	Uncharacterized protein, isoform C OS=Drosophila melanogaster OX=7227 GN=CG17078 PE=1 SV=1
Pcyt1	LD46058p OS=Drosophila melanogaster OX=7227 GN=Pcyt1 PE=1 SV=1
Dmel\CG2260	LD41718p OS=Drosophila melanogaster OX=7227 GN=Dmel\CG2260 PE=1 SV=1
Non2	LD45195p OS=Drosophila melanogaster OX=7227 GN=Non2 PE=1 SV=1
Dmel\CG6617	LD25271p OS=Drosophila melanogaster OX=7227 GN=Dmel\CG6617 PE=1 SV=1
lig	Lingerer, isoform E OS=Drosophila melanogaster OX=7227 GN=lig PE=1 SV=1

Spx	RE50839p OS=Drosophila melanogaster OX=7227 GN=Spx PE=2 SV=1
mre11	Endo/exonuclease Mre11 OS=Drosophila melanogaster OX=7227 GN=mre11 PE=1 SV=1
Gp210	Gp210 ortholog, isoform A OS=Drosophila melanogaster OX=7227 GN=Gp210 PE=1 SV=1
nolo	GH19218p OS=Drosophila melanogaster OX=7227 GN=nolo PE=1 SV=2
Rab14	MIP20481p OS=Drosophila melanogaster OX=7227 GN=Rab14 PE=1 SV=1
CG4554	CG4554 OS=Drosophila melanogaster OX=7227 GN=CG4554 PE=1 SV=2
Naa15-16	N(Alpha)-acetyltransferase 15/16, isoform A OS=Drosophila melanogaster OX=7227 GN=Naa15-16 PE=1 SV=1
Smn	Survival motor neuron protein OS=Drosophila melanogaster OX=7227 GN=Smn PE=1 SV=1
alpha-Spec	Spectrin alpha chain OS=Drosophila melanogaster OX=7227 GN=alpha-Spec PE=1 SV=2
Rtc1	Probable RNA 3'-terminal phosphate cyclase-like protein OS=Drosophila melanogaster OX=7227 GN=Rtc1 PE=2 SV=3
chb	CLIP-associating protein OS=Drosophila melanogaster OX=7227 GN=chb PE=1 SV=1
CG7239	GM05640p OS=Drosophila melanogaster OX=7227 GN=CG7239 PE=2 SV=1
scra	Anillin OS=Drosophila melanogaster OX=7227 GN=scra PE=1 SV=3
d4	D4, isoform A OS=Drosophila melanogaster OX=7227 GN=d4 PE=1 SV=1
egl	Egalitarian, isoform B OS=Drosophila melanogaster OX=7227 GN=egl PE=1 SV=4
Rpn13	Proteasomal ubiquitin receptor ADRM1 homolog OS=Drosophila melanogaster OX=7227 GN=Rpn13 PE=1 SV=1

CG1703	LD35151p (Fragment) OS=Drosophila melanogaster OX=7227 GN=CG1703 PE=2 SV=1
CG7632	Uncharacterized protein, isoform B OS=Drosophila melanogaster OX=7227 GN=CG7632 PE=1 SV=1
enc	Protein encore OS=Drosophila melanogaster OX=7227 GN=enc PE=1 SV=2
Akap200	A kinase anchor protein 200, isoform D OS=Drosophila melanogaster OX=7227 GN=Akap200 PE=1 SV=1
Sgf29	FI01566p OS=Drosophila melanogaster OX=7227 GN=Sgf29 PE=1 SV=2
Ski6	FI07225p OS=Drosophila melanogaster OX=7227 GN=Ski6 PE=1 SV=1
DmRH14	RNA helicase OS=Drosophila melanogaster OX=7227 GN=DmRH14 PE=1 SV=2
MSBP	LD12946p OS=Drosophila melanogaster OX=7227 GN=MSBP PE=1 SV=1
CG4788	RE28931p OS=Drosophila melanogaster OX=7227 GN=CG4788 PE=2 SV=1
CSN4	COP9 signalosome complex subunit 4 OS=Drosophila melanogaster OX=7227 GN=CSN4 PE=1 SV=1
RpL18A	60S ribosomal protein L18a OS=Drosophila melanogaster OX=7227 GN=RpL18A PE=1 SV=1
DIP2	Disco-interacting protein 2 OS=Drosophila melanogaster OX=7227 GN=DIP2 PE=1 SV=2
coro	Coronin OS=Drosophila melanogaster OX=7227 GN=coro PE=1 SV=1
PCB	Pyruvate carboxylase OS=Drosophila melanogaster OX=7227 GN=PCB PE=1 SV=1
E(bx)	Nucleosome-remodeling factor subunit NURF301 OS=Drosophila melanogaster OX=7227 GN=E(bx) PE=1 SV=2
TfIIB	Transcription initiation factor IIB OS=Drosophila melanogaster OX=7227 GN=TfIIB PE=2 SV=1
CG1092	SD15476p OS=Drosophila melanogaster OX=7227 GN=CG1092 PE=2 SV=1

wol	Dolichyl-phosphate beta-glucosyltransferase OS=Drosophila melanogaster OX=7227 GN=wol PE=1 SV=1
Cyt-c1	Cytochrome c1, isoform A OS=Drosophila melanogaster OX=7227 GN=Cyt-c1 PE=1 SV=1
pyd-RJ	MIP18367p OS=Drosophila melanogaster OX=7227 GN=pyd-RJ PE=2 SV=1
Clbn	Nuclear export mediator factor NEMF homolog OS=Drosophila melanogaster OX=7227 GN=Clbn PE=1 SV=2
row	LD41072p OS=Drosophila melanogaster OX=7227 GN=row PE=2 SV=1
par-1	GH14769p OS=Drosophila melanogaster OX=7227 GN=par-1 PE=2 SV=1
	Histone acetyltransferase type B catalytic subunit OS=Drosophila melanogaster OX=7227 PE=2 SV=1
su(r)	Dihydropyrimidine dehydrogenase [NADP(+)] OS=Drosophila melanogaster OX=7227 GN=su(r) PE=1 SV=2
CG10600	Uncharacterized protein, isoform A OS=Drosophila melanogaster OX=7227 GN=CG10600 PE=1 SV=3
Saf-B	Scaffold attachment factor B, isoform D OS=Drosophila melanogaster OX=7227 GN=Saf-B PE=1 SV=1
clu	Protein clueless OS=Drosophila melanogaster OX=7227 GN=clu PE=1 SV=1
	IP07725p (Fragment) OS=Drosophila melanogaster OX=7227 PE=2 SV=1
Lon	Lon protease homolog, mitochondrial OS=Drosophila melanogaster OX=7227 GN=Lon PE=1 SV=1
Pdha	Pyruvate dehydrogenase E1 component subunit alpha OS=Drosophila melanogaster OX=7227 GN=Pdha PE=1 SV=1
Art1	Arginine methyltransferase 1 OS=Drosophila melanogaster OX=7227 GN=Art1 PE=1 SV=1

koi	Klaroid, isoform D OS=Drosophila melanogaster OX=7227 GN=koi PE=1 SV=1
Rpn7	26S proteasome non-ATPase regulatory subunit 6 OS=Drosophila melanogaster OX=7227 GN=Rpn7 PE=2 SV=1
Cp18	Chorion protein S18 OS=Drosophila melanogaster OX=7227 GN=Cp18 PE=2 SV=2
CRIF	CR6-interacting factor OS=Drosophila melanogaster OX=7227 GN=CRIF PE=1 SV=1
Syb	Synaptobrevin OS=Drosophila melanogaster OX=7227 GN=Syb PE=2 SV=3
Dmel\CG3226	LD13807p OS=Drosophila melanogaster OX=7227 GN=Dmel\CG3226 PE=1 SV=1
Desat2	Fatty acid desaturase 2 OS=Drosophila melanogaster OX=7227 GN=Desat2 PE=3 SV=1
Rrp42	IP10364p OS=Drosophila melanogaster OX=7227 GN=Rrp42 PE=1 SV=1
CG8611	Probable ATP-dependent RNA helicase CG8611 OS=Drosophila melanogaster OX=7227 GN=CG8611 PE=1 SV=1
Pop2	GH06247p OS=Drosophila melanogaster OX=7227 GN=Pop2 PE=1 SV=2
CG5380	Probable DNA-directed RNA polymerase III subunit RPC6 OS=Drosophila melanogaster OX=7227 GN=CG5380 PE=2 SV=1
Dmel\CG5854	LD23561p OS=Drosophila melanogaster OX=7227 GN=Dmel\CG5854 PE=1 SV=1
CG4858	Cytosolic Fe-S cluster assembly factor NUBP2 homolog OS=Drosophila melanogaster OX=7227 GN=CG4858 PE=1 SV=1
CG5382	Zinc finger protein-like 1 homolog OS=Drosophila melanogaster OX=7227 GN=CG5382 PE=1 SV=1
l(2)05287	FI12406p OS=Drosophila melanogaster OX=7227 GN=l(2)05287 PE=1 SV=2

eIF5	Eukaryotic translation initiation factor 5 OS=Drosophila melanogaster OX=7227 GN=eIF5 PE=1 SV=1
B4	B4 protein OS=Drosophila melanogaster OX=7227 GN=B4 PE=2 SV=1
CG42674	Uncharacterized protein, isoform D OS=Drosophila melanogaster OX=7227 GN=CG42674 PE=1 SV=1
Aatf	Protein Aatf OS=Drosophila melanogaster OX=7227 GN=Aatf PE=1 SV=1
CG1737	CG1737-PA (Fragment) OS=Drosophila melanogaster OX=7227 GN=CG1737 PE=4 SV=1
tyf	LD29423p OS=Drosophila melanogaster OX=7227 GN=tyf PE=2 SV=1
bip2	Bip2 OS=Drosophila melanogaster OX=7227 GN=bip2 PE=1 SV=1
mRpL9	39S ribosomal protein L9, mitochondrial OS=Drosophila melanogaster OX=7227 GN=mRpL9 PE=2 SV=1
Set1	Histone-lysine N-methyltransferase SETD1 OS=Drosophila melanogaster OX=7227 GN=Set1 PE=1 SV=1
CG6459	CG6459 protein OS=Drosophila melanogaster OX=7227 GN=CG6459 PE=4 SV=1
RanBPM	Ran-binding proteins 9/10 homolog OS=Drosophila melanogaster OX=7227 GN=RanBPM PE=1 SV=1
Rcd-1	GH15157p OS=Drosophila melanogaster OX=7227 GN=Rcd-1 PE=1 SV=1
CG7246	CG7246 (Fragment) OS=Drosophila melanogaster OX=7227 GN=CG7246 PE=4 SV=1
Alg11	HL02815p OS=Drosophila melanogaster OX=7227 GN=Alg11 PE=1 SV=2
l(1)G0007	LD24737p OS=Drosophila melanogaster OX=7227 GN=l(1)G0007 PE=1 SV=2
mip130	LD07342p OS=Drosophila melanogaster OX=7227 GN=mip130 PE=1 SV=3

LpR2	Lipophorin receptor 2, isoform H OS=Drosophila melanogaster OX=7227 GN=LpR2 PE=4 SV=1
Usp10	LD28815p OS=Drosophila melanogaster OX=7227 GN=Usp10 PE=1 SV=2
RhoGEF2-RD	SD10031p OS=Drosophila melanogaster OX=7227 GN=RhoGEF2-RD PE=2 SV=1
l(2)01424	RE34257p OS=Drosophila melanogaster OX=7227 GN=l(2)01424 PE=2 SV=1
CG4877	LD09503p OS=Drosophila melanogaster OX=7227 GN=CG4877 PE=2 SV=1
CG8230	Dymeclin OS=Drosophila melanogaster OX=7227 GN=CG8230 PE=1 SV=1
CG5174	CG5174, isoform B OS=Drosophila melanogaster OX=7227 GN=CG5174 PE=1 SV=1
Ank	Ankyrin, isoform B OS=Drosophila melanogaster OX=7227 GN=Ank PE=1 SV=1
CG14805-RA	FI20216p1 OS=Drosophila melanogaster OX=7227 GN=CG14805-RA PE=1 SV=1
CG11334	Methylthioribose-1-phosphate isomerase OS=Drosophila melanogaster OX=7227 GN=CG11334 PE=2 SV=1
Acf	LD32807p (Fragment) OS=Drosophila melanogaster OX=7227 GN=Acf PE=2 SV=1
GstO2	LD27185p (Fragment) OS=Drosophila melanogaster OX=7227 GN=GstO2 PE=2 SV=1
Cpsf160	Cleavage and polyadenylation specificity factor subunit 1 OS=Drosophila melanogaster OX=7227 GN=Cpsf160 PE=1 SV=1
Dmel\CG14438	Uncharacterized protein, isoform A OS=Drosophila melanogaster OX=7227 GN=Dmel\CG14438 PE=1 SV=2
CG1665	IP19920p (Fragment) OS=Drosophila melanogaster OX=7227 GN=CG1665 PE=2 SV=1
rad50	DNA repair protein RAD50 OS=Drosophila melanogaster OX=7227 GN=rad50 PE=2 SV=4

RasGAP1	GTPase-activating protein OS=Drosophila melanogaster OX=7227 GN=RasGAP1 PE=1 SV=2
nero	Deoxyhypusine hydroxylase OS=Drosophila melanogaster OX=7227 GN=nero PE=2 SV=1
Cg2023	IP18173p OS=Drosophila melanogaster OX=7227 GN=Cg2023 PE=1 SV=1
Mtap	S-methyl-5'-thioadenosine phosphorylase OS=Drosophila melanogaster OX=7227 GN=Mtap PE=1 SV=1
CG17514	Uncharacterized protein, isoform A OS=Drosophila melanogaster OX=7227 GN=CG17514 PE=1 SV=2
snama	MIP16350p OS=Drosophila melanogaster OX=7227 GN=snama PE=1 SV=1
CG17760	SD21019p OS=Drosophila melanogaster OX=7227 GN=CG17760 PE=1 SV=1
5PtaseI	5PtaseI, isoform F OS=Drosophila melanogaster OX=7227 GN=5PtaseI PE=4 SV=1
AIMP1	CG8235 OS=Drosophila melanogaster OX=7227 GN=AIMP1 PE=1 SV=1
dia	Protein diaphanous OS=Drosophila melanogaster OX=7227 GN=dia PE=2 SV=2
eIF4G2	SD03848p OS=Drosophila melanogaster OX=7227 GN=eIF4G2 PE=2 SV=1
CG9286	Protein BCCIP homolog OS=Drosophila melanogaster OX=7227 GN=CG9286 PE=2 SV=2
Elp1	Putative elongator complex protein 1 OS=Drosophila melanogaster OX=7227 GN=Elp1 PE=1 SV=2
poe	Protein purity of essence OS=Drosophila melanogaster OX=7227 GN=poe PE=1 SV=1
Dmel\CG8939	Putative rRNA methyltransferase OS=Drosophila melanogaster OX=7227 GN=Dmel\CG8939 PE=1 SV=1
Ip259	GM13959p OS=Drosophila melanogaster OX=7227 GN=Ip259 PE=2 SV=1
14-3-3epsilon-RD	AT09839p (Fragment) OS=Drosophila melanogaster OX=7227 GN=14-3-3epsilon-RD PE=2 SV=1

CG7611	WD repeat-containing protein 26 homolog OS=Drosophila melanogaster OX=7227 GN=CG7611 PE=1 SV=1
Dmel\CG7488	GH26602p OS=Drosophila melanogaster OX=7227 GN=Dmel\CG7488 PE=2 SV=2
l(3)76BDr	E3 ubiquitin-protein ligase listerin OS=Drosophila melanogaster OX=7227 GN=l(3)76BDr PE=1 SV=2
CG11148	GIGYF family protein CG11148 OS=Drosophila melanogaster OX=7227 GN=CG11148 PE=1 SV=2
fray	Frayed, isoform A OS=Drosophila melanogaster OX=7227 GN=fray PE=1 SV=1
r	CAD protein OS=Drosophila melanogaster OX=7227 GN=r PE=1 SV=3
Rs1	BcDNA.GM05306 (Fragment) OS=Drosophila melanogaster OX=7227 GN=Rs1 PE=2 SV=1
Tor	Serine/threonine-protein kinase Tor OS=Drosophila melanogaster OX=7227 GN=Tor PE=1 SV=1
Acox57D-p	Acyl-coenzyme A oxidase OS=Drosophila melanogaster OX=7227 GN=Acox57D-p PE=2 SV=1
Hsc70-2	Heat shock 70 kDa protein cognate 2 OS=Drosophila melanogaster OX=7227 GN=Hsc70-2 PE=1 SV=2
Dmel\CG1575	LD45266p OS=Drosophila melanogaster OX=7227 GN=Dmel\CG1575 PE=2 SV=1
IntS3	Integrator complex subunit 3 OS=Drosophila melanogaster OX=7227 GN=IntS3 PE=1 SV=1
Uch	Ubiquitin carboxyl-terminal hydrolase OS=Drosophila melanogaster OX=7227 GN=Uch PE=2 SV=2
Ect4	Sterile alpha and TIR motif-containing protein 1 OS=Drosophila melanogaster OX=7227 GN=Ect4 PE=2 SV=1
DNApol-delta	DNA polymerase delta catalytic subunit OS=Drosophila melanogaster OX=7227 GN=DNApol-delta PE=2 SV=2
CG12104	Uncharacterized protein, isoform C OS=Drosophila melanogaster OX=7227 GN=CG12104 PE=4 SV=1

Arpc2	Actin-related protein 2/3 complex subunit 2 OS=Drosophila melanogaster OX=7227 GN=Arpc2 PE=2 SV=2
kuz	Kuzbanian, isoform A OS=Drosophila melanogaster OX=7227 GN=kuz PE=1 SV=1
osa	Trithorax group protein osa OS=Drosophila melanogaster OX=7227 GN=osa PE=1 SV=1
Nrd1	RE02581p OS=Drosophila melanogaster OX=7227 GN=Nrd1 PE=2 SV=1
Adk2	Adenylate kinase OS=Drosophila melanogaster OX=7227 GN=Adk2 PE=1 SV=1
SP2637	LD05256p OS=Drosophila melanogaster OX=7227 GN=SP2637 PE=1 SV=1
Dmel\CG4598	RH73277p OS=Drosophila melanogaster OX=7227 GN=Dmel\CG4598 PE=1 SV=2
hang	Zinc finger protein hangover OS=Drosophila melanogaster OX=7227 GN=hang PE=1 SV=4
Dmel\CG8915	FI18001p1 OS=Drosophila melanogaster OX=7227 GN=Dmel\CG8915 PE=2 SV=1
Dmel\CG7556	GH07340p OS=Drosophila melanogaster OX=7227 GN=Dmel\CG7556 PE=1 SV=1
CG32500	NFU1 iron-sulfur cluster scaffold homolog, mitochondrial OS=Drosophila melanogaster OX=7227 GN=CG32500 PE=2 SV=1
Chchd3	Coiled-coil-helix-coiled-coil-helix domain containing 3 OS=Drosophila melanogaster OX=7227 GN=Chchd3 PE=1 SV=1
AdSS	Adenylosuccinate synthetase OS=Drosophila melanogaster OX=7227 GN=AdSS PE=2 SV=1
fand	FI18620p1 OS=Drosophila melanogaster OX=7227 GN=fand PE=1 SV=1
Xpc	DNA repair protein complementing XP-C cells homolog OS=Drosophila melanogaster OX=7227 GN=Xpc PE=1 SV=2
Dmel\CG9577	RE22677p OS=Drosophila melanogaster OX=7227 GN=Dmel\CG9577 PE=1 SV=2

28571108	LD15807p OS=Drosophila melanogaster OX=7227 GN=28571108 PE=2 SV=2
BcDNA:LD21293	LD18312p (Fragment) OS=Drosophila melanogaster OX=7227 GN=BcDNA:LD21293 PE=2 SV=1
Tom20	LD34461p OS=Drosophila melanogaster OX=7227 GN=Tom20 PE=1 SV=1
cup	Protein cup OS=Drosophila melanogaster OX=7227 GN=cup PE=1 SV=3
Dmel\CG11030	FI04466p OS=Drosophila melanogaster OX=7227 GN=Dmel\CG11030 PE=1 SV=2
CG1681	CG1681 (Fragment) OS=Drosophila melanogaster OX=7227 GN=CG1681 PE=4 SV=1
emb	Exportin-1 OS=Drosophila melanogaster OX=7227 GN=emb PE=1 SV=1
CG7987	SD01232p OS=Drosophila melanogaster OX=7227 GN=CG7987 PE=2 SV=1
eIF3k	Eukaryotic translation initiation factor 3 subunit K OS=Drosophila melanogaster OX=7227 GN=eIF3k PE=2 SV=1
SRPK-RA	RE75274p1 OS=Drosophila melanogaster OX=7227 GN=SRPK-RA PE=2 SV=1
CG2926	Uncharacterized protein, isoform A OS=Drosophila melanogaster OX=7227 GN=CG2926 PE=1 SV=1
mTTF	Transcription termination factor, mitochondrial OS=Drosophila melanogaster OX=7227 GN=mTTF PE=2 SV=1
Cap-D2	Condensin complex subunit 1 OS=Drosophila melanogaster OX=7227 GN=Cap-D2 PE=1 SV=1
Dmel\CG9425	Uncharacterized protein, isoform B OS=Drosophila melanogaster OX=7227 GN=Dmel\CG9425 PE=1 SV=2
LRR	Leucine-rich repeat, isoform C OS=Drosophila melanogaster OX=7227 GN=LRR PE=1 SV=1
Slh	Protein sly1 homolog OS=Drosophila melanogaster OX=7227 GN=Slh PE=2 SV=4
CG9330	RE26764p OS=Drosophila melanogaster OX=7227 GN=CG9330 PE=2 SV=1

HP5	Heterochromatin protein 5, isoform A OS=Drosophila melanogaster OX=7227 GN=HP5 PE=1 SV=1
Msp300	Muscle-specific protein 300 kDa, isoform M OS=Drosophila melanogaster OX=7227 GN=Msp300 PE=1 SV=1
smid	Smallminded protein OS=Drosophila melanogaster OX=7227 GN=smid PE=1 SV=1

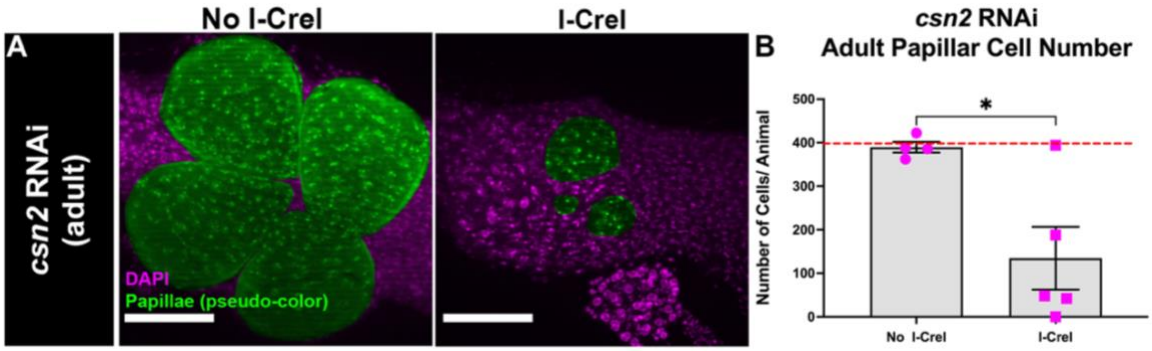

Figure 30: *csn2* is required for papillar cell survival following DSBs

(A) Adult rectum of *csn2* RNAi animals +/- hs-I-CreI. Papillar cells (pseudo-colored), green; DNA (DAPI), magenta. Scale bars = 50μm (B) Quantification of adult papillar cell number in *csn2* RNAi expressing animals +/- hs-I-CreI. Statistical test: Unpaired t-test, p=0.0176. See Methods for statistical notations.

3.2.8 Condensin I complex members interact with Cdt2-GFP after IR in S2 cells

Additional analysis of our Cdt2-IP experiment involved identifying which proteins that interact with Cdt2-GFP following IR also contained a PIP degron consensus sequences. To identify PIP degron-containing proteins, we searched our IR-

specific Cdt2 IP for the following consensus sequence:

[STQN]XX[IMVL]XX[YFV][YFS]XXX[KR] (Fig31A). We identified 27/480 proteins that contained this sequence. Intriguingly, 2/3 proteins that are components of the condensin I complex (CapD2, CapG, SMC2) contained PIP degrons (CapD2 and CapG) (Fig31A-B). [161, 162]. We note that human NCapG, which is homologous to Fly CapG, also contains a conserved PIP box sequence (**Fig31A**). We thus conducted follow-up experiments to validate this complex as a potential target of $CRL4^{CDT2}$ *in vivo*.

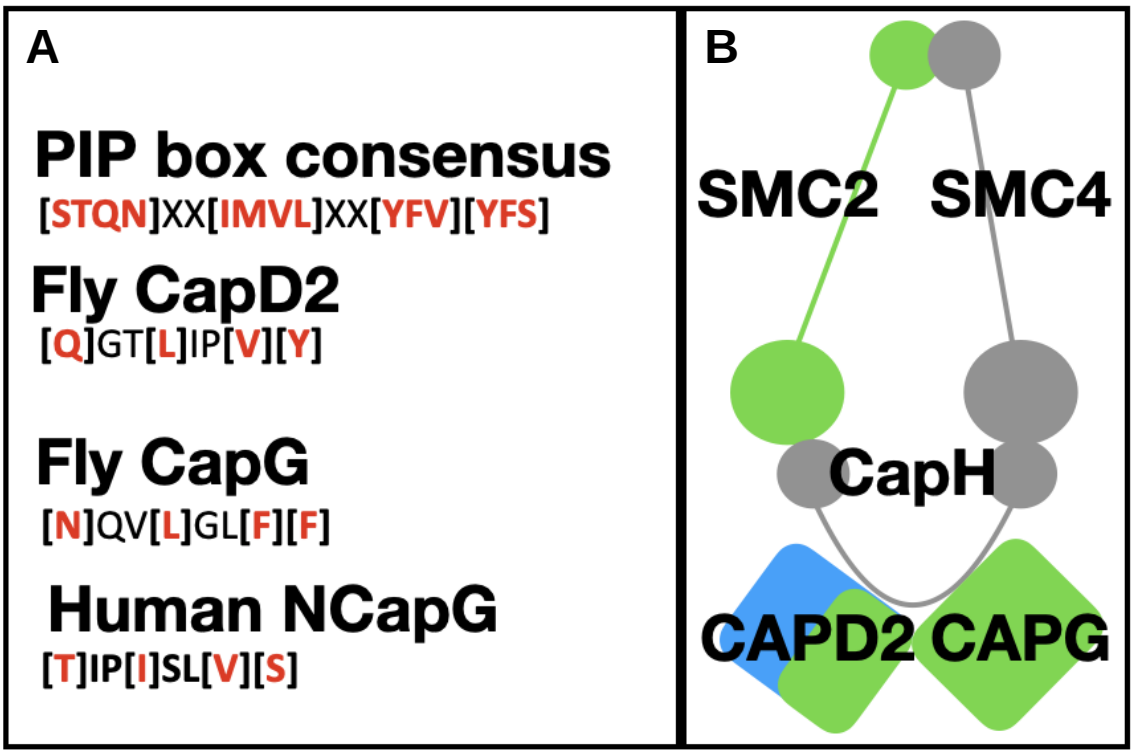

Figure 31: Condensin I proteins interact with Cdt2 after IR

(A) Consensus sequence for PIP box. Fly CapD2 and CapG contain PIP boxes along with Human NCapG. (B) Condensin I complex. Proteins in green were identified in Co-IP with Cdt2-GFP. Blue proteins are identified to have *in vivo* phenotype linked to $CRL4^{CDT2}$.

3.2.9 Cap-D2 localizes to nuclear periphery and MN in *cdt2* RNAi papillar cells following DSBs

Using an antibody for *Drosophila* CapD2, we stained mitotic rectums +/- *cdt2* RNAi after *hs-I-Cre*I-induced DSBs. Our hypothesis was that if $CRL4^{CDT2}$ indeed regulates condensin I following DSBs, then CapD2 expression should increase in *cdt2*

RNAi animals. In WT animals, CapD2 expression remained diffuse across interphase and mitotic nuclei (Fig32A). This is in contrast to what we observed in *cdt2* knockdown animals, in which CapD2 displayed two obvious localization patterns. The first observation was that CapD2 localized to the nuclear periphery of *cdt2* RNAi papillar cells (Fig32C). The relative intensity of CapD2 expression in the nuclear periphery was higher than both inside and outside of the nucleus (Fig32D). This is in contrast to WT animals, which, similar to our observation that CapD2 remains diffuse, CapD2 relative intensity levels remained consistent regardless of the subcellular compartment (Fig32A-B). Our second observation was that CapD2 localized to micronuclei in *cdt2* RNAi animals following mitosis (Fig32C). We also observe increased CapD2 localization on acentric fragments and on the ends of anaphase chromosomes facing acentric fragments during anaphase in *cdt2* RNAi animals compared to WT animals which do not have increased expression on anaphase chromosomes and segregating acentric fragments (data not shown). Our data is consistent with the conclusion that $CRL4^{CDT2}$ is required for condensin I regulation following DSBs during the mitotic stage in papillar cells. When $CRL4^{CDT2}$ is inhibited, CapD2 levels are increased at the nuclear periphery and on micronuclei following mitosis.

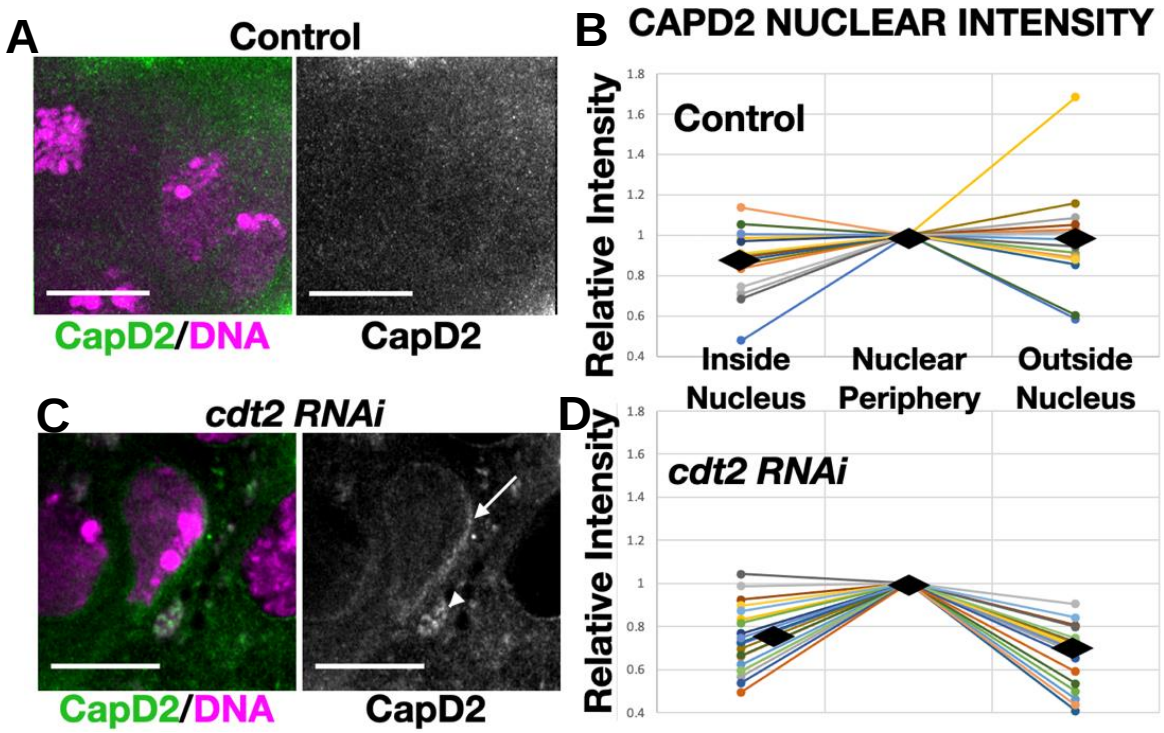

Figure 32: Loss of *cdt2* results in increased Cap-D2 expression on the nuclear periphery and MN

(A) WT mitotic stage rectums with CapD2 antibody staining. CapD2, green; DNA, magenta. Scale bars = 10 μm. (B) Quantification of the relative intensity of CapD2 in WT papillar cells. (C) *cdt2* RNAi mitotic stage rectums with CapD2 antibody staining. White arrows- nuclear periphery staining. White arrowheads – micronuclei. All other labeling as in A. (D) Quantification of the relative intensity of CapD2 in *cdt2* RNAi papillar cells.

3.3 Discussion

Our previous study identified that DNA damage signaling is important for segregating acentric fragments during mitosis when checkpoints are compromised in interphase (Chapter 2). This chapter contributes to our growing knowledge of

mechanisms that cells employ to segregate broken chromosomes in mitosis. Moreover, we have identified two distinct pathways (FA and $CRL4^{CDT2}$), which are required for acentric DNA segregation.

To determine the extent that the FA pathway contributes to acentric DNA segregation and genome stability in checkpoint-inactive cells, we generated three new reagents: (1) a CRISPR mutant lacking the conserved monoubiquitination residue of Fancd2 (*fancd2*^{K595R}), (2) a transgenic animal ubiquitously expressing a GFP-tagged WT Fancd2, and (3) a transgenic animal ubiquitously expressing a GFP-tagged Fancd2 with the K595R point mutation. Additionally, we serendipitously acquired both a Fancd2 deletion and an additional Fancd2 point mutant in a conserved residue (*fancd2*^{D644E}). both which displayed a DSB-specific decrease in adult papillar cell number similar to tested *fancd2*^{K595R} lines suggesting that both these animals have disrupted Fancd2 function. Overall, these reagents will be useful in understanding the role of conserved Fancd2 domains and residues in regulating genome stability in cells with inactive checkpoints and persistent mitotic DNA damage.

Furthermore, revisiting our candidate screen, we also identified the $CRL4^{CDT2}$ as a novel complex to be required for acentric DNA segregation during mitosis. More specifically, *cdt2* is required for acentric DNA segregation. A Co-IP identified two

additional complexes, CSN and condensin I, to interact with Cdt2 following IR *in vitro*. We show *in vivo* that both *csn2* and CapD2 regulation have important roles in DDRs in checkpoint inactive papillar cells. These results signify both a novel role for $CRL4^{CDT2}$ in acentric DNA segregation and novel connection between $CRL4^{CDT2}$ and the condensin I complex.

3.3.1 Expanding on the role of Fancd2 in mediating acentric segregation using new reagents

We generated several genetic tools to study the role of Fancd2 in segregating acentric DNA during mitosis. We have characterized these reagents in both whole fly and tissue-specific contexts. *fancd2*^{K595R} flies are homozygous viable and fertile. The *fancd2*^{K595R} mutation also results in adult eye tumors in the absence of exogenous DNA damage and persistent Mre11 foci during mitosis following DSBs. Further, *fancd2*^{K595R} survival can be rescued with expression of the Ubi-GFP-Fancd2 transgene. We did not observe this rescue in Fancd2 deletion animals, nor can Ubi-GFP-Fancd2 rescue adult rectum phenotypes in Fancd2 deletion animals. Ubi-GFP-Fancd2 displays pan-nuclear expression in cycling cells (mitotic and endocycling) in both developing and adult *Drosophila* tissues. Ubi-GFP-Fancd2 foci are recruited to IR-induced DSBs and these breaks persist in papillar cells similar to *hs-I*-CreI-induced DSBs. However, persistent foci recruitment was not observed in Ubi-GFP-Fancd2 K595R flies.

Understanding Fancd2 modifications, localization, and kinetics are crucial for identifying the contributions of FA proteins in segregating acentric DNA during mitosis. We hypothesize that monoubiquitinated Fancd2 is recruited to resected DNA ends and recruits downstream repair proteins responsible for repairing acentric DNA to the rest of the genome. Future investigations should look further into the role of Fancd2 in promoting acentric DNA segregation through additional post-translational modifications and other protein-protein interactions. Based on our observations and previous studies, our hypothesis is that Fancd2 monoubiquitination is required for Pol Theta recruitment to acentric DNA [116]. Identifying if monoubiquitinated Fancd2 directly or indirectly recruits Pol Theta is crucial in understanding the molecular network involved in repair of acentric DNA as well as the physical connections that promote acentric DNA segregation in mitosis.

Further, identifying the extent, if any, that other posttranslational modifications are required for the role of Fancd2 in acentric DNA segregation is of great interest. As Fancd2 is phosphorylated by various PIKKs in mice and humans, investigating whether *Drosophila* Fancd2 is also phosphorylated will be useful in developing tools in our papillar cell model. Additionally, as Fancd2 is therapeutic target for cancer treatments,

identifying important translational modifications and downstream targets following DSBs will be of interest for future studies [94, 116, 136, 163].

3.3.5 CRL4^{CDT2} is a novel complex implicated in acentric DNA segregation

Every gene in the CRL4^{CDT2} complex is required for adult papillar cell survival following *hs-I-Cre*I-induced DSBs. Further, *cdt2*, which confers substrate specificity for CRL4^{CDT2}, is required for acentric DNA segregation during mitosis and micronuclei prevention. In order to investigate the role of CRL4^{CDT2} in segregating acentric DNA fragments, we identified 480 binding partners for GFP-Cdt2 specifically following IR in S2 cells. Of these 480 proteins, two proteins were a part of the CSN complex, both a known regulator of CRLs and a complex with a component that was identified as hit with our initial candidate screen *in vivo* (*csn2*) [152-155]. 27 of these proteins contained a PIP degron and are therefore putative targets for CRL4^{CDT2} degradation. Two of these 27 proteins were components of the condensin I complex (CapD2 and CapG) while one condensin I member (SMC2) did not contain a PIP degron but did interact with GFP-Cdt2 following DNA damage [161, 162]. To validate that CRL4^{CDT2} impacts condensin I following DSBs *in vivo* we stained WT and *cdt2* RNAi rectums with a CapD2 antibody. We observed that *cdt2* knockdown results in increased CapD2 expression around the nuclear periphery and micronuclei following mitosis and mitosis with failed acentric

DNA segregation, respectively. These results are consistent with a role for $CRL4^{CDT2}$ in regulating condensin I expression following DSBs in cells with persistent broken chromosomes.

We hypothesize that $CRL4^{CDT2}$ promotes chromatin relaxation to allow for the recruitment of DSB repair proteins which facilitate repair and rescue of acentric DNA during mitosis (Fig33A-B). $CRL4^{CDT2}$ is regulated by CSN to allow for regulation of repair similar to its function in cell cycle progression or DNA repair during interphase arrest [144]. $CRL4^{CDT2}$ has been observed to prevent chromatin compaction during DNA replication through degradation of one of its well-known targets, Set8, a histone methyltransferase [164]. It is therefore possible that $CRL4^{CDT2}$ can influence chromatin confirmation during other stages of the cell cycle. Further, $CRL4^{CDT2}$ has been identified to have functions outside of its role in S-phase underscoring the possibility that $CRL4^{CDT2}$ may have various mechanisms of chromatin organization during distinct stages of the cell cycle [158].

We cannot rule out other possible contributions of $CRL4^{CDT2}$ in preventing acentric DNA mis-segregation. $CRL4^{CDT2}$ also regulates cell cycle checkpoints during S-phase and at the G_2/M transition [158]. Papillar cells, along with other endocycled cells, don't appear to arrest their cell cycle during interphase following DNA damage [47, 48,

51, 89, 165]. It is thus possible that $CRL4^{CDT2}$ also controls cell cycle arrest in papillar cells after DSBs. $CRL4^{CDT2}$ targets p21 and Chk1 for destruction, preventing cell cycle arrest. As papillar cells are not responsive to changes in p53 or are dependent on Chk1 and Chk2 kinases, it is possible that $CRL4^{CDT2}$ is responsible for mediating this response. Future studies investigating whether double mutants for *cdt2*, *p21*, and *chk1*/*chk2* can rescue any defects observed in *cdt2* knockdown animals will be of great interest in determining other contributions of $CRL4^{CDT2}$ in segregating acentric DNA in mitosis.

Lastly, we hypothesize that FA proteins and $CRL4^{CDT2}$ represent distinct but possibly overlapping mechanisms of acentric DNA segregation during mitosis. Indeed, FA proteins did were not found in our list of 480 proteins to interact with Cdt2, however proteins from the MRN complex did. It is possible then that Cdt2 is recruited earlier than Fancd2 to prevent both cell cycle arrest and chromatin condensation to facilitate MRN binding upstream of Fancd2 recruitment. Future studies investigating if Fancd2 foci recruitment is dependent on *cdt2* will shed light on whether or not this mechanism is used. Additionally, *Drosophila* Fancd2 does not possess a PIP degron like CapD2 and is not likely targeted for destruction by $CRL4^{CDT2}$. Overall, our studies demonstrate a novel mechanisms of acentric DNA segregation by identifying an interaction with condensin I and $CRL4^{CDT2}$. As both *cdt2* and *fancd2* mutations have been implicated in

various cancers, future studies investigating synthetic lethality between *fancd2*^{K595R} and *cdt2 RNAi* in segregating acentric DNA will also be of interest for its therapeutic applications [157, 163].

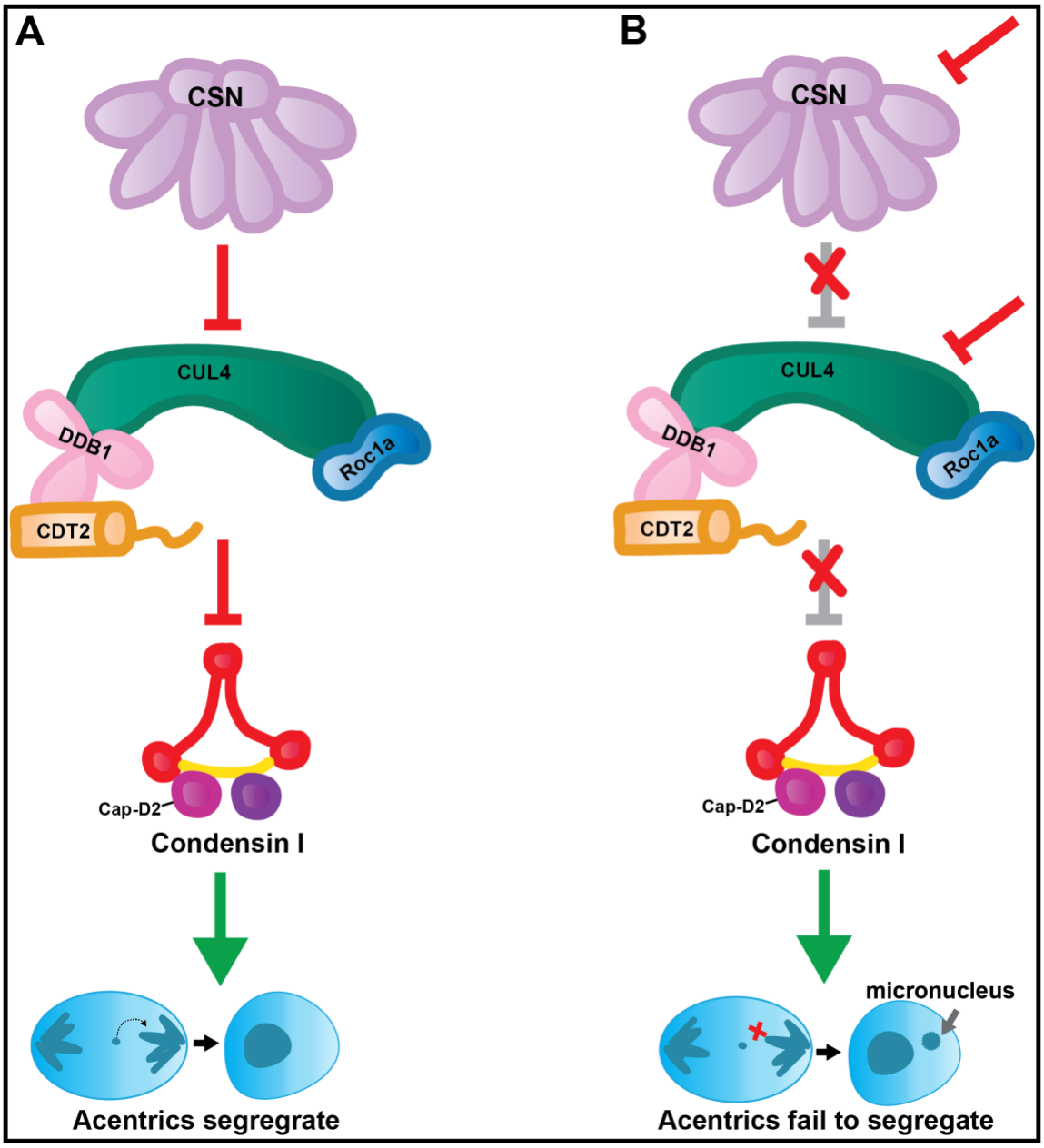

Figure 33: Model Figure - CSN and CRL4^{CDT2} regulate acentric DNA segregation through Condensin I inhibition

(A) In WT papillar cells, CSN regulates CRL4CDT2 activity which is required for condensin I inhibition during acentric DNA segregation. (B) In *cdt2* RNAi animals, condensin I levels remain elevated which prevents acentric from segregating, increases micronuclei, and causes papillar cell loss. Knock down of CSN component, *csn2,* also leads to papillar cell loss following DSBs.

4. Conclusions

This dissertation details mitotic DNA damage responses using *Drosophila* rectal papillar cells as a model. In this final chapter, I will conclude by summarizing my key findings for each chapter. I will then provide additional insights on future directions for this work, propose additional models based on our studies and the current literature, and finally, I will discuss the significance of our findings within the context of the field of mitotic DDRs, polyploid DDRs, and connections to cancer biology.

4.1 Chapter 2 – An alt-EJ repair intermediate promotes acentric DNA rescue during mitosis

Chapter 2 contains my first author publication in which I detail a proposed mechanism for how acentric DNA fragments can physically segregate during mitosis when checkpoints are inactive in interphase. Despite our model system, papillar cells, lacking canonical interphase DNA damage checkpoint features (p53, chk1/chk2, cell cycle arrest, cell death when DSBs are high), these cells can still recruit DNA repair proteins with similar kinetics to cells that have intact DNA damage checkpoints in interphase. The key difference is that while checkpoint-intact larval brain progenitors clear DNA repair protein foci within 24 hours, papillar cells show persistent DNA repair foci recruitment for several days (5-6 d).

These proteins, Mre11, RPA3, and Fancd2, all persist on damaged papillar chromosomes as these cells enter mitosis. During mitosis, RPA3 displays distinct kinetics where as Mre11 and Fancd2 foci are resolved during prophase, prior to NEBD, RPA3 foci persist after NEBD and are mostly resolved by metaphase. RPA3 foci kinetics are regulated by both the monoubiquitinated form of Fancd2 and the alt-EJ protein, Pol Theta. Loss of *polQ* and Fancd2 monoubiquitination mutants results in persistent RPA3 foci lasting past mitosis into the following interphase as well as a failure of acentric DNA to properly segregate during mitosis. Taken together, these data suggest that an alt-EJ repair intermediate promotes acentric DNA segregation during mitosis when DNA damage checkpoints are inactive during interphase.

4.1.1 DNA repair proteins display delayed kinetics in the absence of a DNA damage checkpoint

Cell cycle checkpoints are put in place to allow for adequate surveillance of the genome and to ensure that DNA damage is repaired in a timely fashion [1, 2, 4]. This transcription-mediated response halts the cell cycle and is coordinated with DNA damage repair to allow enough time for cells to repair DNA damage before returning to the cell cycle [166]. Outstanding questions remain regarding how cell cycle checkpoints are coordinated with DNA damage repair [19, 167]. Our study provides evidence for how DNA repair and cell cycle checkpoints may be uncoupled in certain circumstances.

Previous studies have shown that cells can recruit repair proteins when checkpoints are dysregulated. *Drosophila* salivary glands represent an example of this, in which these cells presumably inactivate checkpoints as they undergo several rounds of endocycling during *Drosophila* development. Despite this, *Drosophila* salivary gland cells recruit persistent gH2Av indicating that there is DNA damage signaling occurring in these cells [65]. Furthermore, cancer cells, which largely dysregulate cell cycle checkpoints not only recruit DNA damage proteins, but also upregulate them in response to DNA damage [42, 43].

Coordination of cell cycle checkpoints and DNA repair is thus context specific. Lack of robust cell cycle checkpoints appear to have at least two consequences on DNA repair. Based on our findings that checkpoint-inactive papillar cells show persistent recruitment of Mre11, RPA3, and Fancd2 foci, it is likely that checkpoints ensure that DNA repair takes places efficiently. This is supported by evidence present in the aforementioned studies in which the lack of cell cycle checkpoints results in delayed DNA repair. Second, it is likely that cell cycle checkpoints regulate DNA repair, as DNA repair genes are upregulated in checkpoint-active polyploid cells [42]. As we don't have evidence that papillar cells upregulate DNA repair genes, we can only speculate potential consequences of increased DNA repair capacity. Papillar cells rely on the alt-EJ

gene, *polQ* for regulation of DNA repair kinetics and acentric DNA rescue which is a highly mutagenic pathway. Studies have shown that cancer cells also disproportionately rely on alt-EJ repair compared to noncancerous cycling cells [100, 106, 168, 169]. It is therefore possible that cell cycle checkpoints influence DNA repair pathway decisions, and that loss of cell cycle checkpoints alter pathway choice, leading to more deleterious pathways.

4.1.2 DNA repair proteins are present and dynamic during mitosis

It was previously thought that DNA repair events are largely shut down during mitosis. This idea is constantly being challenged with increasing evidence for repair events occurring during mitosis. Several groups have identified both DNA repair protein recruitment to mitotic chromosomes following DNA damage as well as the occurrence of DNA repair synthesis during mitosis [31, 32, 34-36, 38, 39, 75, 170, 171]. Similarly, we observe Fancd2, Mre11, and RPA3 recruitment to mitotic papillar chromosomes. These proteins have distinct kinetics, indicating that potential repair events may be taking place during this time window. Other groups have described mechanisms of initiated but incomplete repair that starts in S-phase and needs to be resolved by mitosis. Replication stress, underreplication at common fragile sites, and incomplete repair during S-phase are likely to produce DNA catenanes that provide

barriers to successful cell division through the presence of UFBs during mitosis. Similarly, we believe that papillar cells initiate repair events and that these events need to be completed by mitosis in order to prevent broken chromosomes from mis-segregating into a micronucleus.

As mentioned in the Discussion of Chapter 2, we believe there are key differences in the repair intermediates that we observe in papillar cells compared to the UFBs that have been previously described [110, 172, 173]. Alt-EJ requires annealing of short microhomologies around the site of a break as opposed to HR which requires long range end resection and strand invasion. While unwound invaded strands produce long RPA-coated strands, we speculate that alt-EJ repair leads to displaced RPA and subsequent annealing of broken DNA ends by Pol Theta and monoubiquitinated Fancd2. This unwound, annealed DNA may not be able to be detected by using reporters for histones (HisH2Av) or DAPI, but may be detectable using reporters for unwound DNA or proteins believed to be recruited downstream of RPA3 removal. In addition to RPA and BLM, thymidine analogs such as BrdU and EdU also label DAPI negative-UFBs [173-175]. It remains to be determined if EdU or BrdU localizes to gaps between acentric and centric fragments. Thymidine analog incorporation to acentric DNA gaps along with the requirement for Pol Theta for thymidine analog incorporation

to these sites would support our hypothesis that acentric DNA forms an alt-EJ intermediate.

As Pol Theta is both required for RPA3 removal during acentric DNA segregation in papillar cells and progression of alt-EJ repair, future studies addressing if Pol Theta is recruited to acentric/centric DNA gaps will be useful [100]. Further, alt-EJ requires repair synthesis when gap-filling [96, 176]. It remains to be determined the extent to which acentric fragments are repaired and labeling with either BrdU or EdU will elucidate if and when repair is occurring. Additionally experiments to address the timing of DNA repair synthesis may involve use of a cell cycle reporter, such as the RGB cell cycle tracker transgene generated by Handke and colleagues [177].

4.1.3 Monoubiquitinated Fancd2 and Pol Theta work together to promote DNA repair protein resolution and acentric DNA rescue during mitosis

We identified an epistatic interaction between *fancd2*^{K595R} mutants and *polQ* RNAi animals in preventing micronuclei and regulating DNA repair kinetics during mitosis. We thus conclude that both monoubiquitinated Fancd2 and Pol Theta function to promote an alt-EJ repair intermediate that is needed to rescue persistent broken chromosomes during mitosis.

A surprising observation was that neither NHEJ nor HR are required for acentric DNA segregation during papillar cell mitosis (Chapter 2, Fig14; Table 1). In *S. pombe*, acentric chromosome segregation occurs through "noncanonical HR" repair that is not dependent on Rad51 [178]. This is similar to our observation that Rad51 is not required specifically for acentric DNA segregation during mitosis but likely has other requirements for normal development (Chapter 2, Fig14). The question still remains as to why papillar cells would select the alt-EJ repair pathway, which leads to deleterious genomic rearrangements, and not error-free HR [5, 30].

In order for HR to occur, a repair template must be present in the cell which typically occurs in S/G_2 phase of the cell cycle [5, 34, 92]. During the developmental time window that we induce DSBs in papillar cells, these cells are undergoing the endocycle where HR should be the prominent pathway choice [5, 92]. Additionally, Rad51 is recruited to polyploid papillar chromosomes even in the absence of exogenous DNA damage (Chapter 2, Fig14C-D) . Even in *Drosophila* salivary glands which contain polytene cells, Arp2/3-driven relocalization of heterochromatin to the nuclear periphery occurs – similar to what is observed during HR in other *Drosophila* cell types [67, 87]. It is worth noting that in some cases, what are considered "back-up" pathways may be preferable to major DSB repair pathways. For example, in polyploid cells with multiple

homologous chromosomes in organisms that have highly-repetitive genomes, HR may be more deleterious than alt-EJ. HR in such case may result in either an increased likelihood of end to end chromosome fusions if multiple DSBs are present or in more deleterious rearrangements than the inevitable insertions and deletions that occur from alt-EJ [87]. As noted in the **Introduction** chapter, the context in which DNA damage arises is important in understanding repair pathway choice.

Another possibility for as to why alt-EJ is the repair pathway of choice in papillar cells may be due to the chromosome conformation in endocycled cells and the resulting physical restrictions of long-range end resection. It is therefore possible that downstream repair events may be actively inhibited in papillar cells during the endocycle to the first mitotic division. Findings from a previous study [54, 179] identified that papillar chromosomes are polytene following endocycling. Of note, the most dynamic changes we observe with Mre11 and RPA3 recruitment occur during early prophase around the time of NEBD. Indeed, we have reported that papillar cells must reverse polyteny through a cohesion ring opening-mediated mechanism of separating into the most recently replicated sister chromosome so that papillar cells can segregate their chromosomes during mitosis [179]. Based on these two lines of evidence, we hypothesize that papillar cells are capable of recruiting early acting DSB repair

machinery following DNA damage but that repair is halted due to limited end resection in polytene chromosomes. Following interphase, when these cells are no longer polytene, repair is able to progress and is likely mediated through alt-EJ based on the requirement of *polQ* and not HR or cNHEJ machinery.

As DSBs are naturally accumulating during the endocycle in papillar cells as are the exogenous DSBs that we induce using IR/I-CreI, it is possible that resection machinery is present and actively inhibits cNHEJ. Thus, if resected DNA cannot recruit cNHEJ machinery and the chromosome confirmation precludes long-range resection needed for HR or SSA, alt-EJ would likely be the repair pathway of choice.

Furthermore, while we don't have definitive evidence that complete repair of acentric DNA is occuring or if any repair events are happening specifically during mitosis, there is evidence that alt-EJ can occur during mitosis and during the following G_1 [114, 115]. In *Xenopus* mitotic extracts, Pol Theta is important for repair of replication-induced damage specifically during mitosis, where HR and NHEJ are inactive [114]. In human cells, Pol Theta binds to chromatin fractions as cells exit mitotis and enter G_1, even in the absense of DNA damage [115]. Taken together, these findings support a model in which Pol Theta can function during mitosis to displace RPA3 and promote alt-EJ of acentric DNA ends.

4.2 Chapter 3 – A candidate screen identified the FA pathway and CRL4^{CDT2} as regulators of acentric DNA segregation

In Chapter 3, I expand on the contributions of Fancd2 in promoting acentric DNA segregation during mitosis in papillar cells. I generated several genetic tools to understand both the requirement of Fancd2 post-translational modifications and Fancd2 localization. Additionally, I introduced a novel complex to be implicated in promoting acentric DNA segregation, CRL4^{CDT2}. This complex was identified from our initial candidate screen performed in Chapter 2 (Table 1). Follow-up analysis involved performing a Co-IP to identify potential novel targets of CRL4^{CDT2}-mediated degradation. Indeed we have identified a potential target of this complex, condensin I, and hypothesize that CRL4^{CDT2}-mediated regulation of condensin I promotes local chromatin relaxation around the site of papillar cell DSBs, facilitating the recruitment of DSB repair proteins.

4.2.1 Developing tools to uncover mechanisms of Fancd2-mediated acentric DNA segregation We identified a novel complex to be involved

We developed a CRISPR HDR-mediated mutant of Fancd2 in which the conserved monoubiquitination domain was mutated from a lysine to an arginine (*fancd2*^{K595R}). This mutation was identified to prevent Fancd2 monoubiquitination *in vitro* [108]. Additionally, we cloned full length *Drosophila* Fancd2 and Fancd2 with the K595R

point mutation, fused to an eGFP, into a pBID vector for ubiquitous expression in flies. We validated that these transgenic animals display pan-nuclear expression in actively cycling cells and that in the Ubi-Fancd2-GFP WT animals but not in Ubi-Fancd2-GFP K595R animals, Fancd2 foci are recruited following *hs-I-Cre*I and IR mediated DSBs.

While genetic screens performed in *Drosophila* have provided useful insights in the field of DNA damage repair [5, 12], studying individual DNA damage proteins in flies present a few challenges. Limited tools exist in *Drosophila* to study certain DNA repair proteins to due limited conservation between *Drosophila* DNA repair proteins and mice and humans [5]. Therefore novel reagents must be generated to further our understanding of how these proteins function *in vivo* and to enhance the strength of studying DDRs using *Drosophila*, an already strong model for understanding genetic interactions of DDR proteins.

Fancd2 is a great example of a DNA repair protein with conserved function but poor conservation at the sequence level. Indeed, *Drosophila* Fancd2 is only 23% identical to human Fancd2 (compared to 75% identity of mouse Fancd2). Further analysis involving generation of new Fancd2 reagents for *Drosophila* as well as further investigations using the tools created for Chapters 2 and 3 will be crucial in understanding the mechanisms of acentric DNA segregation during mitosis in papillar

cells. We have yet to identify mutants that disrupt Fancd2-GFP kinetics, as Mre11 and RPA are disrupted in *fancd2*^{K595R} mutants. It would be interesting to identify additional downstream targets of Fancd2 to determine the mechanisms of Fancd2 resolution during mitosis. Mitotically active proteins may also be recruited to acentric fragments downstream of Fancd2 removal, making them of great interest to identify so that the nature of the physical tether connecting acentric fragments to its centric partner may be elucidated.

Our *fancd2*^{K595R} mutants thus far have provided strong evidence for the requirement of Fancd2 post-translational modifications in promoting acentric DNA segregation. Additionally analysis may involve the generation of additional double mutants, similar to our experiments with *polQ* RNAi to identify factors that may act together or in parallel with monoubiquitinated Fancd2 (See Subsection 4.2.3 for more details). Further, understanding DNA repair pathway choice may also be of great interest using our *fancd2*^{K595R} mutants. For example, we hypothesize that in addition to recruiting Pol Theta to acentric DNA, monoubiquitinated Fancd2 also prevents cNHEJ through inhibition of Ku binding to short-range resected DNA. Testing the effects of *fancd2*^{K595R} and Ku mutants is a potential future direction for understanding mechanisms of DNA repair pathway choice. Lastly, the generation of these Fancd2 CRISPR mutants

may also shed light on mutations found in human cancers. We serendipitously generated a Fancd2 mutant with a point mutation in a conserved residue (*fancd2*^{D644E}). Interestingly, this mutation (*fancd2*^{D604E}) was found in a breast cancer patient with distance metastasis and relapse [180]. We find that similar to *fancd2*^{K595R} mutants, *fancd2*^{D644E} mutants show a loss in papillar cell number following DSBs. This underscores the feasibility and significance of studying conserved Fancd2 mutations using *Drosophila* as a model.

4.2.2 CRL4^{CDT2} is required for acentric DNA segregation and regulates the condensin I complex during the mitotic window

We identified a novel complex to be involved in acentric DNA segregation, the E3 ubiquitin ligase, CRL4^{CDT2}. This complex has known roles in DNA replication and cell cycle progression, but a mitotic function for CRL4^{CDT2} has yet to be elucidated. We also identified 480 proteins (Table 3) that interact with Cdt2-GFP, a GFP-tagged form of the protein that confers substrate specificity for CRL4^{CDT2}. Of these 480 proteins, 27 are putative targets of CRL4^{CDT2} in that they possess the consensus sequence for the PIP degron, a motif that promotes PCNA-mediated degradation by CRL4^{CDT2}. Of these 27 proteins, we identified two proteins that are a part of the condensin I complex, CapD2 and CapG. We observed that *cdt2* RNAi results in increased CapD2 expression around the nuclear periphery and micronucleus of cells that recently missegregated broken

chromosomes. We proposed a model in which $CRL4^{CDT2}$ promotes inhibition of condensin I to allow for chromatin relaxation at the site of acentric DNA fragments and subsequent DNA repair protein recruitment.

DNA repair protein interactions with condensin I complex members to promote DNA repair has been previously identified in human and mouse cell lines during interphase [181]. It is important to note that this interaction is also specific to SSB as abrogating condensin I had no effect on DSB repair during interphase [181]. Is thus possible that condensin I plays a role in the DNA damage response and that the type of DNA damage may influence condensin I interactions. In line with this logic, human condensin I recruitment to chromatin is also actively inhibited during G_2/M DNA damage checkpoints by Chk2. It is therefore possible that papillar cells, which do not depend on Chk1 or Chk2 kinases and do not arrest their cell cycle, depend on $CRL4^{CDT2}$ to prevent condensin I recruitment to chromatin following DSBs. Condensin I is typically recruited to chromatin following NEBD during prophase [182]. This is during the same timeframe as the resolution of DNA repair proteins that we hypothesize are needed for acentric DNA segregation. Additionally, $CRL4^{CDT2}$ actively inhibits Chk1 in a PCNA-independent manner to prevent cell cycle arrest at G_2/M [156]. We therefore hypothesize that papillar cells may depend on $CRL4^{CDT2}$ to inhibit checkpoints during

interphase while promoting DNA repair through chromatin relaxation at DSBs following DNA damage.

4.2.3 Proposed mechanism for Fancd2 and CRL4^{CDT2} cooperation during acentric DNA segregation – potential targets for synthetic lethality

We thus far have identified at least two distinct mechanisms of acentric DNA rescue during mitosis through the findings that both monoubiquitinated Fancd2 and CRL4^{CDT2} is required for this process. Monoubiquitinated Fancd2 works in concert with alt-EJ protein, Pol Theta to regulate DNA repair protein dynamics at DSBs during mitosis. In contrast, CRL4^{CDT2} interacts with condensin I proteins following DNA damage *in vitro*. These proteins contain a PIP degron consensus sequence needed for CRL4^{CDT2}-mediated degradation through PCNA interactions on chromatin. Further, we show *in vivo* that *cdt2* knockdown leads to increased condensin I localization on the nuclear periphery and micronuclei suggesting that CRL4^{CDT2} regulates chromatin changes through condensins to promote acentric DNA segregation.

Additional experimentation on whether loss of either CRL4^{CDT2} components or Fancd2 impacts the dynamics of the other protein/complex will be interesting. For example, future studies investigating whether *cdt2* knockdown disrupts Fancd2-GFP foci recruitment will be important in pinpointing the timing of CRL4^{CDT2} function. If the

hypothesis is that $CRL4^{CDT2}$ is needed for chromatin changes necessary for DNA repair protein recruitment, *cdt2* RNAi should indeed disrupt Fancd2 foci recruitment. Moreover, Fancd2 monoubiquitination mutants should not impact CapD2 levels if this hypothesis is correct.

Lastly, synthetic lethality is a tool cancer researchers have been investigating to improve therapeutic treatments. An additional future direction for this study should involve testing if $fancd2^{K595R}$ mutants and *cdt2* RNAi animals result in synthetic lethality following DNA damage. More specifically, if $fancd2^{K595R}$; *cdt2* RNAi double mutants show combinatory effects on micronuclei frequency and adult papillar cell loss, this will provide strong evidence for targeting these genes for cancer treatment. As papillar cells already possess overlapping traits to cancer cells that are resistant to traditional DNA-damage causing therapies, this could be a novel combinatorial therapy for treatment-resistance cancers.

4.3 Summary

In summary, DSBs present in mitosis pose a strong threat to genomic integrity and can give rise to neoplasia, cell death, or senescence [34]. This body of work proposes several models of how cells with DSBs present during mitosis prevent loss of genetic material and cell death. This work contributes to the growing knowledge that in

polyploid cells or in cells with inactive or dysregulated cell cycle checkpoints, DDRs are rewired to promote cell viability. Cancer is associated with both polyploidy and inactive checkpoints, therefore this work in papillar cells is of great significance in studying human disease phenotypes and potential therapies.

Appendix A

A.1 Methods and Materials

A.1.1 *Drosophila* Stocks

Table 4: A list of fly stocks used in this thesis

Figure	Reagent	Source Info
All data Figures	*hs-I-Cre*I	Bloomington *Drosophila* Stock Center; RRID:BDSC_6936
4-6,9, 12, 25	*ubi-mre11-GFP (II)*	[38]
4-6,9, 12, 25	*ubi-mre11-GFP (III)*	[38]
7-9, 13, 16, 19	*ubi-RPA3-GFP (II)*	[85]
7-9,	*ubi-RPA3-GFP (III)*	[85]
10-11	*UAS-mre11 RNAi*	Bloomington *Drosophila* Stock Center; RRID:BDSC_39028
9-11, 15-17, 19, 21, 28-30, 32	*byn-Gal4*	[186]
9-11, 15-17, 19, 21, 28-30, 32	*tub-Gal80^{ts}*	Bloomington *Drosophila* Stock Center; RRID:BDSC_ 7018
10-11, 19	*His-2av-GFP*	Bloomington *Drosophila* Stock Center; RRID:BDSC_24163

10-11	*tomato-Cenp-C*	[187]
12, 13	*hisH2AVRFP*	Bloomington *Drosophila* Stock Center; RRID:BDSC_23651
17	*UAS-fancm RNAi*	Vienna *Drosophila* Resource Center VDRC: 104865
17	*UAS-fancl RNAi*	Vienna *Drosophila* Resource Center VDRC: 32025
18, 19, 21, 24-26	$fancd2^{K595R/K595R}$	This study (See *Drosophila* Culture & Genetics)
26	$fancd2^{deletion}$	This study (See *Drosophila* Culture & Genetics)
24	$fancd2^{D644E/D644E}$	This study (See *Drosophila* Culture & Genetics)
20, 26	*Ubi-GFP-Fancd2*	This study (See *Drosophila* Culture & Genetics)
27	*Ubi-GFP-Fancd2 K595R*	This study (See *Drosophila* Culture & Genetics)
19	*UAS-fancd2 RNAi*	[108]
15, 16	*UAS- dna polymerase theta RNAi*	Bloomington *Drosophila* Stock Center; RRID:BDSC_58238
15,16, 21	*UAS- dna polymerase theta RNAi*	Vienna Drosophila Resource Center VDRC: 104788
9	ry^{776+} *gRNA*	[88]
9	*UAS-Cas9*	Bloomington *Drosophila* Stock Center; RRID:BDSC_54594

14	*UAS-rad51 RNAi*	Bloomington *Drosophila* Stock Center; RRID:BDSC_38898
14	*w1118*	Bloomington *Drosophila* Stock Center; RRID:BDSC_3605
29	*UAS-Moesin-GFP*	[188]
28, 32	*UAS-cdt2 RNAi*	Bloomington Drosophila Stock Center; RRID:BDSC_51510
28, 29	*UAS-cdt2 RNAi*	Vienna Drosophila Resource Center VDRC: 31484
28	*UAS-ddb1 RNAi*	Bloomington *Drosophila* Stock Center; RRID:BDSC_41997
28	*UAS-ddb1 RNAi*	Bloomington *Drosophila* Stock Center; RRID:BDSC_33888
28	*UAS-roc1a RNAi*	Bloomington *Drosophila* Stock Center; RRID:BDSC_32362
28	*UAS-roc1a RNAi*	Vienna Drosophila Resource Center VDRC: 32339
28	*UAS-cul4 RNAi*	Bloomington *Drosophila* Stock Center; RRID:BDSC_50614
28	*UAS-cul4 RNAi*	Vienna Drosophila Resource Center VDRC: 105668
30	*UAS-csn2 RNAi*	Bloomington *Drosophila* Stock Center; RRID:BDSC_28908

A.1.2 *Drosophila* Culture & Genetics

Flies were raised on standard fly food (Archon Scientific, Durham, NC) at 22ºC except for when experiments were conducted with *tub-Gal80^{ts}*. In experiments using *tub-Gal80^{ts}*, animals were raised at 18ºC until the second larval instar stage, when DNA damage was induced (see DNA Damage). Those animals were then shifted to 29ºC during the feeding third larval instar stage.

The *fancd2$^{K595R/K595R}$* flies were generated by GenetiVision Corporation (www.genetivision.com). The K595R mutation was created via two steps of CRISPR-Cas9 mediated HDR (homology directed repair) events. In the first step, two CRISPR-Cas9 targets were designed to delete a 490 bp fragment containing the K595. Two guide RNAs were cloned into pCFD3 vector (http://www.flyrnai.org/tools/grna_tracker/web/files/Cloning-with-pCFD3.pdf)

and a donor DNA was created with a GFP cassette flanked by two 1 kb f*ancd2* sequences beyond cleavage sites. Upon co-injection of both DNA constructs, two gRNAs were expressed to direct the double strand break (DSB) by Cas9 (endogenously expressed in the injection stock BL#54591). After the DSB, the GFP cassette was inserted into *fancd2* genome via donor DNA mediated recombination. In the second step, based on the same principle, a 1039 bp DNA containing GFP cassette (plus neighboring *fancd2*

sequences) was substituted by the mutant allele containing K595R using a new set of gRNAs and new donor DNA which is the *fancd2* sequence with K595R mutation introduced.

The *Ubi-GFP-Fancd2* and *Ubi-GFP-Fancd2 K595R* flies were generated by cloning full length *Drosophila* Fancd2 with and without the K595R point mutation, fused to codon optimized GFP and separated by a $(GSSS)_4$ linker at the N-terminus, into a pBID vector (Addgene, TwistBioscience). The resulting plasmid was used to make transgenic flies (Model System Injections).

The stock containing ry^{776+} gRNA (ATTGTGGCGGAGATCTCGA) was made by the Sekelsky lab at UNC Chapel Hill, NC. The guide RNA was cloned into a pCFD3 vector (Fillip Port, Simon Bullock lab, MRC-LMB) and injected at 58A using PhiC 31. The landing site has a 3xP3 DsRed marker and the pCFD3 has a *vermillion+* marker.

A.1.3 DNA Damage

Double-strand breaks (DSBs) were induced using three methods. The first method uses animals expressing the *hs-I-Cre*I transgene. DNA damage was induced using methods in [47]. Animals were heat shocked at 37ºC for 90 min at the second larval instar stage. The second method to induce DSBs was using IR as described in [47]. Fly food containing second larval instar flies were placed in 60 mm petri dishes. The

petri dishes were then place in an X-RAD 160 PXI precision X-ray irradiator (calibrated by a dosimetrist) at 20 Gy. Lastly, DSBs were induced at the *ry* locus using CRISPR-Cas9 (see *Drosophila* Culture and Genetics). Animals expressing the *ry* gRNA were crossed to animals expressing *UAS-Cas9*; *byn-Gal4, tub-Gal80ts*. These animals were raised at 18ºC until the second larval instar stage. Larvae were then shifted to 29ºC for 24 h to allow for expression of Cas9 and subsequent induction of DSBs at the *ry* locus and then shifted back to 18ºC.

A.1.4 Fixed Imaging

Drosophila tissues were dissected in 1X PBS and immediately fixed in 3.7% formaldehyde + 0.3% Triton-X. Immunofluorescence (IF) staining was performed as in [183]. Primary antibodies used in this study were mouse anti-gamma H2Av (1:2,500, Lake et al., 2013), rabbit anti-GFP (1:1,000, Life Technologies), rabbit anti-Rad51 (1:500, A gift from J. Kadonaga, USCD), rabbit anti-RPA (1:1,000, a gift from J. Nordman, generated by P. Fisher), and rabbit anti-Cap-D2 (1:1000, a gift from G. Rogers). Tissue was stained with DAPI at 5 μg/ml.

All fixed images presented in figures were acquired using Zeiss 880 Airyscan Inverted Confocal using 20x/0.80 (420650-9901): Plan-Apochromat, NA: 0.80, air and 63x/1.4 (420782-9900): Plan-Apochromat, NA: 1.4, Oil objectives. 405 nm Diode, Argon/2

488, and 561 nm Diode lasers were used on a Zeiss Axio Observer Z1 with Definite Focus2. The system was controlled by Zeiss Zen 2.3. Adult rectum images were acquired using Zeiss AxioImager M.2 with Apotome processing using 20x objective. Additional imaging used for quantitation only were performed using Andor Dragonfly 505 unit with Borealis illumination spinning disk confocal with Andor iXon Life 888 1024x1024 EMCCD camera and using 63x/1.47 TIRF HC PL APO CORR (Leica 11506319) Oil objective (405 nm (100 mw), 488 nm (150 mW), and 561 nm (100 mW) diodes) on a Leica DMi8 microscope. The system was controlled by Fusion software.

A.1.5 Live Imaging

Tissues were prepared for live imaging as described in previous studies [89, 184] Images were acquired on spinning disk confocal (Yokogawa CSU10 scanhead) on an Olympus IX-70 inverted microscope using a 60×/1.3 NA UPlanSApo Silicon oil, 488 and 568 nm Kr-Ar laser lines for excitation, and an Andor Ixon3 897 512 electron-multiplying charge-coupled device camera. The system was controlled by MetaMorph 7.7

A.1.6 Image Analysis

All image analysis was performed using ImageJ [185]. Focus index was determined as the percentage of cells with at least one DNA repair focus. Individual foci

were not counted due to somatic chromosome pairing, in which foci in these cells can coalesce into a single focus. Mre11-GFP foci in fixed tissues were not as distinguishable as RPA3-GFP foci and thus were determined using co-localization with gH2AV antibody. Focus index, micronuclei frequency, and adult papillar cell number were quantified using Image J Cell Counter plugin. Foci Intensity was calculated by measuring mean fluorescence intensity of individual foci. Images were converted to grayscale and individual ROIs were drawn around multiple foci within each cell across different stages of cell division (interphase, prophase (pre and post NEBD), metaphase, anaphase, and interphase following the first division). Measurements of individual ROIs were taken using the mean gray value. ROIs of the same size were taken from background on the same stack and timepoint as the relevant foci and mean intensity values were averaged and subtracted from each focus mean intensity value.

A.1.7 Statistics

All statistics were computed in Prism (versions 8 and 9, GraphPad, La Jolla, CA). Adult papillar cell number and micronuclei frequency for animals expressing various RNAi constructs were analyzed using an unpaired t test (no DNA damage versus DNA damage). Focus index and fluorescence intensity measurements were analyzed using ordinary one-way ANOVA with multiple comparisons (data points compared to no

DNA damage control). P-values and N values are indicated in figure legends. Statistical notations used in figures: NS= not significant, *=$P \leq 0.05$, **= $P \leq 0.01$, ***=$P \leq 0.001$, ****= $P \leq 0.0001$.

References

1. Harper, J.W. and S.J. Elledge, *The DNA Damage Response: Ten Years After.* Molecular Cell, 2007. 28(5): p. 739-745.

2. Ciccia, A. and S.J. Elledge, *The DNA damage response: making it safe to play with knives.* Mol Cell, 2010. 40(2): p. 179-204.

3. Finn, K., N.F. Lowndes, and M. Grenon, *Eukaryotic DNA damage checkpoint activation in response to double-strand breaks.* Cell Mol Life Sci, 2012. 69(9): p. 1447-73.

4. Jackson, S.P. and J. Bartek, *The DNA-damage response in human biology and disease.* Nature, 2009. 461(7267): p. 1071-8.

5. Sekelsky, J., *DNA Repair in Drosophila: Mutagens, Models, and Missing Genes.* Genetics, 2017. 205(2): p. 471-490.

6. Chatterjee, N. and G.C. Walker, *Mechanisms of DNA damage, repair, and mutagenesis.* Environmental and Molecular Mutagenesis, 2017. 58(5): p. 235-263.

7. Fishel, R., *Mismatch repair.* The Journal of biological chemistry, 2015. 290(44): p. 26395-26403.

8. Yang, W. and Y. Gao, *Translesion and Repair DNA Polymerases: Diverse Structure and Mechanism.* Annual Review of Biochemistry, 2018. 87(1): p. 239-261.

9. Kastan, M.B., *DNA Damage Responses: Mechanisms and Roles in Human Disease.* 2007 G.H.A. Clowes Memorial Award Lecture, 2008. 6(4): p. 517-524.

10. Cannan, W.J. and D.S. Pederson, *Mechanisms and Consequences of Double-Strand DNA Break Formation in Chromatin.* Journal of Cellular Physiology, 2016. 231(1): p. 3-14.

11. Scully, R., et al., *DNA double-strand break repair-pathway choice in somatic mammalian cells.* Nat Rev Mol Cell Biol, 2019. 20(11): p. 698-714.

12. Holsclaw, J.K., T. Hatkevich, and J. Sekelsky, *Chapter 9 - Meiotic and Mitotic Recombination: First in Flies*, in *Genome Stability*, I. Kovalchuk and O. Kovalchuk, Editors. 2016, Academic Press: Boston. p. 139-154.

13. Cussiol, J.R.R., B.L. Soares, and F.M.B.d. Oliveira, *From yeast to humans: Understanding the biology of DNA Damage Response (DDR) kinases.* Genetics and molecular biology, 2019. 43(1 suppl 1): p. e20190071-e20190071.

14. Chen, Y., et al., *Drosophila RecQ5 is required for efficient SSA repair and suppression of LOH in vivo.* Protein & cell, 2010. 1(5): p. 478-490.

15. Holsclaw, J.K. and J. Sekelsky, *Annealing of Complementary DNA Sequences During Double-Strand Break Repair in Drosophila Is Mediated by the Ortholog of SMARCAL1.* Genetics, 2017. 206(1): p. 467-480.

16. Castedo, M., et al., *Cell death by mitotic catastrophe: a molecular definition.* Oncogene, 2004. 23(16): p. 2825-2837.

17. Blackford, A.N. and S.P. Jackson, *ATM, ATR, and DNA-PK: The Trinity at the Heart of the DNA Damage Response.* Mol Cell, 2017. 66(6): p. 801-817.

18. Hafner, A., et al., *The multiple mechanisms that regulate p53 activity and cell fate.* Nat Rev Mol Cell Biol, 2019. 20(4): p. 199-210.

19. Barnum, K.J. and M.J. O'Connell, *Cell cycle regulation by checkpoints.* Methods in molecular biology (Clifton, N.J.), 2014. 1170: p. 29-40.

20. Delacôte, F. and B.S. Lopez, *Importance of the cell cycle phase for the choice of the appropriate DSB repair pathway, for genome stability mintenance: the trans-S double-strand break repair model.* Cell Cycle, 2008. 7(1): p. 33-38.

21. McArt, D.G., et al., *Comet sensitivity in assessing DNA damage and repair in different cell cycle stages.* Mutagenesis, 2010. 25(3): p. 299-303.

22. Scully, R. and A. Xie, *In my end is my beginning: control of end resection and DSBR pathway 'choice' by cyclin-dependent kinases.* Oncogene, 2005. 24(17): p. 2871-2876.

23. Mao, Z., et al., *DNA repair by nonhomologous end joining and homologous recombination during cell cycle in human cells.* Cell Cycle, 2008. 7(18): p. 2902-6.

24. Jeggo, P.A., *Studies on mammalian mutants defective in rejoining double-strand breaks in DNA.* Mutat Res, 1990. 239(1): p. 1-16.

25. Kakarougkas, A. and P.A. Jeggo, *DNA DSB repair pathway choice: an orchestrated handover mechanism.* The British Journal of Radiology, 2014. 87(1035): p. 20130685.

26. Shrivastav, M., L.P. De Haro, and J.A. Nickoloff, *Regulation of DNA double-strand break repair pathway choice.* Cell Research, 2008. 18(1): p. 134-147.

27. Li, J. and X. Xu, *DNA double-strand break repair: a tale of pathway choices.* Acta Biochimica et Biophysica Sinica, 2016. 48(7): p. 641-646.

28. Grabarz, A., et al., *Initiation of DNA double strand break repair: signaling and single-stranded resection dictate the choice between homologous recombination, non-*

homologous end-joining and alternative end-joining. Am J Cancer Res, 2012. 2(3): p. 249-68.

29. Ferretti, L.P., L. Lafranchi, and A.A. Sartori, *Controlling DNA-end resection: a new task for CDKs.* Frontiers in genetics, 2013. 4: p. 99-99.

30. Iliakis, G., T. Murmann, and A. Soni, *Alternative end-joining repair pathways are the ultimate backup for abrogated classical non-homologous end-joining and homologous recombination repair: Implications for the formation of chromosome translocations.* Mutat Res Genet Toxicol Environ Mutagen, 2015. 793: p. 166-75.

31. Thompson, R., R. Gatenby, and S. Sidi, *How Cells Handle DNA Breaks during Mitosis: Detection, Signaling, Repair, and Fate Choice.* Cells, 2019. 8(9): p. 1049.

32. Blackford, A.N. and M. Stucki, *How Cells Respond to DNA Breaks in Mitosis.* Trends in Biochemical Sciences, 2020. 45(4): p. 321-331.

33. Ferrari, S. and C. Gentili, *Maintaining Genome Stability in Defiance of Mitotic DNA Damage.* Frontiers in Genetics, 2016. 7(128).

34. Bakhoum, S.F., et al., *Mitotic DNA Damage Response: At the Crossroads of Structural and Numerical Cancer Chromosome Instabilities.* Trends in Cancer, 2017. 3(3): p. 225-234.

35. Heijink, A.M., M. Krajewska, and M.A.T.M. van Vugt, *The DNA damage response during mitosis.* Mutation Research/Fundamental and Molecular Mechanisms of Mutagenesis, 2013. 750(1): p. 45-55.

36. Bakhoum, S.F., et al., *DNA-Damage Response during Mitosis Induces Whole-Chromosome Missegregation.* Cancer Discovery, 2014. 4(11): p. 1281-1289.

37. Leimbacher, P.-A., et al., *MDC1 Interacts with TOPBP1 to Maintain Chromosomal Stability during Mitosis.* Molecular Cell, 2019. 74(3): p. 571-583.e8.

38. Landmann, C., et al., *The Mre11-Rad50-Nbs1 complex mediates the robust recruitment of Polo to DNA lesions during mitosis in Drosophila.* J Cell Sci, 2020. 133(13).

39. Gomez Godinez, V., et al., *DNA damage induced during mitosis undergoes DNA repair synthesis.* PLOS ONE, 2020. 15(4): p. e0227849.

40. Davoli, T. and T. de Lange, *The Causes and Consequences of Polyploidy in Normal Development and Cancer.* Annual Review of Cell and Developmental Biology, 2011. 27(1): p. 585-610.

41. Illidge, T.M., et al., *Polyploid giant cells provide a survival mechanism for p53 mutant cells after DNA damage.* Cell Biol Int, 2000. 24(9): p. 621-33.

42. Zheng, L., et al., *Polyploid cells rewire DNA damage response networks to overcome replication stress-induced barriers for tumour progression.* Nature Communications, 2012. 3(1): p. 815.

43. Ivanov, A., et al., *Endopolyploid cells produced after severe genotoxic damage have the potential to repair DNA double strand breaks.* Journal of Cell Science, 2003. 116(20): p. 4095-4106.

44. Chitnis, M.M., et al., *IGF-1R inhibition enhances radiosensitivity and delays double-strand break repair by both non-homologous end-joining and homologous recombination.* Oncogene, 2014. 33(45): p. 5262-5273.

45. Colin, D.J., et al., *The role of reactive oxygen species and subsequent DNA-damage response in the emergence of resistance towards resveratrol in colon cancer models.* Cell Death & Disease, 2014. 5(11): p. e1533-e1533.

46. Shang, Z.-F., et al., *Inactivation of DNA-Dependent Protein Kinase Leads to Spindle Disruption and Mitotic Catastrophe with Attenuated Checkpoint Protein 2 Phosphorylation in Response to DNA Damage.* Cancer Research, 2010. 70(9): p. 3657-3666.

47. Bretscher, Heidi S. and Donald T. Fox, *Proliferation of Double-Strand Break-Resistant Polyploid Cells Requires Drosophila FANCD2.* Developmental Cell, 2016. 37(5): p. 444-457.

48. Fox, D.T. and R.J. Duronio, *Endoreplication and polyploidy: insights into development and disease.* Development, 2013. 140(1): p. 3-12.

49. Peterson, N.G. and D.T. Fox, *Communal living: the role of polyploidy and syncytia in tissue biology.* Chromosome Res, 2021: p. 1-16.

50. Edgar, B.A. and T.L. Orr-Weaver, *Endoreplication Cell Cycles: More for Less.* Cell, 2001. 105(3): p. 297-306.

51. Schoenfelder, K.P. and D.T. Fox, *The expanding implications of polyploidy.* Journal of Cell Biology, 2015. 209(4): p. 485-491.

52. Fox, D.T., et al., *Polyploidy: A Biological Force From Cells to Ecosystems.* Trends in Cell Biology, 2020. 30(9): p. 688-694.

53. Orr-Weaver, T.L., *When bigger is better: the role of polyploidy in organogenesis.* Trends in Genetics, 2015. 31(6): p. 307-315.

54. Stormo, B.M. and D.T. Fox, *Polyteny: still a giant player in chromosome research.* Chromosome Research, 2017. 25(3): p. 201-214.

55. Adachi, S., et al., *Programmed induction of endoreduplication by DNA double-strand breaks in Arabidopsis.* Proceedings of the National Academy of Sciences, 2011. 108(24): p. 10004-10009.

56. Radziejwoski, A., et al., *Atypical E2F activity coordinates PHR1 photolyase gene transcription with endoreduplication onset.* The EMBO Journal, 2011. 30(2): p. 355-363.

57. Pampalona, J., et al., *Progressive Telomere Dysfunction Causes Cytokinesis Failure and Leads to the Accumulation of Polyploid Cells.* PLOS Genetics, 2012. 8(4): p. e1002679.

58. Davoli, T., E.L. Denchi, and T. de Lange, *Persistent Telomere Damage Induces Bypass of Mitosis and Tetraploidy.* Cell, 2010. 141(1): p. 81-93.

59. Chitikova, Z.V., et al., *Sustained activation of DNA damage response in irradiated apoptosis-resistant cells induces reversible senescence associated with mTOR downregulation and expression of stem cell markers.* Cell Cycle, 2014. 13(9): p. 1424-1439.

60. Mehrotra, S., et al., *Endocycling cells do not apoptose in response to DNA rereplication genotoxic stress.* Genes Dev, 2008. 22(22): p. 3158-71.

61. Zhang, B., et al., *Low Levels of p53 Protein and Chromatin Silencing of p53 Target Genes Repress Apoptosis in Drosophila Endocycling Cells.* PLOS Genetics, 2014. 10(9): p. e1004581.

62. Hassel, C., et al., *Induction of endocycles represses apoptosis independently of differentiation and predisposes cells to genome instability.* Development (Cambridge, England), 2014. 141(1): p. 112-123.

63. Delmas, S., et al., *Mre11-Rad50 Promotes Rapid Repair of DNA Damage in the Polyploid Archaeon Haloferax volcanii by Restraining Homologous Recombination.* PLOS Genetics, 2009. 5(7): p. e1000552.

64. Yarosh, W. and A.C. Spradling, *Incomplete replication generates somatic DNA alterations within Drosophila polytene salivary gland cells.* Genes & development, 2014. 28(16): p. 1840-1855.

65. Andreyeva, E.N., et al., *Local DNA underreplication correlates with accumulation of phosphorylated H2Av in the Drosophila melanogaster polytene chromosomes.* Chromosome Research, 2008. 16(6): p. 851-862.

66. Lilly, M.A. and A.C. Spradling, *The Drosophila endocycle is controlled by Cyclin E and lacks a checkpoint ensuring S-phase completion.* Genes Dev, 1996. 10(19): p. 2514-26.

67. Dialynas, G., L. Delabaere, and I. Chiolo, *Arp2/3 and Unc45 maintain heterochromatin stability in Drosophila polytene chromosomes.* Experimental Biology and Medicine, 2019. 244(15): p. 1362-1371.

68. Hannibal, R.L., et al., *Copy Number Variation Is a Fundamental Aspect of the Placental Genome.* PLOS Genetics, 2014. 10(5): p. e1004290.

69. Bentchikou, E., et al., *Additive Effects of SbcCD and PolX Deficiencies in the In Vivo Repair of DNA Double-Strand Breaks in Deinococcus radiodurans.* Journal of Bacteriology, 2007. 189(13): p. 4784-4790.

70. Alexander, J.L., et al., *Multiple mechanisms contribute to double-strand break repair at rereplication forks in Drosophila follicle cells.* Proceedings of the National Academy of Sciences of the United States of America, 2016. 113(48): p. 13809-13814.

71. Hart, M., S.D. Adams, and V.M. Draviam, *Multinucleation associated DNA damage blocks proliferation in p53-compromised cells.* Communications biology, 2021. 4(1): p. 451-451.

72. Lu, K.L. and Y.M. Yamashita, *Germ cell connectivity enhances cell death in response to DNA damage in the Drosophila testis.* eLife, 2017. 6: p. e27960.

73. Zack, T.I., et al., *Pan-cancer patterns of somatic copy number alteration.* Nature Genetics, 2013. 45(10): p. 1134-1140.

74. Newcomb, R., et al., *Context-dependent effects of whole-genome duplication during mammary tumor recurrence.* Scientific Reports, 2021. 11(1): p. 14932.

75. Petsalaki, E. and G. Zachos, *DNA damage response proteins regulating mitotic cell division: double agents preserving genome stability.* Febs j, 2020. 287(9): p. 1700-1721.

76. Syed, A. and J.A. Tainer, *The MRE11–RAD50–NBS1 Complex Conducts the Orchestration of Damage Signaling and Outcomes to Stress in DNA Replication and Repair.* Annual Review of Biochemistry, 2018. 87(1): p. 263-294.

77. Tisi, R., et al., *Functional and structural insights into the MRX/MRN complex, a key player in recognition and repair of DNA double-strand breaks.* Computational and structural biotechnology journal, 2020. 18: p. 1137-1152.

78. Rong, Y.S., et al., *Targeted mutagenesis by homologous recombination in D. melanogaster.* Genes Dev, 2002. 16(12): p. 1568-81.

79. Royou, A., et al., *BubR1- and Polo-coated DNA tethers facilitate poleward segregation of acentric chromatids.* Cell, 2010. 140(2): p. 235-45.

80. Jaklevic, B., et al., *Contribution of growth and cell cycle checkpoints to radiation survival in Drosophila.* Genetics, 2006. 174(4): p. 1963-1972.

81. Royou, A., H. Macias, and W. Sullivan, *The Drosophila Grp/Chk1 DNA damage checkpoint controls entry into anaphase.* Curr Biol, 2005. 15(4): p. 334-9.

82. Peterson, C., et al., *reaper is required for neuroblast apoptosis during Drosophila development.* Development, 2002. 129(6): p. 1467-1476.

83. Furuta, T., et al., *Phosphorylation of Histone H2AX and Activation of Mre11, Rad50, and Nbs1 in Response to Replication-dependent DNA Double-strand Breaks Induced by Mammalian DNA Topoisomerase I Cleavage Complexes* *. Journal of Biological Chemistry, 2003. 278(22): p. 20303-20312.

84. Nakamura, K., et al., *Collaborative action of Brca1 and CtIP in elimination of covalent modifications from double-strand breaks to facilitate subsequent break repair.* PLoS Genet, 2010. 6(1): p. e1000828.

85. Murcia, L., et al., *Selective Killing of RAS-Malignant Tissues by Exploiting Oncogene-Induced DNA Damage.* Cell Reports, 2019. 28(1): p. 119-131.e4.

86. Iwaki, D.D. and J.A. Lengyel, *A Delta–Notch signaling border regulated by Engrailed/Invected repression specifies boundary cells in the Drosophila hindgut.* Mechanisms of Development, 2002. 114(1): p. 71-84.

87. Chiolo, I., et al., *Double-Strand Breaks in Heterochromatin Move Outside of a Dynamic HP1a Domain to Complete Recombinational Repair.* Cell, 2011. 144(5): p. 732-744.

88. Carvajal-Garcia, J., et al., *DNA polymerase theta suppresses mitotic crossing over.* PLOS Genetics, 2021. 17(3): p. e1009267.

89. Fox, D.T., J.G. Gall, and A.C. Spradling, *Error-prone polyploid mitosis during normal Drosophila development.* Genes Dev, 2010. 24(20): p. 2294-302.

90. Cohen, E., et al., *Physiology, Development, and Disease Modeling in the Drosophila Excretory System.* Genetics, 2020. 214(2): p. 235-264.

91. Kondo, S. and N. Perrimon, *A genome-wide RNAi screen identifies core components of the G_2-M DNA damage checkpoint.* Science signaling, 2011. 4(154): p. rs1-rs1.

92. Ceccaldi, R., B. Rondinelli, and A.D. D'Andrea, *Repair Pathway Choices and Consequences at the Double-Strand Break.* Trends in Cell Biology, 2016. 26(1): p. 52-64.

93. Wright, W.D., S.S. Shah, and W.D. Heyer, *Homologous recombination and the repair of DNA double-strand breaks.* J Biol Chem, 2018. 293(27): p. 10524-10535.

94. Ceccaldi, R., et al., *Homologous-recombination-deficient tumours are dependent on Polθ-mediated repair.* Nature, 2015. 518(7538): p. 258-62.

95. Chang, H.H.Y., et al., *Non-homologous DNA end joining and alternative pathways to double-strand break repair.* Nature Reviews Molecular Cell Biology, 2017. 18(8): p. 495-506.

96. Beagan, K., et al., *Drosophila DNA polymerase theta utilizes both helicase-like and polymerase domains during microhomology-mediated end joining and interstrand crosslink repair.* PLOS Genetics, 2017. 13(5): p. e1006813.

97. Beagan, K. and M. McVey, *Linking DNA polymerase theta structure and function in health and disease.* Cellular and molecular life sciences : CMLS, 2016. 73(3): p. 603-615.

98. Chan, S.H., A.M. Yu, and M. McVey, *Dual Roles for DNA Polymerase Theta in Alternative End-Joining Repair of Double-Strand Breaks in Drosophila.* PLOS Genetics, 2010. 6(7): p. e1001005.

99. Hanscom, T. and M. McVey, *Regulation of Error-Prone DNA Double-Strand Break Repair and Its Impact on Genome Evolution.* Cells, 2020. 9(7).

100. McVey, M. and S.E. Lee, *MMEJ repair of double-strand breaks (director's cut): deleted sequences and alternative endings.* Trends Genet, 2008. 24(11): p. 529-38.

101. Kent, T., et al., *Mechanism of microhomology-mediated end-joining promoted by human DNA polymerase θ.* Nat Struct Mol Biol, 2015. 22(3): p. 230-7.

102. Sharma, S., et al., *Homology and enzymatic requirements of microhomology-dependent alternative end joining.* Cell Death & Disease, 2015. 6(3): p. e1697-e1697.

103. Ahmad, A., et al., *ERCC1-XPF Endonuclease Facilitates DNA Double-Strand Break Repair.* Molecular and Cellular Biology, 2008. 28(16): p. 5082-5092.

104. Ma, J.-L., et al., *Yeast Mre11 and Rad1 Proteins Define a Ku-Independent Mechanism To Repair Double-Strand Breaks Lacking Overlapping End Sequences.* Molecular and Cellular Biology, 2003. 23(23): p. 8820-8828.

105. Liang, L., et al., *Modulation of DNA end joining by nuclear proteins.* J Biol Chem, 2005. 280(36): p. 31442-9.

106. Wood, R.D. and S. Doublié, *DNA polymerase θ (POLQ), double-strand break repair, and cancer.* DNA Repair (Amst), 2016. 44: p. 22-32.

107. Rodríguez, A. and A. D'Andrea, *Fanconi anemia pathway.* Curr Biol, 2017. 27(18): p. R986-r988.

108. Marek, L.R. and A.E. Bale, *Drosophila homologs of FANCD2 and FANCL function in DNA repair.* DNA Repair (Amst), 2006. 5(11): p. 1317-26.

109. Yang, H., et al., *Methods Favoring Homology-Directed Repair Choice in Response to CRISPR/Cas9 Induced-Double Strand Breaks.* International Journal of Molecular Sciences, 2020. 21(18): p. 6461.

110. Liu, Y., et al., *The origins and processing of ultra fine anaphase DNA bridges.* Curr Opin Genet Dev, 2014. 26: p. 1-5.

111. Harper, J.W. and S.J. Elledge, *The DNA damage response: ten years after.* Mol Cell, 2007. 28(5): p. 739-45.

112. Lord, C.J. and A. Ashworth, *The DNA damage response and cancer therapy.* Nature, 2012. 481(7381): p. 287-294.

113. Thyme, S.B. and A.F. Schier, *Polq-Mediated End Joining Is Essential for Surviving DNA Double-Strand Breaks during Early Zebrafish Development.* Cell reports, 2016. 15(4): p. 707-714.

114. Deng, L., et al., *Mitotic CDK Promotes Replisome Disassembly, Fork Breakage, and Complex DNA Rearrangements.* Molecular Cell, 2019. 73(5): p. 915-929.e6.

115. Fernandez-Vidal, A., et al., *A role for DNA polymerase θ in the timing of DNA replication.* Nature Communications, 2014. 5(1): p. 4285.

116. Kais, Z., et al., *FANCD2 Maintains Fork Stability in BRCA1/2-Deficient Tumors and Promotes Alternative End-Joining DNA Repair.* Cell Reports, 2016. 15(11): p. 2488-2499.

117. Muzzini, D.M., et al., *Caenorhabditis elegans POLQ-1 and HEL-308 function in two distinct DNA interstrand cross-link repair pathways.* DNA Repair (Amst), 2008. 7(6): p. 941-50.

118. Ward, T.A., P.J. McHugh, and S.T. Durant, *Small molecule inhibitors uncover synthetic genetic interactions of human flap endonuclease 1 (FEN1) with DNA damage response genes.* PLOS ONE, 2017. 12(6): p. e0179278.

119. Minocherhomji, S. and I.D. Hickson, *Structure-specific endonucleases: guardians of fragile site stability.* Trends in Cell Biology, 2014. 24(5): p. 321-327.

120. Peterson, N.G., et al., *Cytoplasmic sharing through apical membrane remodeling.* eLife, 2020. 9: p. e58107.

121. Shen, H., D.M. Moran, and C.G. Maki, *Transient Nutlin-3a Treatment Promotes Endoreduplication and the Generation of Therapy-Resistant Tetraploid Cells.* Cancer Research, 2008. 68(20): p. 8260-8268.

122. Shen, H., et al., *Two 4N Cell-Cycle Arrests Contribute to Cisplatin-Resistance.* PLOS ONE, 2013. 8(4): p. e59848.

123. Szakács, G., et al., *Targeting multidrug resistance in cancer.* Nat Rev Drug Discov, 2006. 5(3): p. 219-34.

124. Marcozzi, A., F. Pellestor, and W.P. Kloosterman, *The Genomic Characteristics and Origin of Chromothripsis.* Methods Mol Biol, 2018. 1769: p. 3-19.

125. Zhang, C.-Z., et al., *Chromothripsis from DNA damage in micronuclei.* Nature, 2015. 522(7555): p. 179-184.

126. Nazaryan-Petersen, L., et al., *Chromothripsis and DNA Repair Disorders.* J Clin Med, 2020. 9(3).

127. Crasta, K., et al., *DNA breaks and chromosome pulverization from errors in mitosis.* Nature, 2012. 482(7383): p. 53-58.

128. McLaughlin, M., et al., *Inflammatory microenvironment remodelling by tumour cells after radiotherapy.* Nat Rev Cancer, 2020. 20(4): p. 203-217.

129. Liu, H., et al., *Nuclear cGAS suppresses DNA repair and promotes tumorigenesis.* Nature, 2018. 563(7729): p. 131-136.

130. Mackenzie, K.J., et al., *cGAS surveillance of micronuclei links genome instability to innate immunity.* Nature, 2017. 548(7668): p. 461-465.

131. Harding, S.M., et al., *Mitotic progression following DNA damage enables pattern recognition within micronuclei.* Nature, 2017. 548(7668): p. 466-470.

132. Bakhoum, S.F., et al., *Chromosomal instability drives metastasis through a cytosolic DNA response.* Nature, 2018. 553(7689): p. 467-472.

133. Fang, C.-B., et al., *Fanconi Anemia Pathway: Mechanisms of Breast Cancer Predisposition Development and Potential Therapeutic Targets.* Frontiers in Cell and Developmental Biology, 2020. 8(160).

134. Niraj, J., A. Färkkilä, and A.D. D'Andrea, *The Fanconi Anemia Pathway in Cancer.* Annual review of cancer biology, 2019. 3: p. 457-478.

135. Singh, S., et al., *Genetic and physical interactions between the yeast ELG1 gene and orthologs of the Fanconi anemia pathway.* Cell cycle (Georgetown, Tex.), 2013. 12(10): p. 1625-1636.

136. Ceccaldi, R., P. Sarangi, and A.D. D'Andrea, *The Fanconi anaemia pathway: new players and new functions.* Nature Reviews Molecular Cell Biology, 2016. 17(6): p. 337-349.

137. Liu, W., et al., *Fanconi anemia pathway as a prospective target for cancer intervention.* Cell & Bioscience, 2020. 10(1): p. 39.

138. Liang, C.C., et al., *UHRF1 is a sensor for DNA interstrand crosslinks and recruits FANCD2 to initiate the Fanconi anemia pathway.* Cell Rep, 2015. 10(12): p. 1947-56.

139. Thompson, E.L., et al., *FANCI and FANCD2 have common as well as independent functions during the cellular replication stress response.* Nucleic acids research, 2017. 45(20): p. 11837-11857.

140. Boisvert, R.A. and N.G. Howlett, *The Fanconi anemia ID2 complex: dueling saxes at the crossroads.* Cell Cycle, 2014. 13(19): p. 2999-3015.

141. Geiss-Friedlander, R. and F. Melchior, *Concepts in sumoylation: a decade on.* Nature Reviews Molecular Cell Biology, 2007. 8(12): p. 947-956.

142. Moldovan, G.-L. and A.D. D'Andrea, *How the Fanconi Anemia Pathway Guards the Genome.* Annual Review of Genetics, 2009. 43(1): p. 223-249.

143. Panagopoulos, A., et al., *CRL4^{Cdt2}: Coupling Genome Stability to Ubiquitination.* Trends in Cell Biology, 2020. 30(4): p. 290-302.

144. Abbas, T. and A. Dutta, *CRL4Cdt2: master coordinator of cell cycle progression and genome stability.* Cell cycle (Georgetown, Tex.), 2011. 10(2): p. 241-249.

145. Havens, C.G. and J.C. Walter, *Mechanism of CRL4Cdt2, a PCNA-dependent E3 ubiquitin ligase.* Genes & Development, 2011. 25(15): p. 1568-1582.

146. Pan, W.-W., et al., *Ubiquitin E3 Ligase CRL4^{CDT2/DCAF2} as a Potential Chemotherapeutic Target for Ovarian Surface Epithelial Cancer **. Journal of Biological Chemistry, 2013. 288(41): p. 29680-29691.

147. Han, C., et al., *Cdt2-mediated XPG degradation promotes gap-filling DNA synthesis in nucleotide excision repair.* Cell Cycle, 2015. 14(7): p. 1103-1115.

148. Moss, J., et al., *Break-induced ATR and Ddb1-Cul4(Cdt)² ubiquitin ligase-dependent nucleotide synthesis promotes homologous recombination repair in fission yeast.* Genes & development, 2010. 24(23): p. 2705-2716.

149. Nguyen, H.C., W. Wang, and Y. Xiong, *Cullin-RING E3 Ubiquitin Ligases: Bridges to Destruction.* Sub-cellular biochemistry, 2017. 83: p. 323-347.

150. Lydeard, J.R., B.A. Schulman, and J.W. Harper, *Building and remodelling Cullin–RING E3 ubiquitin ligases.* EMBO reports, 2013. 14(12): p. 1050-1061.

151. Fouad, S., et al., *Cullin Ring Ubiquitin Ligases (CRLs) in Cancer: Responses to Ionizing Radiation (IR) Treatment.* Frontiers in Physiology, 2019. 10(1144).

152. Wei, N. and X.W. Deng, *The COP9 Signalosome.* Annual Review of Cell and Developmental Biology, 2003. 19(1): p. 261-286.

153. Cope, G.A. and R.J. Deshaies, *COP9 Signalosome: A Multifunctional Regulator of SCF and Other Cullin-Based Ubiquitin Ligases.* Cell, 2003. 114(6): p. 663-671.

154. Cavadini, S., et al., *Cullin–RING ubiquitin E3 ligase regulation by the COP9 signalosome.* Nature, 2016. 531(7596): p. 598-603.

155. Hannß, R. and W. Dubiel, *COP9 signalosome function in the DDR.* FEBS Letters, 2011. 585(18): p. 2845-2852.

156. Huh, J. and H. Piwnica-Worms, *CRL4(CDT2) targets CHK1 for PCNA-independent destruction.* Molecular and cellular biology, 2013. 33(2): p. 213-226.

157. Olivero, M., et al., *The stress phenotype makes cancer cells addicted to CDT2, a substrate receptor of the CRL4 ubiquitin ligase.* Oncotarget, 2014. 5(15): p. 5992-6002.

158. Kim, Y., N.G. Starostina, and E.T. Kipreos, *The CRL4Cdt2 ubiquitin ligase targets the degradation of p21Cip1 to control replication licensing.* Genes & development, 2008. 22(18): p. 2507-2519.

159. Sansam, C.L., et al., *DTL/CDT2 is essential for both CDT1 regulation and the early G2/M checkpoint.* Genes & development, 2006. 20(22): p. 3117-3129.

160. Prestel, A., et al., *The PCNA interaction motifs revisited: thinking outside the PIP-box.* Cellular and Molecular Life Sciences, 2019. 76(24): p. 4923-4943.

161. Green, L.C., et al., *Contrasting roles of condensin I and condensin II in mitotic chromosome formation.* Journal of cell science, 2012. 125(Pt 6): p. 1591-1604.

162. Paul, M.R., A. Hochwagen, and S. Ercan, *Condensin action and compaction.* Current genetics, 2019. 65(2): p. 407-415.

163. Jenkins, C., J. Kan, and M.E. Hoatlin, *Targeting the Fanconi Anemia Pathway to Identify Tailored Anticancer Therapeutics.* Anemia, 2012. 2012: p. 481583.

164. Centore, R.C., et al., *CRL4(Cdt2)-mediated destruction of the histone methyltransferase Set8 prevents premature chromatin compaction in S phase.* Molecular cell, 2010. 40(1): p. 22-33.

165. Øvrebø, J.I. and B.A. Edgar, *Polyploidy in tissue homeostasis and regeneration.* Development, 2018. 145(14).

166. Paulovich, A.G., D.P. Toczyski, and L.H. Hartwell, *When Checkpoints Fail.* Cell, 1997. 88(3): p. 315-321.

167. Campos, A. and A. Clemente-Blanco, *Cell Cycle and DNA Repair Regulation in the Damage Response: Protein Phosphatases Take Over the Reins.* Int J Mol Sci, 2020. 21(2).

168. Beagan, K. and M. McVey, *Linking DNA polymerase theta structure and function in health and disease.* Cell Mol Life Sci, 2016. 73(3): p. 603-15.

169. Patel, P.S., A. Algouneh, and R. Hakem, *Exploiting synthetic lethality to target BRCA1/2-deficient tumors: where we stand.* Oncogene, 2021. 40(17): p. 3001-3014.

170. Derive, N., et al., *Bub3–BubR1-dependent sequestration of Cdc20Fizzy at DNA breaks facilitates the correct segregation of broken chromosomes.* Journal of Cell Biology, 2015. 211(3): p. 517-532.

171. Naim, V. and F. Rosselli, *The FANC pathway and BLM collaborate during mitosis to prevent micro-nucleation and chromosome abnormalities.* Nature Cell Biology, 2009. 11(6): p. 761-768.

172. Chan, Y.W., K. Fugger, and S.C. West, *Unresolved recombination intermediates lead to ultra-fine anaphase bridges, chromosome breaks and aberrations.* Nature Cell Biology, 2018. 20(1): p. 92-103.

173. Fernández-Casañas, M. and K.L. Chan, *The Unresolved Problem of DNA Bridging.* Genes (Basel), 2018. 9(12).

174. Chan, K.-L., P.S. North, and I.D. Hickson, *BLM is required for faithful chromosome segregation and its localization defines a class of ultrafine anaphase bridges.* The EMBO Journal, 2007. 26(14): p. 3397-3409.

175. Umbreit, N.T., et al., *Mechanisms generating cancer genome complexity from a single cell division error.* Science, 2020. 368(6488): p. eaba0712.

176. Sallmyr, A. and A.E. Tomkinson, *Repair of DNA double-strand breaks by mammalian alternative end-joining pathways.* J Biol Chem, 2018. 293(27): p. 10536-10546.

177. Handke, B., et al., *Towards Long Term Cultivation of Drosophila Wing Imaginal Discs In Vitro.* PLOS ONE, 2014. 9(9): p. e107333.

178. Ohno, Y., et al., *Acentric chromosome ends are prone to fusion with functional chromosome ends through a homology-directed rearrangement.* Nucleic Acids Research, 2015. 44(1): p. 232-244.

179. Stormo, B.M. and D.T. Fox, *Distinct responses to reduplicated chromosomes require distinct Mad2 responses.* eLife, 2016. 5: p. e15204.

180. Yates, L.R., et al., *Genomic Evolution of Breast Cancer Metastasis and Relapse.* Cancer Cell, 2017. 32(2): p. 169-184.e7.

181. Heale, J.T., et al., *Condensin I interacts with the PARP-1-XRCC1 complex and functions in DNA single-strand break repair.* Molecular cell, 2006. 21(6): p. 837-848.

182. Hirota, T., et al., *Distinct functions of condensin I and II in mitotic chromosome assembly.* J Cell Sci, 2004. 117(Pt 26): p. 6435-45.

183. Sawyer, J., E. Cohen, and D. Fox, *Inter-organ regulation of Drosophila intestinal stem cell proliferation by a hybrid organ boundary zone.* Development, 2017. 144: p. dev.153114.

184. Schoenfelder, K.P., et al., *Indispensable pre-mitotic endocycles promote aneuploidy in the Drosophila rectum.* Development, 2014. 141(18): p. 3551-3560.

185. Schneider, C.A., W.S. Rasband, and K.W. Eliceiri, *NIH Image to ImageJ: 25 years of image analysis.* Nature Methods, 2012. 9(7): p. 671-675.

186. Singer, J.B., et al., *Drosophila brachyenteron regulates gene activity and morphogenesis in the gut.* Development, 1996. 122(12): p. 3707-3718.

187. Althoff, F., R.E. Karess, and C.F. Lehner, *Spindle checkpoint–independent inhibition of mitotic chromosome segregation by Drosophila Mps1.* Molecular Biology of the Cell, 2012. 23(12): p. 2275-2291.

188. Edwards, K.A., et al., *GFP-Moesin Illuminates Actin Cytoskeleton Dynamics in Living Tissue and Demonstrates Cell Shape Changes during Morphogenesis inDrosophila.* Developmental Biology, 1997. 191(1): p. 103-117.

Biography

Delisa Clay received her Bachelor of Science degree in Biology with a minor in Chemistry from Virginia Commonwealth University (VCU) , in Richmond, VA. She attended VCU from 2012-2016. She published a first author paper titled, "Persistent DNA Damage Signaling and DNA Polymerase Theta Promote Broken Chromosome Segregation" in the Journal of Cell Biology in 2021. She received the Duke BioCoRE Program Award (NIH, T32) and the Duke School of Medicine Biomedical Graduate Fellowship in 2016, the National Science Foundation Graduate Research Fellowship in 2018, the Michelle P. Winn Inclusive Excellence Award and the Best Graduate Student Talk Award at the Annual Triangle Fly Symposium in 2019, and the ASCB Inclusivity Grant in 2020. She was appointed by Dean Paula McClain and President Vincent Price as a member of the Duke Graduate School Board of Visitors in 2019.